TolC imaging and its time-resolved production dynamics.

by

Alexander Mircea Petrescu

a Thesis submitted in partial fulfillment

of the requirements for the degree of

Doctor of Philosophy

in Biochemical Engineering

Approved Dissertation Committee

Prof. Dr. Mathias Winterhalter

Jacobs University Bremen

Prof. Dr. Roland Benz

Jacobs University Bremen

Prof. Dr. Malcolm Page

Basilea Pharmaceutica Ltd.

Prof. Dr. Jean-Michel Bolla

Aix-Marseille Université

Date of Defense: 11th of May 2016

Department of Life Sciences and Chemistry

Statutory Declaration

(Declaration on Authorship of a Dissertation)

I, Alexander Mircea Petrescu hereby declare, under penalty of perjury, that I am aware of the consequences of a deliberately or negligently wrongly submitted affidavit, in particular the punitive provisions of § 156 and § 161 of the Criminal Code (up to 1 year imprisonment or a fine at delivering a negligent or 3 years or a fine at a knowingly false affidavit).

Furthermore, I declare that I have written this PhD thesis independently, unless where clearly stated otherwise. I have used only the sources, the data and the support that I have clearly mentioned.

This PhD thesis has not been submitted for the conferral of a degree elsewhere.

Bremen, the 11th of May 2017

Signature

Table of Contents

Acknowledgements

I would like to express my sincere and immense gratitude to Prof. Mathias Winterhalter for all the support, trust and confidence he has placed in me over the years. Chapeau!

I am thankful to the members of the committee evaluating this work, especially to Prof. Malcolm Page for his wise and kind comments and suggestions.

I would like to acknowledge my loving parents, Elisabeta and Constantin, for all the sacrifices they have made such that my brother and I pursue the educations we want. You have been and are a humbling example for me.

My brother Dragoş has always been there for me, a listening ear, a helping hand and always supportive. Thank you!

And lastly, I thank my sweet Victoria for being such a supportive, gentle and cheerful presence in my life. Thank you, love.

1 TolC imaging and time-resolved production via fluorescent labeling in *Escherichia coli*

1.1 Declaration of contribution

I have conceived the study and designed all experiments. I have done all the cloning, functionality tests, Western blots, quantitative real time RT PCR, most microscopy and some of the growth curve/time-resolved fluorescence measurements. The remaining microscopy and time-resolved fluorescence experiments I did together Xizhou Zhang, in the framework of her bachelor thesis, under my supervision. I wrote this manuscript and planned further experiments.

1.2 Abstract

TolC is a component of the protein complex that forms the main bacterial efflux system involved in expelling out of the cell numerous harmful antibacterial chemicals such as antibiotics and detergents. TolC is the outer membrane component of the system and it connects with an inner membrane energy-demanding pump, which can be either an ABC transporter or a proton antiporter. A periplasmic membrane fusion protein seals the connection of the two. TolC is able to bind a multitude of such transporters which have very different substrate specificities thus TolC part-taking in the efflux of dozens of substrates. This makes TolC be a main participant in the phenomenon of multidrug efflux and a better understanding of its behavior in vivo is thus required. In the present study, the spatial localization and time-resolved dynamics of TolC production in live cells is described. This is achieved by labeling the TolC protein genomically with an oxidation-resistant variant of GFP, superfolder GFP. The labelled protein is fully functional and shows a growth medium-dependent expression. Furthermore, certain antibiotics increase its production in a concentration-dependent manner. This is the first time such a behavior was shown and opens new ways for further research.

1.3 Introduction

1.3.1 The bacterial envelope and transport

Gram-negative bacteria are surrounded by a very distinct cell envelope that is made of two individual membranes. Sharff et al. (2001) give a comprehensive account on the peculiarities of this envelope: The inner membrane is in contact with the cytosol and it is a normal phospholipid bilayer. The outer membrane faces the cell's exterior and the lipids of the outer leaflet have attached to them poly-saccharides with polar sugar head groups. These lipopoly-saccharides

confer the bacteria unique physical-chemical features and are a characteristic of bacteria. They are often the ones inducing an immunogenic response in hosts. Between the two lipid bilayers there is a 100 to 250 Å-long space (Graham, 1991), the periplasm, inside which a peptidoglycan wall is built to confer mechanical strength to the bacterium. Because of the outer membrane porins, most of which are basically open, the periplasmic space is in ionic equilibrium with the exterior, fact that leads to a series of problems and interesting solutions to these problems. More accurately, due to the fixed charged (polar) groups on the outer membrane the periplasm is in Donnan equilibrium (Hellman, 1998). The problems mentioned are referring to the mechanistic challenge the bacterium is faced with when having to secrete/excrete molecules across the periplasm. Energy is required to move molecules across the periplasm in the case of excreted waste and virulence factors, and energy has to go into fighting a concentration gradient in the case of drug influx. In order to get this energy, ATP could be hydrolyzed or electrochemical gradients could be utilized. However, since the periplasm is in equilibrium with the outside environment, ATP concentrations cannot be sustained in the periplasm nor can electrochemical gradients be established. Therefore, outer membrane proteins cannot benefit from such forms of energy and they cannot do the active transport. The active energy-consuming step has to be driven at the inner membrane level, from the cytoplasm. And here comes the mechanistic problem: with the active transport step at the level at the inner membrane molecules from the cytoplasm and from within the inner membrane (such as lipophilic drugs) have to be put across two membrane and the 100-250 Å of the periplasm (Graham, 1991).

There are no less than five (I to V) systems developed through evolution that successfully transport various substrates in the outside environment. These systems are summarized by Sharff et al. (2001): in type II and V the transport isn't continuous, but it is accomplished in two steps being fragmented in the periplasm where the substrate is free for some time. In type II, proteins with specific N-terminus localization signals are the substrates and they are transported in an ATP-dependent manner cotranslationally across the inner membrane through the Sec pump. In the periplasm they fold and translocation across the outer membrane takes place. Type III processes are complicated; they transport folded proteins that have certain signals requiring approx. 20 other auxiliary proteins. DNA is transported through a continuous pilus in the type IV mechanism.

Type I transport is maybe the most interesting of all since is one of the main players in conferring bacteria the so-called multidrug resistance, a phenomenon with a rapidly growing importance of clinical relevance (Paulsen, 1997) In type I a continuous channel that spans the two membranes plus the periplasmic space is created through a multiprotein complex. The complex consists of

three elements: an inner membrane translocator, an outer membrane pore and a periplasmic membrane fusion protein that connects the two establishing a continuous channel (Johnson, 1999). The inner membrane translocator can mostly be either an ATP-binding cassette (ABC) protein or a proton antiporter. The periplasmic fusion protein depends on the translocator and the outer membrane component.

1.3.2 The outer membrane protein TolC

The most prominent outer membrane component of the type I efflux system is the protein TolC from *E. coli*. TolC represents a ubiquitous large family of porins throughout Gram-negative bacteria: approximately 100 members have been found in 30 bacterial species (Paulsen, 1997), indicating the importance this protein has.

TolC is able to interact with a large range of different transporters depending on the nature of the transported substrate (Paulsen, 1997) and ca thus complete the export of a variety of unrelated antimicrobials being thus very important in the phenomenon of multidrug efflux (Nikaido, 1996). Studies show that *E. coli* lacking the TolC protein are susceptible to a multitude of toxic agents such as bile salts, detergents, organic solvents (Bina, 2001 and Aono, 1998) which attests its role in MDR. TolC has a high versatility when it comes to the inner membrane transporter partner: although this partner can be an ABC transporter, it is mostly a proton antiporter belonging to the RND (resistance nodulation division) or to the MFS (major facilitator superfamily) families consisting of many transporters. In *E. coli* TolC is able to bind no less than 30 translocators, like EmrAB of the MFS family and AcrAB of the RND family (Saier, 1998). Figure 1 shows how such a type I complex looks like.

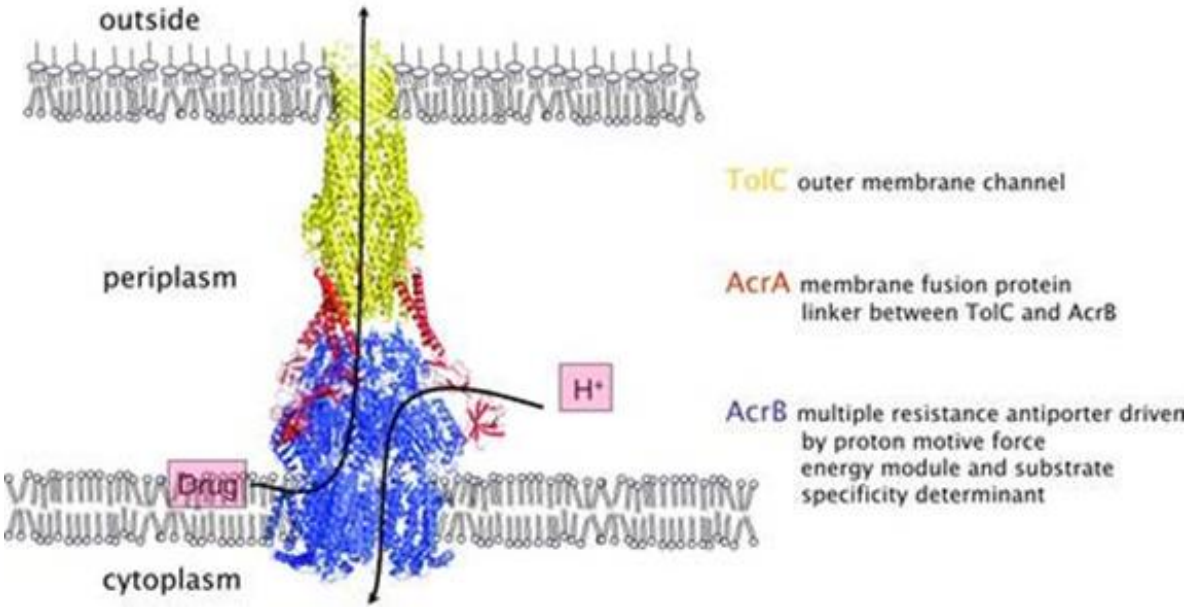

Figure 1: Example of a type I system involving TolC. TolC is shown interacting with the proton antiporter MDR family translocator AcrAB. The interaction is reversible and TolC can attach to up to 30 other translocators in *E. coli* participating in the efflux of many different substrates (picture from Eicher et al., 2009)

By binding those 30 potential transporter partners TolC gets involved in the efflux of literally hundreds of substrates, most of which are toxic to the bacterium. To get an idea of the proportions of this phenomenon below are the substrate specificities of three TolC-containing *E. coli* efflux systems (Koronakis, 2004):

AcrAB (RND family)/ TolC: acriflavin, azithromycin, β-lactams, bile salts, cholate, chloramphenicol, crystal violet, ciprofloxacin, deoxycholate, ethidium bromide, erythromycin

AcrEF (RND family)/ TolC: fatty acids, fluoroquinolones, fusidic acid, nalidixic acid, novobiocin, rifampicin, SDS, Triton X-100

EmrAB (MFS family)/ TolC: lipophilic cations, carbonyl cyanide m-chlorophenilhydrazone, nalidixic acid

TolC thus becomes an essential player in the rapidly-increasing process of bacterial multidrug resistance, being very important to the survivability of pathogens in hosts during infections (Aono, 1998, Paulsen 1997 and Nikaido, 1996). Therefore, studying this protein under all possible aspects is crucial. The aspects advanced in this work for investigation are the spatial distribution and production dynamics of TolC. These aspects have not yet been investigated and represent a new approach to understanding the phenomenon of multidrug resistance. For example, TolC is the Omp conducing the substrates of all those pumps outside the cell, but is there a specific arrangement on the geometry of the cell that makes antibiotic efflux so efficient? Is this arrangement different prior to the apparition of the stressor (antibiotic), and how does it change

after? Is TolC production upregulated after antibiotic exposure and how fast? These are all very important questions that if answered would shed some light on the phenomenon of MDR.

1.3.3 Other roles of TolC

However, in addition to its drug efflux activity, TolC is used for a multitude of biological roles. Some of the processes TolC takes part in are useful for the cell, while others are detrimental.

Iron is an essential element required for the growth of many organisms. Its ability to change oxidation stated between +2 and +3 make it vital for redox reactions in the electron transfer chain. In mammals, it is also essential as an O_2/CO_2 binder – as part of the heme. Iron is therefore a limited resource, either in the context of microbial life where most microorganisms will compete for it, or in the context of a host's body where the pathogenic bacteria compete with the very host they are infecting for it. In order to sequester the scarce iron in their environment, bacteria have developed the ability to synthesize, secrete and retrieve very strong iron chelators, the siderophores. The siderophore produced by the organism *Escherichia coli* is enterobactin. Until recently it was not known how enterobactin is getting secreted, which molecular pathway it takes. Vega and Young (Vega and Young, 2014) found that the outer membrane channel required for enterobactin secretion is TolC. They observed that when cells are grown in media lacking iron, and are therefore induced to produce and secrete enterobactin, the cells swell and elongate (Figure 2). In their work, they show the swelling is due to the enterobactin which is getting produced but cannot leave the cell, the conclusion being that TolC is utilized for enterobactin secretion.

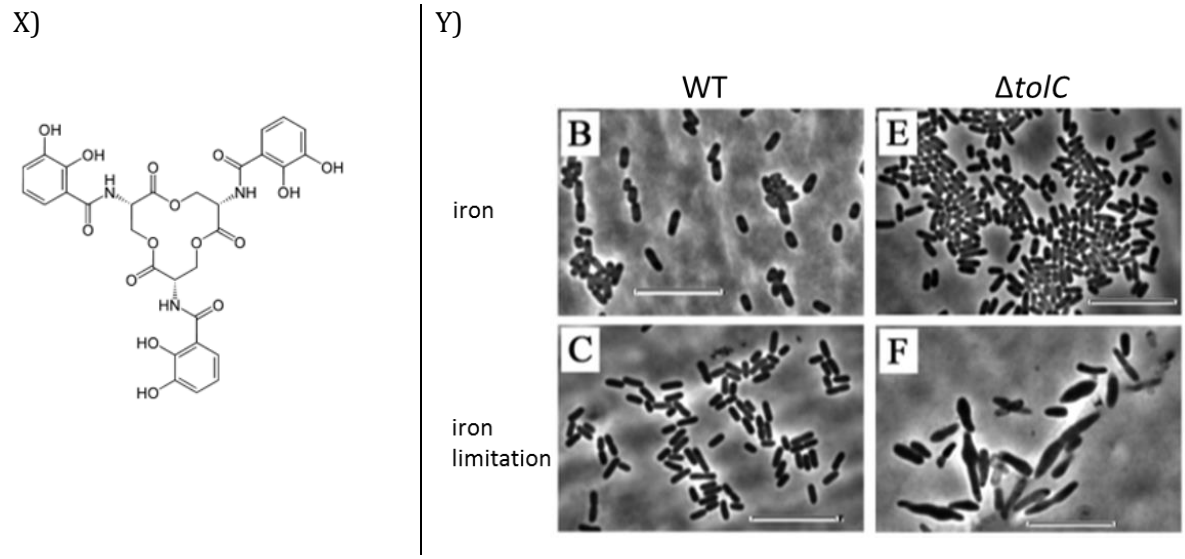

Figure 2: Enterobactin, the *E. coli* siderophore. X) the chemical structure of enterobactin and Y) *E. coli* morphology as a function of TolC and iron limitation: WT cells have similar morphology independent of iron (B) and C) inlets), whereas Δ*tolC* look elongated and swollen under iron limitation due to enterobactin accumulation in the periplasm (F) inlet) (picture from Vega and Young, 2014)

Siderophores help bacteria capture and retrieve the available iron, but there are also mechanisms helping them make more iron available to them. These mechanisms consist of producing protein toxins which are capable of multimerizing and forming large pores into erythrocytes, which then leads to a massive release of iron-containing hemoglobin. *Staphylococcus aureus* is widely known for being able to produces several such proteins, the hemolysins. However, also some pathogenic *E. coli* strains produce such toxins, the α-hemolysin (Skals et al., 2009). α-Hemolysin is produce in the cytoplasm and, in order to be secreted, it uses a dedicated inner membrane transporter, HlyB. HlyB forms a complex with TolC, TolC being essential for hemolysin secretion in *E. coli*.

Colicins are bactericidal peptides produced by certain strains of *E. coli* against others, aiding their fight for resources. Colicins require a receptor on the surface of the cell, and a channel to translocate into the periplasmic space. Once there they might undergo folding/maturation which renders them active. Some of them act directly in the periplasm inserting into the inner membrane and creating pores which disrupt the membrane potential, while others act in the cytoplasm as DNases/RNases. Colicin E1 is using the vitamin B12 as a receptor and TolC as the channel to go through (Masi et al., 2007). This is a remarkable use of the fact that TolC is such an important protein for *E. coli*, and it *must* be there, therefore a good place for "high jacking".

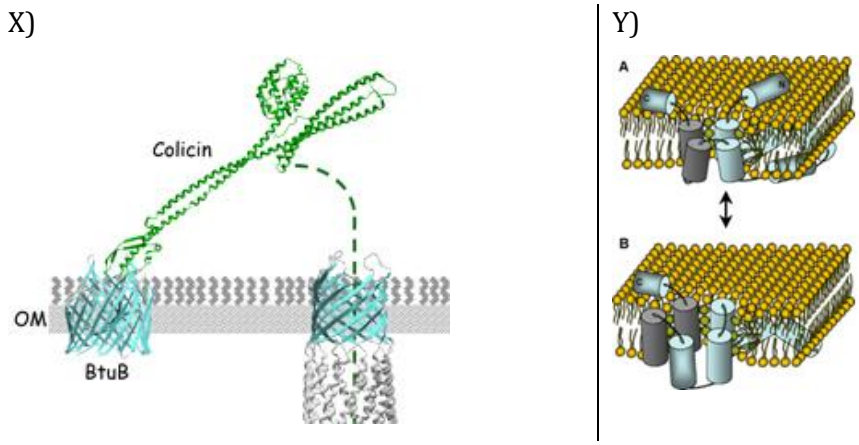

Figure 3: Colicin E1 entry into the cell. X) Once docked onto the BtuB receptor, the peptide binds and translocate through TolC (image from Masi et al., 2007) and Y) the pore-forming domain of Colicin E1 as it inserts and forms a channel into the inner membrane (image from Sobko et al., 2006)

Colicin E1 thereafter forms inserts into the inner membrane with its pore-forming domain, creating large holes which lead to membrane depolarization (Sobko et al., 2006).

1.3.4 Protein labeling and omps.

Previous studies on LamB (maltose uptake outer membrane protein porin) spatial distribution (Vos-Scheperkeuter, 1984 and Jaffe, 1985) done using indirect immunogold electron microscopy involving an anti-LamB primary antibody and a protein A-gold probe on fixed cells have been

unable to correctly asses LamB spatial distribution. This was in part due to the bad antibody staining because of the difficult access to LamB as a result of the intricate lipopoly-saccharide (LPS) layer (Voorhout, 1986), and due to the fixation of cells, which affects the outer membrane integrity. Therefore, investigating the spatial distribution of Omps is better preferred in live cells.

In fact, it was long-proven that indirect immuno-labeling does not provide an accurate description of the outer membrane since the chemical fixation method seems to be responsible for extracting proteins (Palade, 1952), thus live-imaging is essential for maintaining the native Omps distribution.

If modern live-cell imaging using GFP and its derivatives can be successfully applied for cytoplasmic and inner membrane proteins (Feilmeier, 2000) it has been shown that this method cannot be used on outer membrane proteins because GFP fails to fold correctly when exported from the cytoplasm (Feilmeier, 2000) into the periplasm and therefore there is little, almost non-existing information on the localization of Omps.

One of the very few studies investigating outer membrane proteins organization is that of Gibbs et al. (2004). They have found way of investigating the spatial distribution and dynamics of LamB. Using the information that the lambda bacteriophage uses LamB as receptor when infecting bacteria, they produced lambda phage tails, which they afterwards fluorescently labeled. These tails are natural ligands of LamB and therefore they can be used as probes when labeled. This method was good both for LamB spatial localization and for live-imaging showing how the spatial pattern changes over time. The results were interesting revealing not a uniformly distributed pattern, but a spiral-shaped localization consisting of one LamB moving population and another LamB resting population.

When GFP and derivatives are fused to proteins that exit the cytoplasm they fail to fold correctly and do not fluoresce unless they are exported using the Tat export pathway (Feilmeier, 2000). The Tat pathway exports proteins in a fully folded state and it is not the route taken by most exported proteins, including the omps. Omps take a different export route, the Sec pathway which transports them in a linear form in the periplasm where they are welcomed by chaperons aiding their refolding which evidently fails for GFP and derivatives. Pedelacq et al. (Pédelacq et al., 2006) developed a robust derivative of GFP with improved folding and stability, termed superfolder GFP – sfGFP. Aronson et al. (Aronson et al., 2011) showed that the superfolder GFP is able to fold and fluoresce in the *Escherichia coli* periplasm, making it an suitable reporter for the thus-far „inaccessible“ periplasm.

Structurally, TolC is a homo-trimieric protein, composed of 12 strads that form a continuous 140Å-long channel spanning the outer membrane and reaching deep into the periplasm (Koronakis et al., 2004). Each monomer contributes 3 of the strands, which, in the outer membrane form a β-barrel that is continues by long α-helical barrel followed by a mixed α/β barrel. This third domain of the protein, the equatorial one, harbors the protein's C-terminus. The C-terminus is pointing outwards toward the periplasm, hanging freely (Koronakis et al., 2004; Zgurskaya et al., 2011)

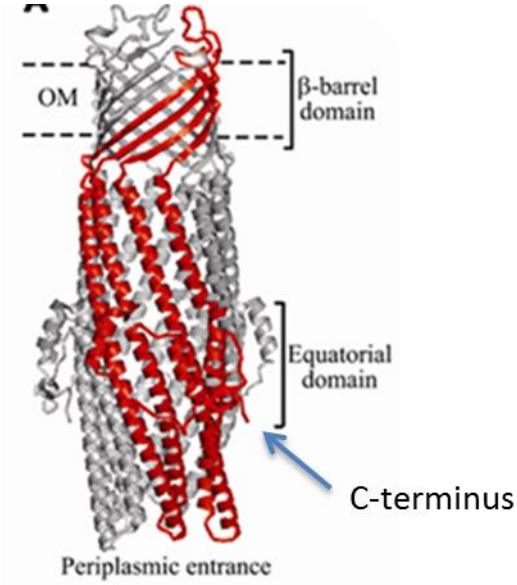

Figure 4: TolC structure. Arrow points to the C-terminus, in the equatorial domain of the protein (picture from Zgurskaya et al., 2011)

As the C-terminus of TolC hangs on the outside of the protein exposed to the periplasm (Figure 4), it seemed like a suitable strategy to fuse the sfGFP translationally to it. The sfGFP protein would be linked to TolC, on the side, hopefully not impeding TolC's functions. The novel protein proved to be both functional and fluorescent and revealed previously unknown interesting facts.

1.4 Materials and Methods

1.4.1 Genomic insertions of mutations

The protocol for Red/ ET® recombination by Gene Bridges GmbH and the original study by Datsenko and Wanner (Datsenko and Wanner, 2000) were adopted and modified in order to generate both the CSH50 Δ*tolC::bla* and CSH50 *tolC-sfgfp-bla* strains.

The plasmid containing the Red/ET over-expression, pSC101-BAD-gbaA^{tet}, was transformed into chemically competent CSH50 cells. Recovery and incubation were done at 30 °C overnight on a LB agar plate containing 3 µg/ml of tetracycline. Next, a single colony was inoculated at 30 °C overnight at 150 rpm in 3 mL LB medium containing 3 µg/mL tetracycline. From this preculture a 1:100 dilution in 200 mL LB medium containing 3 µg/mL tetracycline was prepared in a 1 L culture flask and it was further incubated at 30 °C at 150 rpm. It was grown until it reached an OD_{600} of 0.4-0.6 when the temperature was raised to 37 °C and 6 mL of 10 % L-arabinose was added to induce Red/ET expression. The induced culture was incubated for another hour at the same conditions (37 °C, 150 rpm). Next, the culture was chilled on ice followed by a centrifugation at 3000 rpm for 10 min at 4 °C. The pellet was washed once with cold ddH_2O, re-centrifuged and then washed again with cold ddH_2O containing 10% glycerol. After the last washing and centrifugation, the OD_{600} was adjusted to 0.4-0.6 with ddH_2O containing 10% glycerol and arching was tested with a BIO-RAD Mircopulser™ electroporator. Lastly, the cell suspension was frozen in liquid nitrogen in 80 µL aliquots and then stored at -80 °C.

The *bla* ampicillin resistance gene and *sfgfp-bla* respectively were amplified by PCR (50 ng pBAD24/pBSK*sfgfp* plasmid template, 10 µL 15x GC buffer, 1.5 µL DMSO, 500 nM forward primer, 500 nM reverse primer, 200 µM dNTPs, 0.5 µL Phusion polymerase, and ddH2O up to total volume of 50 µL). The PCR reaction was carried on at 98 °C for 2 min, then 25 cycles of 98 °C for 10 s, 51/58 °C for 30 s, 72 °C for 40s/3 min, and finally 72 °C for 10 min and 4 °C until the end. Gel electrophoresis was performed for verification, on a 1 % agarose gel. The primers were 5'-aattttacagtttgatcgcgctaaatactgcttcaccacaaggaatgcaaatgagtattcaacatttccg and 5'-atctttacgttgccttacgttcagacggggccgaagccccgtcgtcgtcattaccaatgcttaatcagtg for amplifying *bla*, and 5'-gcaaacatccgcacgcactaccaccagtaacggtcataacccttttccgtaacctcgagggtggcgcggat and 5'-atctttacgttgccttacgttcagacggggccgaagccccgtcgtcgtcattaccaatgcttaatcagtgag for amplifying *sfgfp-bla*. The PCR products were incubated with DpnI restriction enzyme for 1 h at 37 °C and then for 20 min at 80 °C for inactivation. Gel electrophoresis was performed with the resulting product on a 1 % agarose gel with SYBR Green®. The PCR products were gel-purified using the NucleoSpin® Extract II kit.
300 ng of the purified PCR products were added to the previously made recombination competent cells. A BIO-RAD Mircopulser™ electroporator was used with 2.5 kV/5 ms for transformation. The cells were then incubated for 1 h at 37 °C in rich dYT medium. The transformations were plated on ampicillin plates and incubated overnight at 37°C.

Single colonies were picked from the transformed cells and resuspended in 50 µL ddH_2O. The samples were placed in a heating block for 5 min at 95 °C under vigorous shaking. Next, the tubes

were shortly centrifuged and 5 µL of the cells solution was taken out and used as DNA template for PCR verification. The PCR mix was added (5 µL 10x ThermoPol buffer, 200 nM forward primer and 200 nM reverse primer, 200 µM dNTPs, 0.5 µL 1000 U/mL Vent polymerase, and ddH2O) up to total volume of 50 µL. The PCR reaction was performed at 95 °C for 5 min, then 30 cycles of 95 °C for 45 s, 49/52 °C for 45 s, 72 °C for 45/120 s, and finally 72 °C for 5 min and 4 °C until the end. Primers that amplify the *tolC* gene (5'-catgaagaaattgctccccattc and 5'-acgcgtcgactcagttacggaaagggttatg) were used to check its successful deletion; for the *sfgfp-bla* insertion, the *tolC-sfgfp* junction was checked with primers 5'-cattgttgatgtgttggatgc and 5'-gtcagggtagtcaccagagtc – expected product size of 534 bp. The products were checked on a1 % agarose gel.
All enzymes used were from New England BioLabs, Frankfurt, Germany.

The pBSK*sfgfp* plasmid was a much-appreciated kind gift from Dr. Thomas G. Bernhardt.

1.4.2 Minimal Inhibitory Concentration determination

For all tested antibiotics except for novobiocin, the MIC was determined using bioMerieux's ETEST® antibiotic strips on LB agar plates following the protocol given by the manufacturer.
For novobiocin the serial dilution method was used. In a 96-well microtiter plate 180 µL of Müller-Hinton broth was added in the first row of wells and 100 µL of Müller-Hinton broth was added to the following rows. 20 µL of 32 mg/mL of novobiocin solution was added to the first row. The antibiotic was well mixed in the first well and 100 µL were taken out and placed in the well of the second row. This was again mixed and 100 µL of the second row were transferred into the third etc. until the last row, where the last 100 µL were discarded. Bacteria that were previously grown in fresh overnight cultures were suspended in sterile water in a 1.5 mL tube. A dilution was prepared to adjust the OD_{600} to 1.0 (approximately 10^9 bacterial cells/mL). The suspension was further diluted 1:10 with sterile water. Then, a 1:50 dilution with Müller-Hinton broth was prepared giving a concentration of $2*10^6$ cells/mL. Of this dilution 100 µL were added to each well. The pipetting was stared at the well with the lowest concentration of antibiotics and then it was moved up to the wells with higher concentration. The cells were left to grow in the incubator overnight, and the MIC was read.

1.4.3 Colicin E1 killing test

Overnight cultures of the cells were diluted in LB to OD600= 0.4 and plated evenly using a sterile cotton swab on LB agar plates. A solution of 33.3 µM Colicin E1 was diluted 100 fold to get the starting concentration. This dilution was further diluted 10 fold 5 more times. Each solution was dropped on the plated bacteria in 5 µL drops.

1.4.4 Real Time RT PCR

Cells were grown identically to those for online fluorescence monitoring, in the fluorimeter in a 96-well plate and in biological triplicates. The cells were collected from multiple wells and the RNA was extracted with the RNAEasy kit. QuantiTect SYBR Green one-step Quantitative PCR (Qiagen GmbH, Germany) was used to conduct the qRT-PCR in a Mx3000PTM Real Time cycler (Stratagene, USA). The primers used to the quantitate the *tolC* transcript were 5'-ggaattgcgtaagtctgccg and 5'-ggtagccgttgctataggtg amplifying 100 bp from the beginning of the transcript, and for the *rrsA* control 5'-ctcctacgggaggcagcag and 5'-gtattaccgcggctgctg. The program consisted of the following steps: 1x50°C for 10min, 1x95°C for 16min, 40x95°C for 30s, 58°C for 30s, 72°C for 30s.

Prior to the data analysis, the average PCR efficiencies for the amplicons were calculated using the LinRegPCR software (Ramakers et al., 2003).

1.4.5 Western Blot

Cells were grown in the fluorimeter as in the time-resolved fluorescence experiments. After 18h of growth cells from multiple wells were collected for verification of TolC-sfGFP amounts in the M9 vs. the M9 plus iron growth media. The cell pellets were resuspended in the resuspension/sonication buffer (10 mM Tris-HCl pH 8.0, 0.1 mM EDTA, 10 mM $MgCl_2$, 0.1 mM DTT, 5 % Glycerin, 230 mM NaCl). For protein extraction, the samples were sonicated for 30 s (90 % power) and then put on ice for 1 min. This was repeated 8 times. Then, the samples were centrifuged for 30 min at 13 000 rpm at 4 °C. The supernatants were collected in fresh tubes and stored at -20 °C. To determine the protein concentration of the crude protein extracts the Pierce™ BCA Protein Assay Kit was used following the kit manual. For detection, the Tecan Infinite® M200PRO multimode reader machine in conjunction with Magellan software was used.

On a 10% SDS-PAGE gel 5 µg of each sample were loaded. For reference 10 µL of ColorPlusPrestained Protein Marker, Broad Range (7-175 kDa) (New England BioLabs, Frankfurt, Germany) was chosen. The conditions for running the gel were 80 V for 20 min followed by 110 V for 1.5 h or alternatively it was stopped when the running front reached the bottom of the gel.

For the Western blot the Glassycarbon Semidry Transfer System (Schleicher & Schnell, Dassel, Germany) was used. The proteins were transferred on a nitrocellulose membrane (Schleicher & Schnell, Dassel, Germany), by blotting for 1.5 h using an electric current of mA equal to the total area of the gels blotted in cm. Afterwards Ponceau S solution was used for staining the membranes to verify the transfer. With 0.1 NaOH the staining solution was removed and then the membrane

was washed with Tris-Buffered Saline plus Tween-20 (TBST). The membrane was then incubated with 5 % powder milk in TBST for overnight at 4 °C on a rocking table for blocking the membranes. For detection on the membrane the ECF™ kit (GE Healthcare, Munich, Germany) was applied. The primary mouse anti GFP antibody (Neoclone, Madison, USA) was diluted 1:1000000 in 1 % skim milk in TBST. The blocked membrane was incubated with the primary antibody for 2 h at room temperature on a rocking table. The membrane was washed 3 times with TBST for 10 min. Next, the secondary anti-mouse IgG AP-linked antibody (Cell Signaling Technology, Inc., Danvers, MA, USA) were added subsequently and incubated each for 1 h. A washing step followed with washing 3 times for 7 min with TBST. Next ECF (GE Healthcare, Munich, Germany) was added and incubated for 5 min. Fluorescence was recorded with Fuji Phosphoimager FLA7000 (Fujifilm, Tokyo, Japan) and for the quantification AIDA 2D densitometry analysis, version 4.0 was used.

1.4.6 Setting up online measurements

Depending on the experiment (either only OD_{600} or both OD_{600} and fluorescence) the strains that were used were: CSH50 WT, CSH50 Δ*tolC::bla*, CSH50 *tolC-sfgfp-bla*. The cells were plated on LB agar plates containing 50 µg/mL ampicillin, except for WT that was plated without antibiotic. Single colonies (3 for each strain) were then inoculated in 2 – 3 mL of LB containing 50 µg/mL ampicillin (except for WT) in glass tubes and incubated at 37°C while shaking at 150 rpm in a CERTOMAT® BS-1 incubator. The next day, prior to using these cultures as inoculums for the main experiment in the fluorimeter, the overnight OD_{600} of all strains and replicates (that are part of the same experiment) were brought to the same value. 1 mL of each overnight culture was pelleted at 6000 rpm for 3 min in a table-top centrifuge and then subsequently washed twice with ddH2O in order to wash away all iron contained in the overnight LB cultures. The OD_{600} of a 1:10 dilution of the final resuspended pellets was measured and all OD_{600} were brought to the same value via dilution in ddH2O. These same OD_{600} samples were used as inoculums in a 96 – well plate for online OD_{600} and fluorescence measurement.

1.4.7 Online Optical Density and Fluorescence measurement

The online measurement is carried out in minimal medium M9 and in M9 plus iron. M9 is made according to the following scheme (Sambrook and Russell, 2001):

Table 1: Recipe for making 200 mL minimal medium M9

5x M9 Salts (autoclaved)	40 mL
ddH_20	149 mL
1 M $MgSO_4$ (filter sterilized)	1 mL
20 % Glucose (filter sterilized)	10 mL
10 % Thiamine (filter sterilized)	200 µL

105 mg/mL L-proline (filter sterilized)	200 µL
1 M $CaCl_2$ (filter sterilized)	20 µL

The components were added in the order given in Table 1.
1 L of 5 times concentrated M9 salts consists of: 64 g $Na_2HPO_4 \cdot 7H_2O$, 2.5 g NaCl, 15 g KH_2PO_4, and 5 g NH_4Cl and ddH_2O (up to 1 L).

In order to prepare the iron containing condition, 10 mM $FeSO_4$ was added to M9 to a final concentration of 10 µM. In addition to M9 and M9 plus iron, the cells were also grown in the presence of several antibiotics in these media. For details see Table 2. The OD600– normalized washed overnight cultures were inoculated in a 96 – well plate in a 1:200 dilution. 150 µL of media/media plus antibiotic were added to each well and then 0.75 µL of the overnight culture were added. The plate was a Corning 96 Flat Bottom black, clear bottom Polystyrol type. The entire length of the online measurement was 18 h, at 37 °C in a Tecan Infinite® 200 PRO fluorimeter. The measurement consisted of cycles of 10 min, out of which 6 min were for shaking at 180 rpm and 4 min for measuring. The optical density was followed at 600 nm. For fluorescence, GFP was excited at 488 nm and emission was measured at 530 nm. Each well was measured at 4 different locations for a better precision.

1.4.8 Antibiotics for online measurements

In order to test the responsiveness of the reporter strain to antibiotics, antibiotics were chosen to represent various modes of action. The concentrations were chosen to be below the MIC, but high enough to stress the cells (to affect the growth). For testing for concentration – dependent effects, 3 different antibiotics concentrations were tried out.
Table 2: List of antibiotics used for the online measurement and their final concentrations.

Antibiotics	**Concentrations**
Chloramphenicol	1, 2, 3 µg/mL
Clarythromycin	1, 2, 3 µg/mL
Erythromycin	1, 2, 3 µg/mL
Kanamycin	0.5, 1, 2 µg/mL
Novobiocin	25, 50, 100 µg/mL
Tetracycline	0.1, 0.2, 0.3 µg/mL
Trimethoprim	0.25, 0.5, 1 µg/mL
Linezolid	32, 64, 128 µg/mL

The final concentrations were from diluting laboratory stocks into media.

1.4.9 Data analysis for the time – resolved measurements

In order to generate the growth curve: the average OD_{600} value of the blank (M9 or M9 + Fe^{2+}) was subtracted from the optical density value at each point on the measurement. For each strain and condition there were biological triplicates and an average and standard error was calculated at each time point. This value was plotted against time with the standard error as error bars

In order to generate the Fluorescence/OD_{600}: for each strain and condition the optical density was treated as above. The fluorescence, the emission at 530 nm, was at first corrected by subtraction of the average fluorescence value of the blank (M9 or M9 + Fe^{2+}). For each time point and for each one of the replicates, the fluorescence over optical density, the value F/OD_{600} was calculated using the corrected F and $OD_{600.}$ As for each strain there were biological triplicates, average F/OD_{600} and standard errors could be calculated. The F/OD_{600} is an indication of how much fluorescence per cell there is. As of interest there is only the fluorescence coming from sf GFP, the background fluorescence of the cell has to be subtracted. Therefore, from the average F/OD_{600} of the CSH50 *tolC-sfgfp-bla* the average F/OD_{600} of the CSH50 WT cells is subtracted at each time point. This value represents the F/OD_{600}, fluorescence per cell, or more broadly the protein production and is plotted against time to error bars.

1.4.10 Microscopy and cell fixation

Cultures from the 96 well plate were fixed using 5% of a 1 M phosphate buffer and 10% of 37 % formaldehyde for 30 min. The fixed samples were centrifuged at 4,000 g for 3 min and pellets were resuspended in an according volume PBS and stored at 4 °C. Imaging was done within 24 hours.

For nucleoid staining the cells were incubated with 10 µM DRAQ5 for 5 min at room temperature, afterwards centrifuged at 3000 rmp for 5 min and resuspended in PBS.

For membrane staining the cells were incubated for 10 min at room temperature with 5 µg/mL FM4-64 dye, centrifuged at 3000 rpm for 5 min and resuspended in PBS.

The microscopy was carried out using a confocal laser scanning microscope LSM 510 Meta. The images were taken using the 75x objective with oil immersion. The images were analyzed using the LSM 510 software, Release 3.0 (Carl Zeiss Jena GmbH), and ImageJ. sfGFP fluorescence was detected using excitation at 514 nm and recording the emission signal with a broad-pass filter ranging from 530 to 600 nm. All images to be compared were taken using the same settings.

1.5 Results and Discussion

1.5.1 The constructs

As described in the introduction, 2 different strains were generated using the method described by Datsenko and Wanner (Datsenko and Wanner, 2000). CSH50 Δ*tolC::bla* and CSH50 *tolC-sfgfp-bla* were thus generated, a schematic representation of which can be seen in Figure 5.

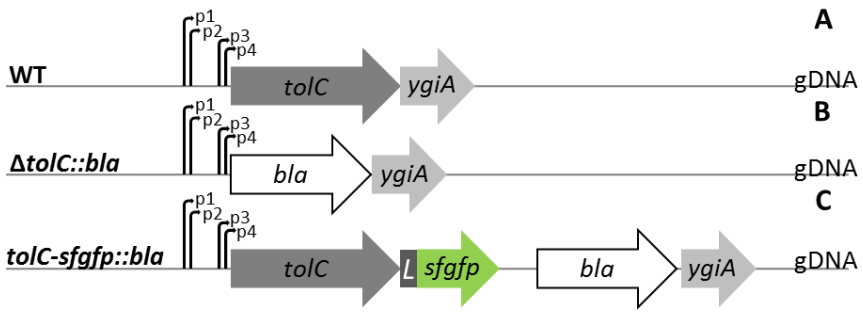

Figure 5: Schematic representation of the 3 strains used in the study. gDNA stands for genomic DNA. A) wilde-type *tolC* genomic context. B)Δ*tolC* genomic context of the *tolC* region and C) the *tolC-sfgfp* context

The correct insertions were checked by PCR performed on genomic DNA as template (gels of the results in Supplemental Figure 1)

1.5.2 Functionality testing

A wide selection of antibiotics representing functionally different groups was chosen to test the functionality of the superfolder GFP labeled TolC (henceforth TolC-GFP for simplicity). For the purpose of this study it is essential that TolC-GFP is still able to interact with AcrAB and form a functional extrusion pump. As can be seen in Table 3 all antibiotics (marked in yellow) for which TolC plays a role (as seen in the severely decreased MIC of the *tolC* mutant) are efficiently expelled via the TolC-GFP as well: the MIC for the *tolC-gfp* strain is similar to that of the wild type. The MICs were determined using the Etest strips for all antibiotics except for novobiocin where the serial dilution method was used. All MICs were determined in biological duplicates.

Table 3: : Functionality test: Antibiotic resistance, E-test, concentration [µg/mL], AM (Ampicillin), OX (Oxacillin), PM (Cefepime), CZ (Ceftizoxime), ETP (Ertapenem), MP (Meropenem), EM (Erythromycin), CH (Clarithromycin), NX (Norfloxacin), EF (Enrofloxacin), LE (Levofloxacin), TR (Trimethoprim), TC (Tetracycline), CL (Chloramphenicol), KM (Kanamycin), LZ (Linezolid), PO (Polymyxin B), CO (Colistin), NV (Novobiocin).

	CSH50 WT 1	CSH50 WT 2	CSH50 Δ*tolC* 1	CSH50 Δ*tolC* 2	CSH50 *tolC-gfp* 1	CSH50 *tolC-gfp* 2
AM	4	4	full	full	full	full
OX	full	full	full	full	full	full
PM	0.023	0.023	0.016	0.016	0.023	0.023
CZ	0.047	0.047	0.032	0.032	0.047	0.047
ETP	0.016	0.016	0.016	0.016	0.016	0.016
MP	0.064	0.064	0.064	0.064	0.064	0.064

EM	24	24	3	3	24	32
CH	32	32	4	4	48	48
NX	0.094	0.094	0.016	0.016	0.064	0.064
EF	0.094	0.094	0.003	0.003	0.064	0.064
LE	0.047	0.047	0.006	0.006	0.032	0.032
TR	2	2	0.38	0.38	2	3
TC	3	4	2	2	3	6
CL	3	4	0.75	0.75	4	6
KM	3	3	2	3	3	3
LZ	full	full	3	4	full	full
PO	0.5	0.5	0.5	0.5	0.5	0.5
CO	0.19	0.19	0.19	0.19	0.19	0.19
NV	400	400	3.125	3.125	400	400

Below the scans of the Etest plates corresponding to Linezolid and Erythromycin are shown for clarity. The inhibition ellipse is visibly larger in the case of the deletion mutant than both for WT and *tolC-gfp*.

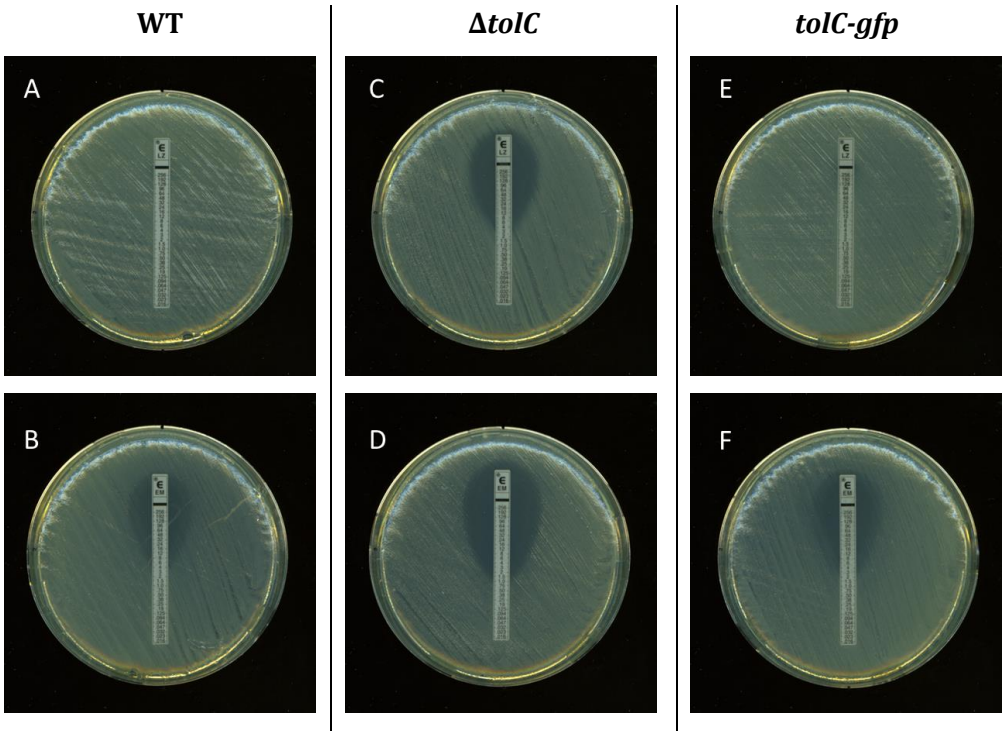

Figure 6: Antibiotic resistance, Etest examples for Linezolid in A), C) and E), and for Erythromycin in B), D) and F).

Colicins are bactericidal toxin proteins produced by bacteria to fend off other bacteria. They can interfere with RNA, DNA and cell wall synthesis as well as depolarize the inner membrane. Colicin E1 is a channel-forming colicin and acts by forming channels in the inner membrane and thus

destroying the membrane potential. Colicin E1 uses TolC as a way into the cell (Masi et al., 2007). Therefore, cells expressing functional TolC should be susceptible to this colicin.

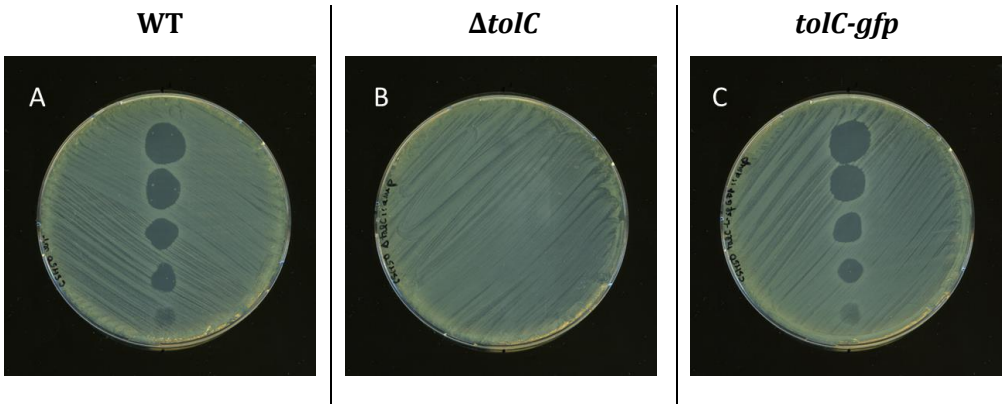

Figure 7: Functionality test: Colicin E1 uptake, decreasing concentrations of Colicin E1 spotted on plated bacteria. Concentration range 333 nM to 33 pM.

Colicin E1 in a concentration series of 333 nM, 33.3 nM, 3.33 nM, 333 pM, 33.3 pM was spotted in 5 µL drops on the plates with evenly distributed bacteria. The result is very clear, with no inhibition of growth in the case of Δ*tolC* (perhaps a small shallow spot is visible at the highest concentration) and clear hollow spots that decrease in size with colicin concentration for both WT and *tolc-gfp*.

As the functionality of TolC-GFP was proven with regard to 2 main functions of TolC, the next step is to see its membrane localization via fluorescence microscopy. WT and *tolC-gfp* cells were grown in LB up until OD600of 0.5 (exponential growth phase) and the cells were labeled with membrane-binding dye FM4-64 prior to being formaldehyde-fixed.

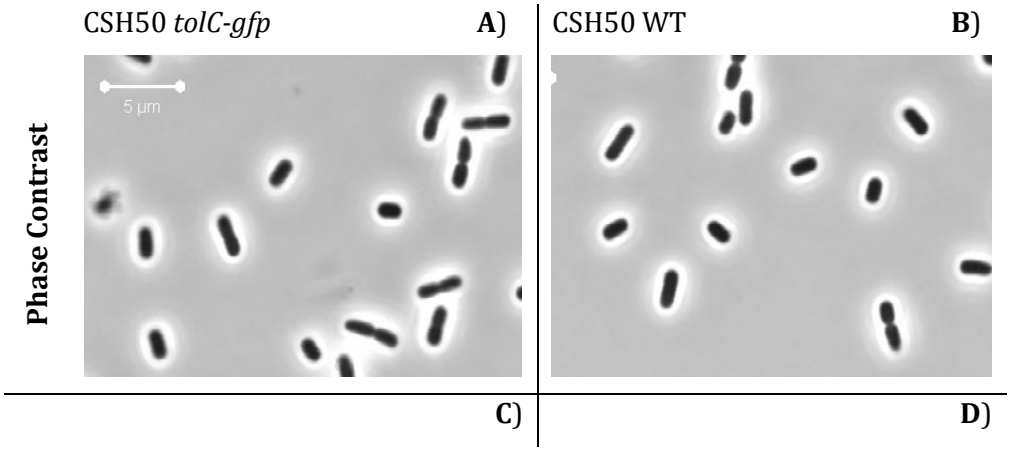

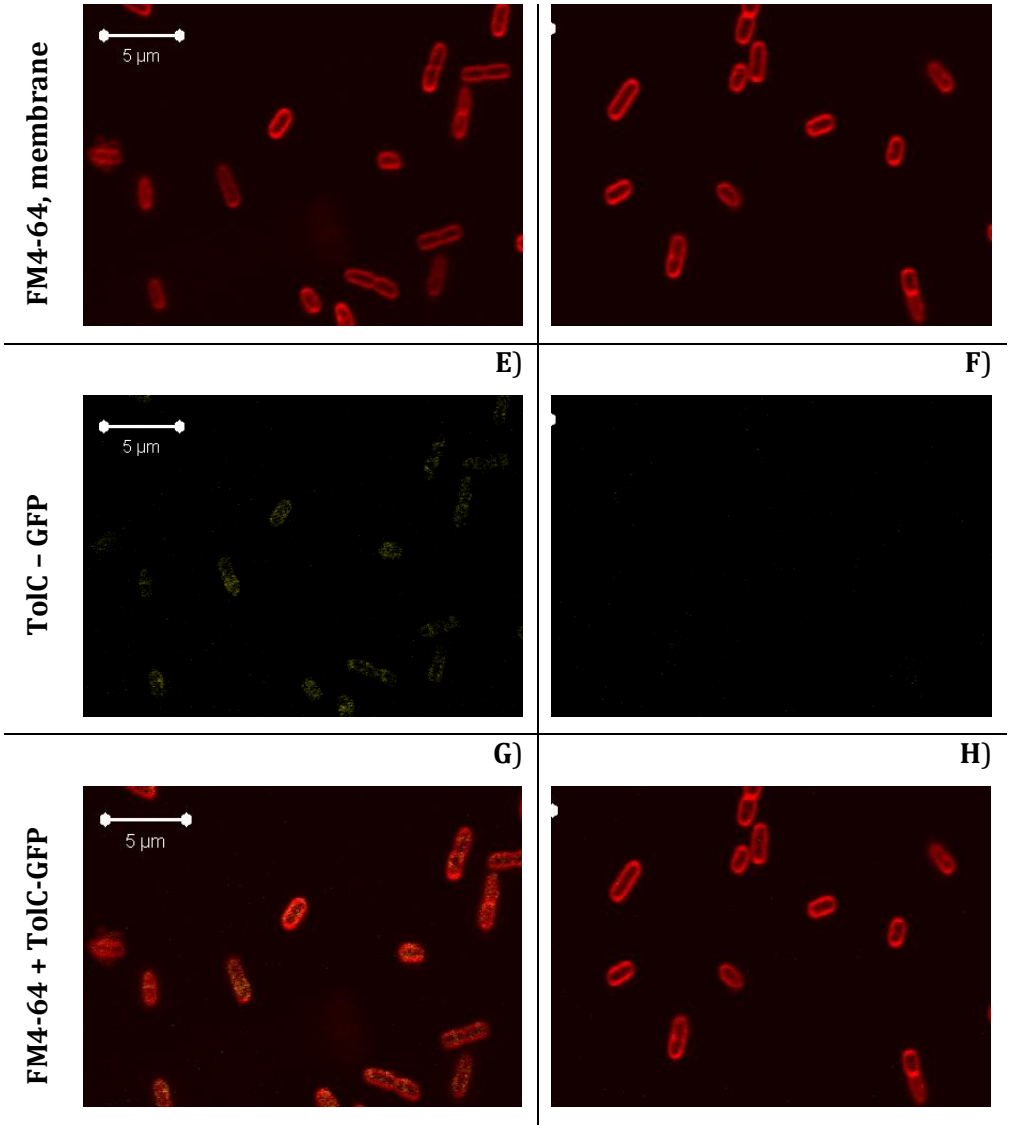

Figure 8: Membrane localization of TolC-GFP. Exponentially growing cells were imaged. E) TolC-GFP signal shows membrane localization and colocalizes with the membrane dye FM4-64 G). WT cells show now fluorescence F).

The membrane labeling with a dye of a different color (FM4-64) has been performed to point unequivocally to the membrane (Figure 8 C) and D)). The signal coming from TolC-GFP does indeed colocalize with that of FM4-64 (Figure 8 E))

A recently found (Bleuel et al., 2005; Vega and Young, 2014) role of TolC shows it is also the exit route of enterobactin. Enterobactin is a siderophore that bacteria secrete in iron-limiting conditions to sequester and retrieve the metal ion. Vega and Young (Vega and Young, 2014) found that in *E. coli* lacking TolC and under iron depletion growth conditions, enterobactin is produced but unable to exit the cell. It therefore accumulates in the periplasm enlarging and deforming the cells and hindering cell growth. It therefore seemed like a good functionality test for the TolC-GFP. The results of Vega and Young were reproduced, with the deletion mutant showing a clear phenotype in M9 medium. Both WT and *tolc-gfp* have normal morphology showing the functionality of TolC-GFP.

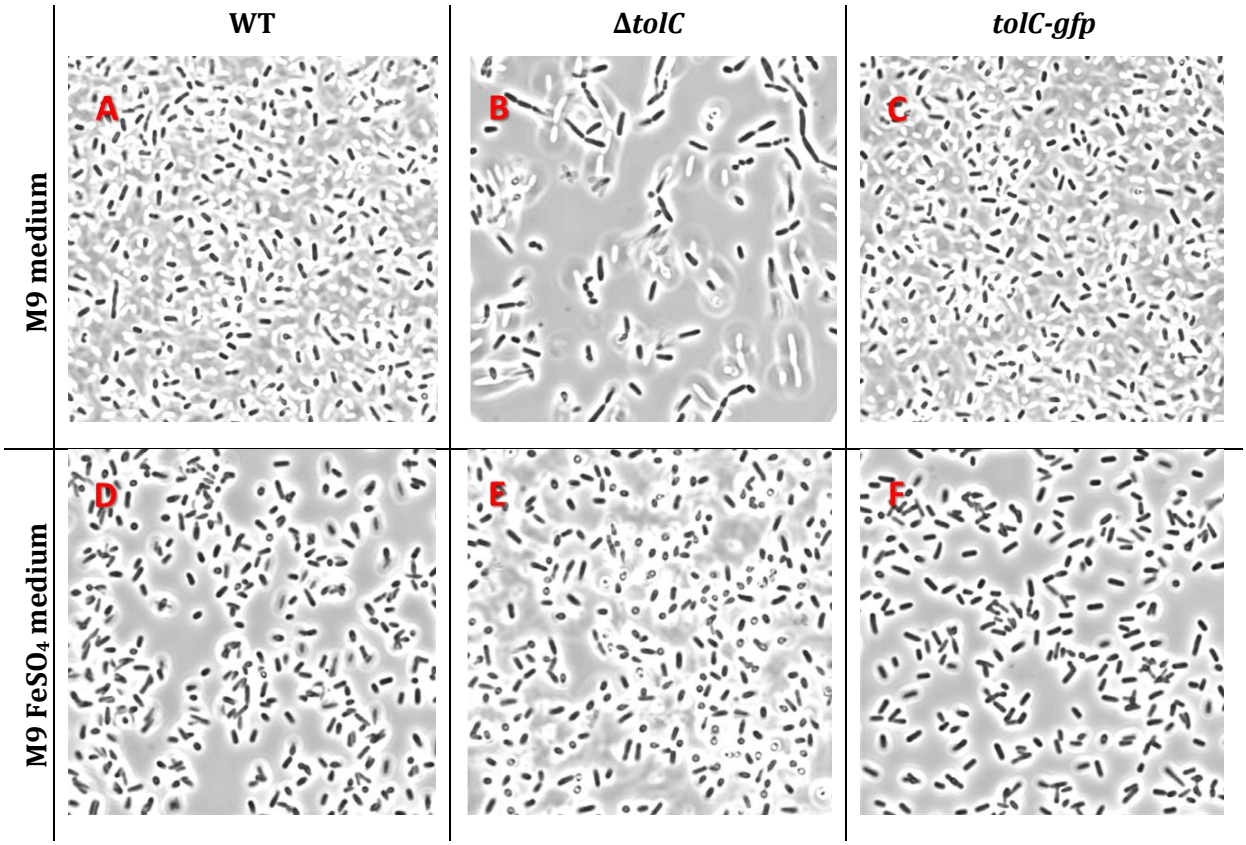

Figure 9: Enterobactin secretion: in M9 (no iron) in Δ*tolC* cells enterobactin accumulates in the periplasm deforming the cells B).

Worth mentioning, the Δ*tolC* phenotype does not manifest in M9 medium plus $FeSO_4$, when enterobactin production is not needed (Figure 9 E)).

A) | B)

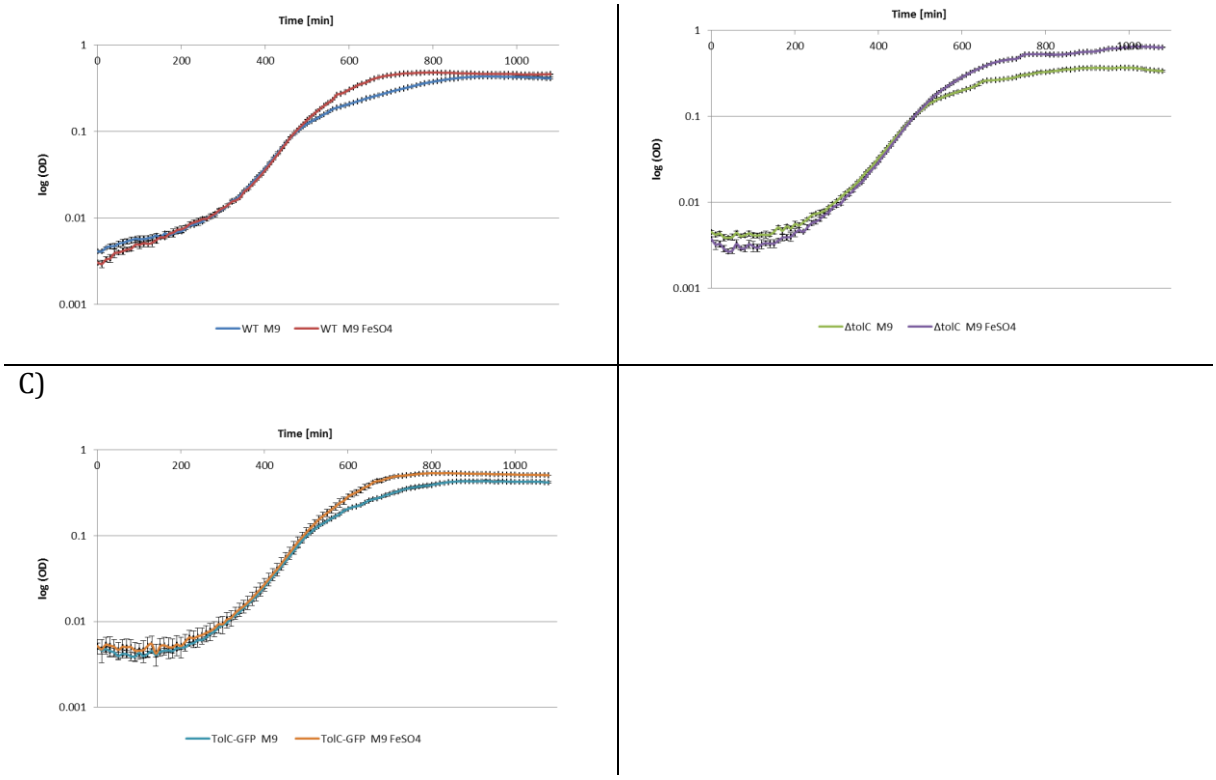

Figure 10: Enterobactin secretion, growth curves in presence/absence of Iron.

The WT-like proper functioning of TolC-GFP with regard to enterobactin secretion is also apparent from growth curves showing the growth in M9 medium and M9 plus iron. Δ*tolC* grows worse M9 than in M9 plus iron and reached a lower final OD600(Figure 10 B)).

1.5.3 Time-resolved fluorescence measurements

After the functionality of TolC-GFP was proven, the next goal was to monitor the production of TolC-GFP in time-resolved fluorescent measurements. This type of measurements is carried out continuously throughout the duration of the experiment (18h) and every 10 min an OD_{600} and a fluorescence measurement is taken. It is then possible to determine the Fluorescence divided by the Optical Density (F/OD) (corrected for with the WT), a unitless quantity that is proportional to the fluorescence of one cell. One could also regard this kind of data as "protein production" (as the fluorescence per cell is in direct relation with the number of GFP molecules in the cell and therefore the number of TolC molecules).

In Figure 11 the OD_{600} and the F/OD are plotted against time. In addition, the dOD/dt is plotted as well.

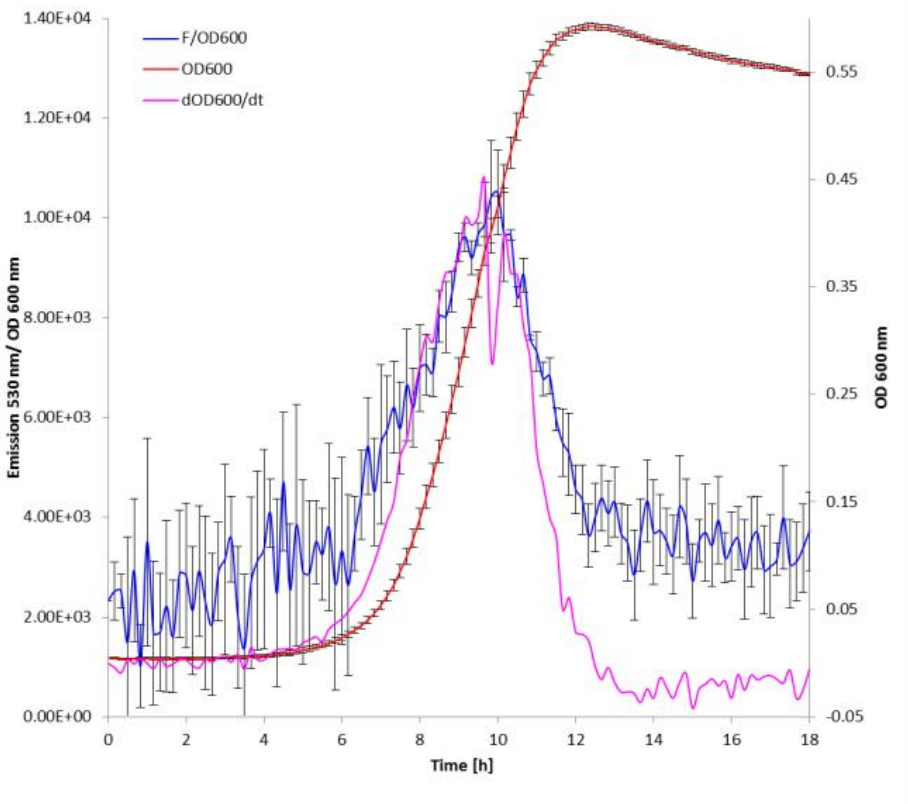

Figure 11: Correlation between F/OD$_{600}$ and dOD$_{600}$/dt when the cells are grown in minimal medium M9 plus iron

The first thing to be mentioned in Figure 11 is the fluorescence peak that is visible during growth in M9 $FeSO_4$. These are conditions where the cells have minimal but sufficient nutrients and salts and therefore grow normal. The peak in F/OD shows that TolC production is increased as the cells start doubling and is maximal when cells are dividing the fastest. TolC production then decreases as the cells divide slower, eventually dropping to the initial level when the cells stop dividing entirely. As this peak was reminiscent of the shape of the first derivative of a sigmoidal curve, the first derivative of the OD600curve was also calculated as dOD/dt. Indeed when plotted together, as in Figure 11, the similarity is apparent. Just to see how similar the two curves are, the Pearson correlation was calculated between the values of the F/OD and dOD/dt. The correlation was found to be **0.92228,** a high value indicating almost perfect coupling. This coupling of TolC production to the rate of growth indicates the very important role TolC has in cell division. An important role in cell division has been largely speculated on with regard to TolC, but what exactly that role is remains elusive.

Since TolC is important for enterobactin secretion under conditions of iron deprivation (Figure 2 and Figure 9), in parallel to cells grown in M9 plus iron, the cells were also grown in M9 alone. The growth curves and the respective F/OD are plotted in Figure 12 against time.

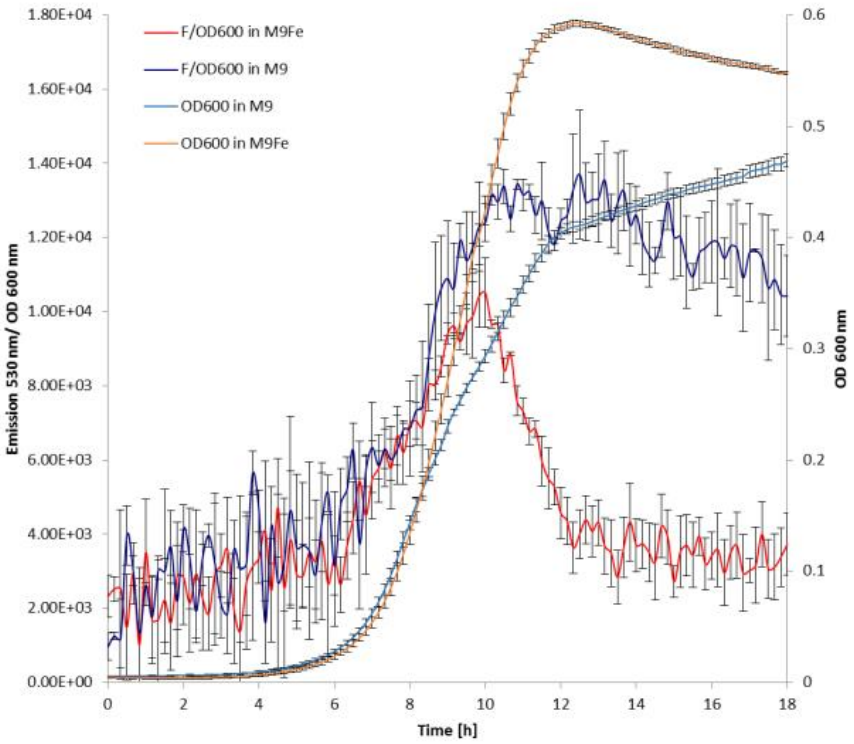

Figure 12: Time-resolved TolC production as followed by GFP F/OD. Lack of iron induces TolC production.

As it can be seen, although the growth in M9 is poorer than that in M9 plus iron, the TolC production (measured as F/OD) is increased, with a final value of around 2.5 times greater. This would make sense since TolC is needed for enterobactin secretion. Bleuel et al. (Bleuel et al., 2005) checked for mRNA levels of TolC with and without iron and found no difference between the conditions, concluding that although TolC is needed for enterobactin export, it is not upregulated by a lack of iron. However, they harvested the cells used for mRNA extraction during the logarithmic growth phase only, where, according to Figure 12 there is not much difference in F/OD between the two conditions.

As a confirmation for the findings from the time-resolved fluorescence measurement, cells were also investigated with microscopy. Cells grown in the same conditions, in the fluorimeter, in a 96-well plate, were taken out at the end of the growth (18h) and fixed for imaging. Three biological replicates were taken for certainty.

CSH50 *tolC-gfp* **M9 18h** **A)** | CSH50 WT **M9 $FeSO_4$ 18h** **B)**

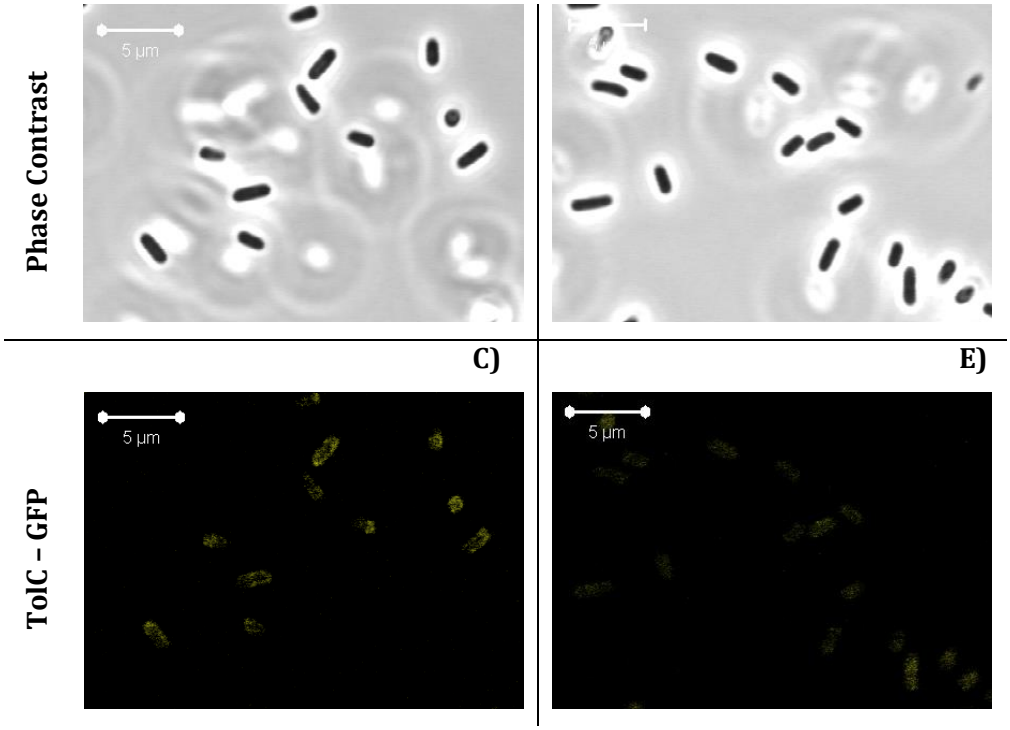

Figure 13: Microscopy of M9/M9Fe grown *tolC-gfp* cells. Lack of iron C) increases the production TolC as cells are more fluorescent than E).

As it can be seen the cells grown in absence of iron are indeed more fluorescence than those grown with (Figure 13). For the other 2 biological replicates see Supplemental Figure 2. The difference in fluorescence is visible, but the flurescence levels are low – this is due to the fact the fluorescent label is coupled to a gene, chromosomally. It is therefore in single-copy and under a native promoter, leading to physiological levels of expression, rather low for excellent confocal imaging. While scanning the microscopy slide for cells and focus plane, care had to be taken not to bleach the fluorophore.

1.5.4 Western Blot

In order to further validate the fluorescence and microscopy results, western blot was carried out with cells grown in the same conditions and coming from the same plate. The experiment was done in biological triplicates. After the cells were disrupted and the protein extracts quantified, 5 µg protein of each sample was loaded on a gel and blotted. TolC-GFP was detected with an anti-GFP antibody. As can be seen in Figure 14 A) the fusion protein runs around the 80 kDa marker band (marked with X on the blot). TolC is reported to have a molecular weight of 51.5 kDa (Koronakis et al., 1997) and GFP 27, together 78.5 kDa. In order not to saturate the signal and to make the differences in protein amount between the 2 growth conditions visible, a very diluted (1:1000000) primary anti-GFP antibody had to be used. Hence the faint bands in Figure 14.

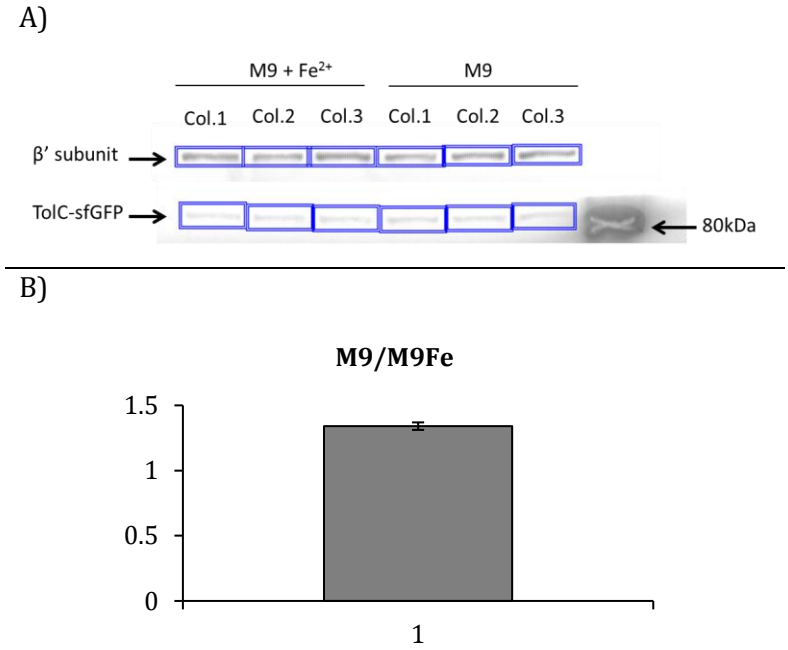

Figure 14: Western Blot of TolC-GFP and beta prime. A) raw data B) analyzed data

To correct for loading errors, a different protein β' (beta prime RNAP subunit) with stable expression was taken as a normalizer. The blots are shown in Figure 14 A), the fusion protein TolC-GFP can be seen around the expected size. The bands were quantified and for each sample the ratio of signal from TolC-GFP to that of β' in that sample was calculated. This ratio represents the amount of TolC-GFP in that sample. In Figure 14 B) a ratio of the value obtained for cells grown in M9 to those grown in M9Fe is shown. Also by Western Blot the cells grown in M9 are shown to have more (1.34 times) more TolC-GFP than those grown in presence of iron.

1.5.5 Real Time RT PCR

Finally, after all previous experiments showed that there is a difference in TolC-GFP levels based on whether the cells are grown in presence of iron or not, quantitative real time RT PCR was carried out to elucidate if the *tolC* transcript levels are corresponding to those of the protein/fluorescence. In addition Bleuel et al. (Bleuel et al., 2005) found no difference in transcript levels, but they only examined cells in the logarithmic growth phase. They concluded that TolC production is not affected by presence/absence of iron.

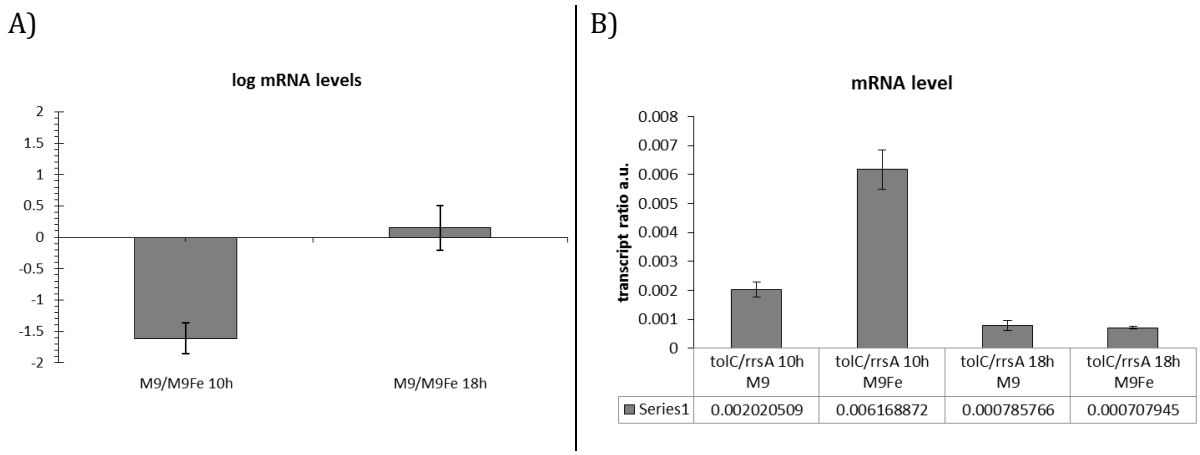

Figure 15: Q-RT PCR of *tolC* mRNA in M9/M9Fe (normalized to *rrsA* mRNA). A) log2 plots of the M9/M9Fe ratios and B) normalized transcript levels in M9 and M9Fe.

The cells were grown identically to the previous experiments, in plates, in the fluorimeter. But in addition to taking the cells only at the end of the 18h, for this experiment samples were also taken after approximatively 10h of growth, corresponding to the beginning of the drop of the physiological TolC peak (Figure 12). This was done to offer a clearer picture as to how these mRNA levels fluctuate. Three biological replicates were considered, and the RT PCR reaction was also performed in technical duplicates for each sample. The PCR quantitated the *tolC-gfp* mRNA by amplifying 100bp from the beginning of the gene (*tolC*). *rrsA* was quantitated in addition to serve as an internal normalizer (the amplification plots for the *tolC-gfp* transcript can be found in Supplemental Figure 3, each curve represents the average of 2 technical replicates). *rrsA* is the gene coding for the 16S RNA ribosomal subunit, and is considered suitable normalizer of gene expression (Bleuel et al., 2005). For each sample then the ratio of *tolC-gfp* transcript to that of *rrsA* transcript is calculated. In Figure 15 A) the results are reported as ratios between M9 and M9Fe. The results are plotted on a log2 scale, such that 0 means no difference, and -1 twice as little, -2 four times as little.

As it can be seen in Figure 15 A), the mRNA levels of *tolC-gfp* are exactly the same at the end of 18h in both M9 and M9 plus iron. Even more interestingly, after 10h of growth, there seems to be more *tolC-gfp* transcript in the cells grown in M9 plus $FeSO_4$ (about 3 times more), although the fluorescence in those cells is declining at that moment (Figure 12), and the fluorescence in the M9-grown sample is higher. Figure 15 B) shows the absolute levels of *tolC-gfp*/*rrsA* transcript ratios in the four samples, for comparison. This finding hints to the fact that the *tolC* mRNA is utilized differently in the 2 conditions.

The construct generated in this work shows therefore its usefulness as via fluorescence one can derive information about the protein level directly.

What is in accordance between the time-resolved fluorescence data and the RT PCR data is that for both conditions the *tolC-gfp* mRNA levels drop from the 10th hour to the 18th hour, as drops the fluorescence. The fluorescence only drops a little in the case of M9, but still drops. The drop in mRNA is to the same level between the 2 conditions, but the fluorescence levels are largely different at the end of the growth (=protein amounts).

To reiterate, Bleuel et al. (Bleuel et al., 2005) found that mRNA of *tolC* does not differ between cells grown in M9 or M9 plus iron, but they only considered logarithmic cells. However, via time-resolved fluorescence, microscopy and western blot, the present study showed that there is indeed a difference which becomes very noticeable in the later growth phases, there being more TolC-GFP in absence of iron.

1.5.6 Antibiotic response

Having proved the functionality of TolC-GFP and the usefulness of time-resolved fluorescence measurements, the question asked next is whether TolC levels change as a function of antibiotic exposure and weather the described system can catch that change. Time-resolved fluorescence measurements were therefore carried out in presence of various antibiotics. The antibiotics for these experiments were picked based on the results shown in Table 3. Antibiotics for which TolC plays no role (same MIC in the case of WT and *tolC--gfp* as in the case of Δ*tolC*) and antibiotics for the extrusion of which TolC is essential (lower MIC for Δ*tolC* than for WT and *tolC-gfp*) were considered.

Based on the response the strain had to the chosen antibiotics, the antibiotics can be divided in the 3 classes (error bars were omitted hence-forth to simplify the figures and allow for comparisons):

1. **NO MIC difference** between CSH50 WT and Δ*tolC* ***and*** no TolC response.

This is the case for tetracycline and kanamycin. Three concentrations of each were tried out. As it can be seen for both antibiotics and both growth conditions, with and without iron, the fluorescence peak/curve looks identical between no antibiotic treatment and the treatments. The only difference being a shift in time corresponding to the delay in growth induced by the noxious

activity of the sub-lethal antibiotic concentrations. Most clear, this effect is seen when cells grown in M9Fe are treated with tetracycline (Figure 16 A))

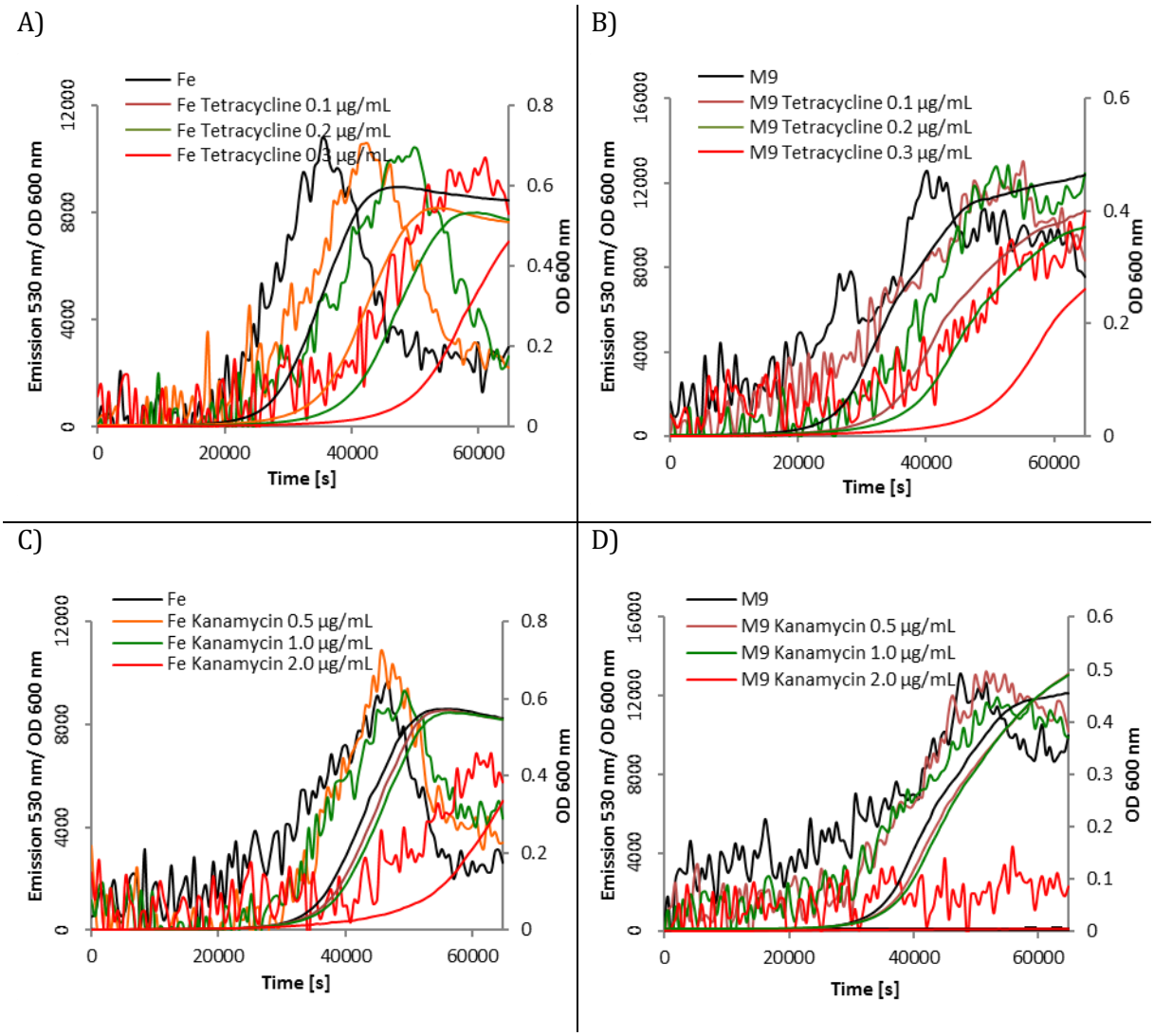

Figure 16: Time-resolved TolC production as followed by GFP F/OD in presence of antibiotics. A) and B) in presence of Tetracycline. C) and D) in presence of Kanamycin. A) and C) cells were grown in M9Fe. B) and D) cells were grown in M9.

2. **MIC difference** between CSH50 WT and Δ*tolC* ***and*** no TolC response.

This is the case for chloramphenicol, trimethoprim and linezolid. Although there is a generous difference in their MICs between the deletion mutant and the WT and *tolC-gfp*: 3-4 to 0.75 µg/mL in the case of chloramphenicol, 2 to 0.38 µg/mL in the case of trimethoprim and >256 to 3/4 µg/mL (Figure 6, A) and C)), there is no effect on the TolC production as evidenced by the time-resolved fluorescence experiments. The only effect is, like for tetracycline and kanamycin, a delay of the fluorescence pattern/peak that corresponds to the delay brought about by the activity of the antibiotic.

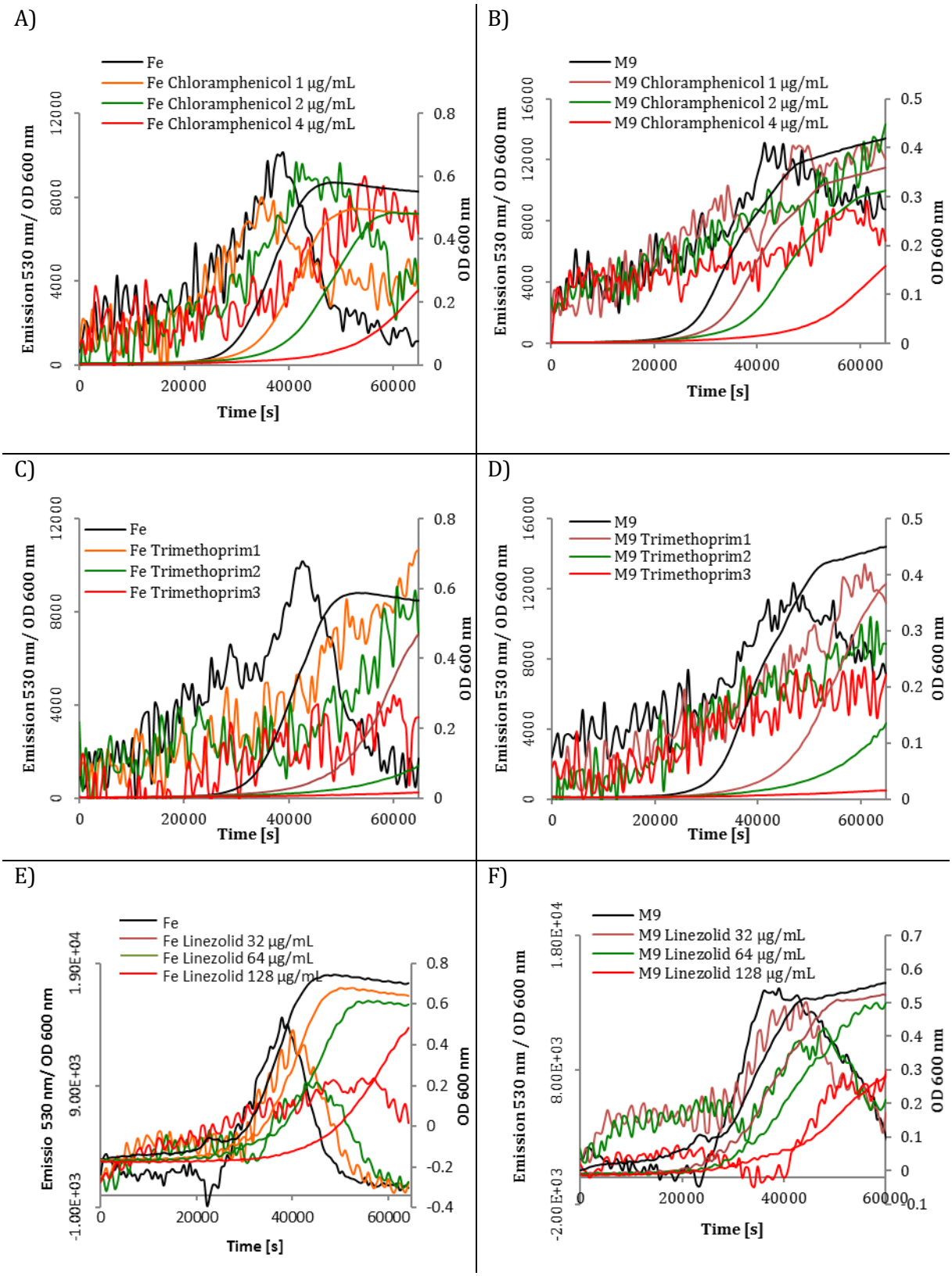

Figure 17: Time-resolved TolC production as followed by GFP F/OD in presence of antibiotics. A) and B) in presence of Chloramphenicol. C) and D) in presence of Trimethoprim. E) and F) in presence of Linezolid. A), C) and E) cells were grown in M9Fe. B), D) and F) cells were grown in M9.

3. **MIC difference** between CSH50 WT and Δ*tolC* ***and*** a concentration-dependent TolC response.

This is the case for Erythromycin, Clarythromycin and Novobiocin. The effect of these antibiotics on TolC-GFP response is not only a delay of the fluorescence pattern in time, coupled to a delayed growth as a consequence of the antibiotic treatment. But also a concentration-dependent increase in the fluorescence peak (in the case of cells grown in M9Fe) and final level of fluorescence (in the case of cells grown in M9). In M9, during the 18 hours of the growth, the bacteria do not reach stationary phase, therefore the F/OD is still high/peaking, but the beginning of a decrease is observable. Should the cells in M9 be allowed to grow for longer, the drop in fluorescence would most probably continue.

These concentrations-dependent increases in fluorescence/TolC production are remarkable and show an unprecedented result. The respective antibiotics are "sensed" by the *E. coli* which increases the production of TolC, involved in their excretion. The increase in the fluorescence peak for cells grown in M9Fe is about 2.5 fold for all 3 antibiotics, and under conditions of iron limitations the increase is about 3/3.5 fold, these extra TolC aiding the bacterium.

A)

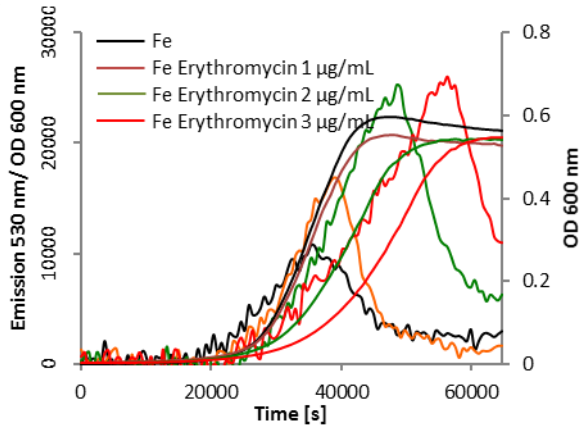

B)

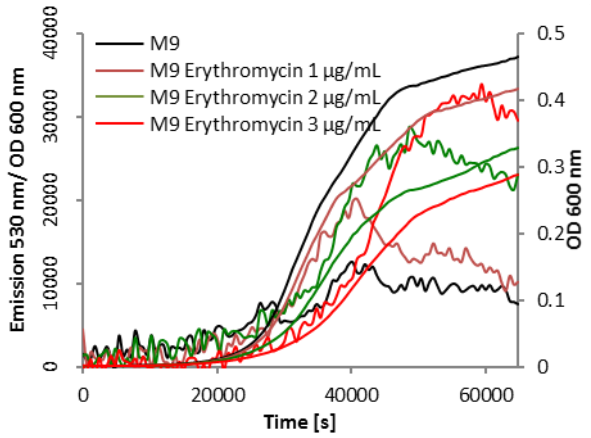

C)

D)

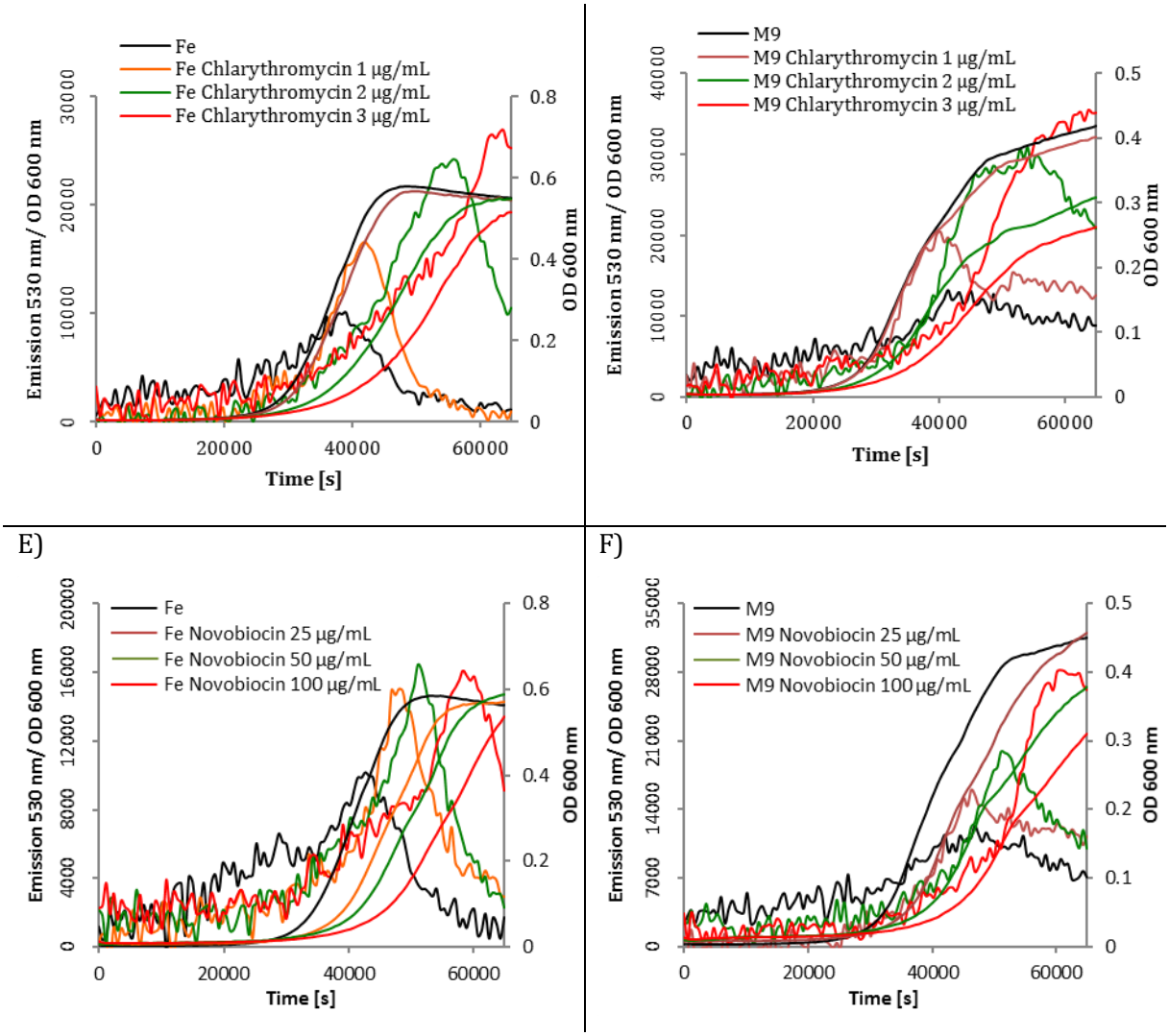

Figure 18: Time-resolved TolC production as followed by GFP F/OD in presence of antibiotics. A) and B) in presence of Erythromycin. C) and D) in presence of Clarithromycin. E) and F) in presence of Novobiocin. A), C) and E) cells were grown in M9Fe. B), D) and F) cells were grown in M9.

1.5.7 Antibiotic response – Microscopy

As a verification of the main finding, namely that Erythromycin, Clarithromycin and Novobiocin induce a concentration-dependent increase in TolC levels as judged by GFP fluorescence/OD, cells were grown in M9, M9 plus iron respectively, with the highest antibiotic concentrations that elicited the response but still allowed the cells to grow. The results were reproducible, and all 3 antibiotics led to a quantitative increase in fluorescence (Figure 19)

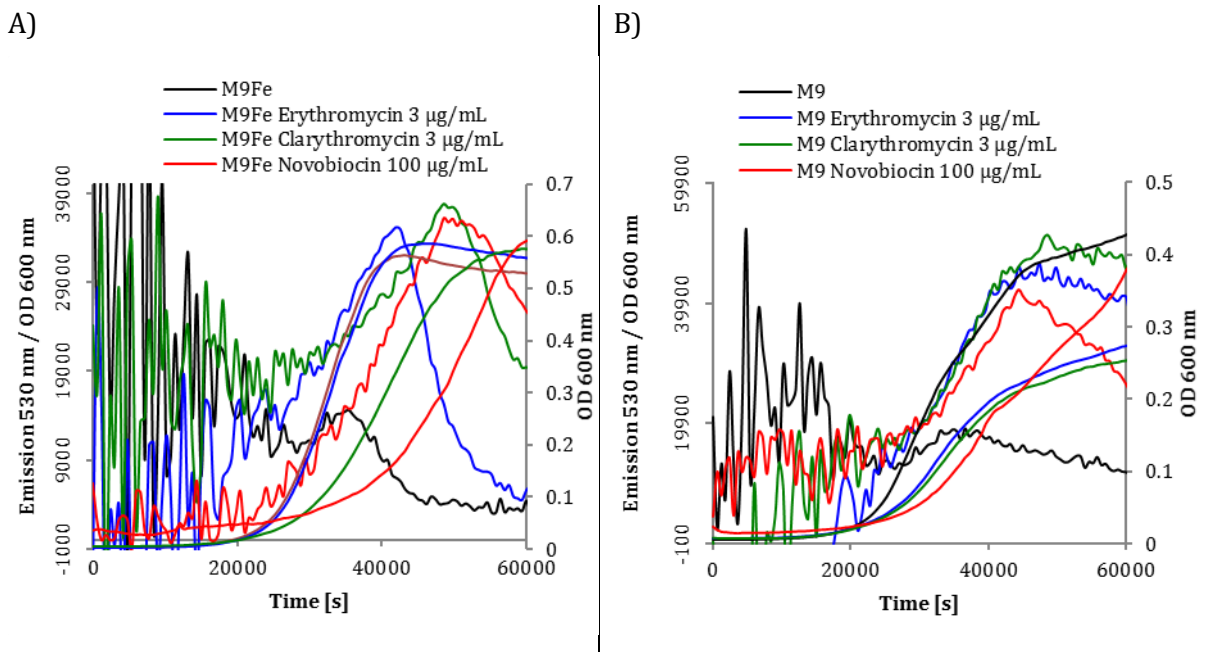

Figure 19: Bacteria grown in M9/M9Fe with Erhythromycin (3 µg/mL), Clarithromycin (3 µg/mL) and Novobiocin (100 µg/mL). A) shows growth in M9Fe and B) in M9.

In the above graphs, the F/OD values in the beginning of the growth fluctuate largely, presumably because of very low inoculation optical densities that leads to an inaccurate and inconsistent fluorescence read. When cells accumulate, their fluorescent signal is more robust and can be read consistently. However, such a noisy F/OD trace was not the case most times experiments of this sort were performed.

To be noted is that the F/OD scale is not the same for cells grown M9Fe (39000 a.u.) and M9 (59900 a.u.). The absence of iron is again leading to higher TolC levels. The cells were harvested directly after the 18h-growth period from the plate, and fixed microscopy. The induction of the antibiotics was checked, as well as the influence on iron. A general remark to reiterate (as for Figure 13) is that low levels of physiological expression make the GFP fusion protein hard to image accurately due to the higher laser intensity that is used, which leads to rapid bleaching. This becomes less of a problem when the cells are expressing TolC-GFP at higher levels, and the signal is more robust. The highest level of F/OD after the 18h as judged by Figure 19, is achieved under Clarithromycin treatment with around 50000 a.u. in M9 and 20000 a.u. in M9Fe. Imaged cells from this condition are shown below in Figure 20. Two of the three colonies used in the experiment were imaged. For each colony and condition 2 view fields were taken for checking the consistency of the signal throughout the microscopy slide. Imaged cells from all other treatments, and both colonies are found in the Appendix (Supplemental Figure 5 to Supplemental Figure 11)

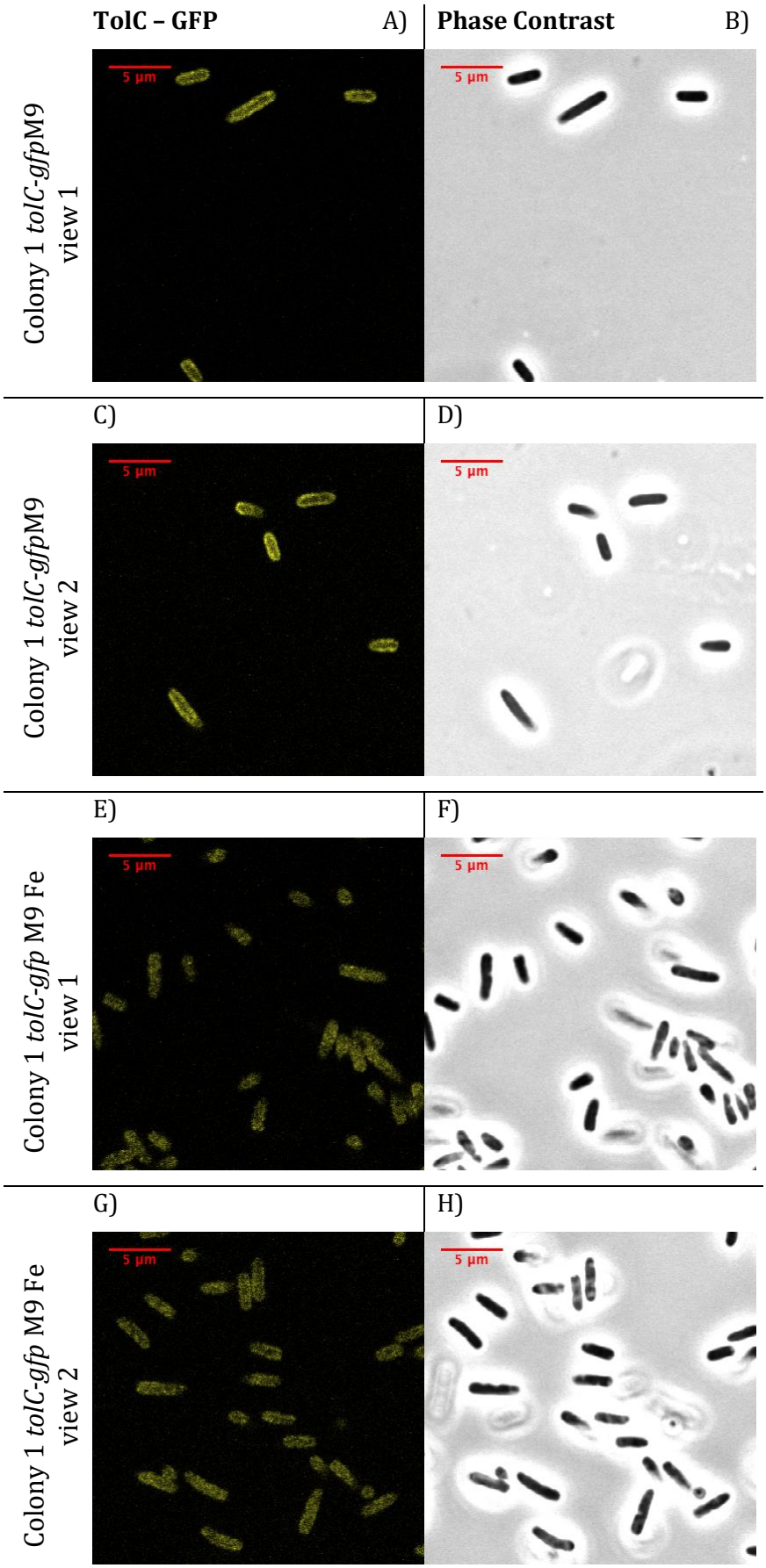

Figure 20: Cells from Colony 1 grown in the presence of Clarythromycin (3 µg/mL). A), B), C) and D) in M9. E), F), G) and H) in M9Fe.

It is clear the that the fluorescence is increased as compared to the no treatment control (Supplemental Figure 5), and that the lack of iron brings TolC levels even higher (Figure 20 A), C) compared to E), G)). As noticed from F/OD graphs, the fluorescence starts to decrease and is not the highest at the end of the growth. Microscopy images of all other antibiotic treatments largely match the F/OD levels in both imaged colonies: Erythromycin and Clarithromycin elicit a strong response and Novobiocin a lower one (Supplemental Figure 5 to Supplemental Figure 11) – at the end of the 18h that is. Optimally, microscopy should be done with cells harvested in the middle of their logarithmic growth, when they are dividing the fastest. For that, the different treatments/conditions should be done separately as the growth curves are offset one from another. Microscopy is a good way of checking for changes in fluorescence, but due to reasons mentioned above is not ideal. In this sense, the time-resolved fluorescence measurements are more accurate as they are ensemble measurements. In this case, the summed fluorescence of 10^6-10^8 cells is measured collectively and the differences between conditions, and variations in time are much more quantitative, reproducible and robust.

1.6 Conclusion

Using superfolder GFP, a GFP derivative recently shown to fold and fluoresce when exported to the bacterial periplasm (Aronson et al., 2011; Pédelacq et al., 2006), a TolC construct was genomically engineered. The construct is a translational fusion of *tolC* and *sfgfp*, inserted in the *tolC* native locus, thus being under all the regulatory elements the wild type protein would be. This TolC-GFP fusion protein was shown to be functional with regard to a number of functions that TolC normally carries. It was shown to be as effective as the wild type protein in participating in the efflux of a variety of antibiotics (Table 3). Colicin E1 is a toxin that utilizes TolC to enter the cell and form channels in its inner membrane, leading to the cell's death. Cells expressing *tolc-gfp* were as susceptible to Colicin E1 as WT cells (Figure 7). Last but not least, TolC was shown to be the exit path for the siderophore enterobactin (Bleuel et al., 2005; Vega and Young, 2014), and the *tolC-gfp* strain was fully capable of doing that judging by the cells morphology (Figure 9) or growth curves in absence and presence of iron (Figure 10).

Taken together these results show that the fluorescent TolC-GFP is functional under all aspects tested. Since there is a scarcity of *in vivo* outer membrane protein studies in the literature, and since TolC is such an important outer membrane protein itself, this strain will offer unique insights into TolC physiology.

In the present work, by studying the time-resolved fluorescence per OD_{600} during the bacterial growth cycle, several new insights surfaced:

Firstly, when cells are growing under minimal but sufficient conditions (M9 plus $FeSO_4$) TolC production (as seen by GFP fluorescence) is strongly coupled to the growth of the cells. The faster the cells grow, the more TolC they produce, and conversely when they slow down, TolC production decreases as well (Figure 12). This coupling was evidenced by a correlation factor of ~0.92 between the F/OD_{600} signal and the derivative of the growth curve. This fact indicates that TolC is important for cell division and/or growth-coupled bacterial physiology.

With regard to cell division, Hiraga et al. (Hiraga et al., 1989) found that the *tolC* deletion leads to the production of anucleated cells. Furthermore, ther AcrEF-TolC was found to play a crucial role in cell division, mutations leading to severe defects (Lau and Zgurskaya, 2005).

Physiologically, TolC seems to play an important role as well: cAMP binds to the CRP protein (cAMP receptor protein) which in turn starts activating catabolic genes and repressing anabolism. cAMP must therefore be extruded efficiently during fast growth, and TolC is responsible for that (Hantke et al., 2011). In addition TolC has been found to be required in porphyrins efflux (Tatsumi and Wachi, 2008). Porphyrins are very useful molecules required in the electron transfer chain and absolutely required when cells are growing fast, but when found in too high concentrations they can cause oxidative stress with mutagenic effects (Tatsumi and Wachi, 2008). The amino acid Cystein, required for growth, is as well toxic when in high amounts because of the high reactivity of its thiol group (Ohtsu et al., 2010), and not surprisingly is being effluxed by TolC (Wiriyathanawudhiwong et al., 2009).

Secondly, there is big difference in TolC production under conditions of iron limitations. TolC levels, as seen by fluorescence over OD_{600}, are maintained high until the end of the 18h, and do not decrease as much as in case of cells grown in the presence of iron. This finding was verified by microscopy (Figure 13) and western blots (Figure 14). However, the mRNA levels of *tolC-gfp* are the same as seen by quantitative real time RT PCR (Figure 15). So, although the mRNA levels are the same, the protein levels differ. This fact points to a different utilization of the mRNA as a function of iron presence/absence. A non-linear relationship between mRNA levels and protein levels is also seen by looking at the mRNA after only 10h growth (Figure 15) when there is more mRNA in the M9Fe sample, but the fluorescence is reversed. Since the *tolC* gene has 4 known regulators as seen Figure 21 it is natural that its transcription is regulated in a complex manner.

The ferric uptake regulator is a general repressor of gene expression. It represses many genes, especially those involved in enterobactin production and secretion. When it is bound to iron it

exerts it repressor function by binding to the DNA in the promoter region of the target gene, and when iron levels drop, it dissociates from iron, undergoes a conformational change and derepresses the target gene (Porcheron and Dozois, 2015). One of the primary targets of Fur repression is a noncoding RNA called RyhB. RyhB in turn regulates many other genes. One of the genes that RyhB is repressing is *marA*, one of the 4 *tolC* activators (Urban and Vogel, 2007; Wright et al., 2013). This could explain why after 10h of growth there is more transcript in the M9Fe sample than in the M9 one. Because, if at stage in growth MarA is the main regulator of TolC, then *marA* will get repressed by RyhB (which in turn will have been derepressed by Fur due to iron limitations).

Parker and Gottesman (Parker and Gottesman, 2016) found that there is a small regulatory RNA called SdsR which represses *tolC* expression by binding in its 5' untranslated region. Interestingly SdsR is produced physiologically in stationary phase. This could explain why TolC levels go down in stationary phase in cells grown in the presence of iron. They also found that over-expression of *sdsR* is leading to increased susceptibility to Novobiocin. Therefore, SdsR is a good candidate for being responsible for some of the effects described in this study.

Thirdly, several antibiotics in the efflux of which TolC is required, as evidenced by much lower MIC values for the Δ*tolC* strain, are triggering a dose-dependent increase in the production of TolC-GFP. Erythromycin, clarithromycin and novobiocin are doing that (Figure 18). This result is remarkable because it means that the cell possesses a mechanism(s) that sense these antibiotics and consequently upregulate TolC production (and potentially other multidrug associated proteins) to help extrude the antibiotics. *tolC* has 4 known regulators, MarA, Rob, SoxS, and PhoP (Figure 21), none of which is known to respond to antibiotics in general, especially these 3. However, this finding is not valid for all antibiotics for which TolC plays a role. For example, chloramphenicol, trimethoprim and linezolid are not eliciting such a response (Figure 17) although the MIC of the Δ*tolC* is substantially diminished (Table 3). This gives even more validity to the finding that *some* antibiotics modulate TolC production, as it points to a certain specificity of the mechanism involved.

1.6.1 Outlook

In order to elucidate the mechanism through which erythromycin, clarithromycin and novobiocin increase TolC production 2 types of studies will be carried out. Firstly, all knows regulators of *tolC*, namely Rob, SoxS, MarA and PhoP (Figure 21) will be deleted one by one from the CSH50 *tolC-gfp* strain. The time-resolved fluorescence measurements will be repeated and the ability of the

respective antibiotics to still increase TolC production or not, will make it clear if the respective regulator was responsible for the response or not. Secondly, the promoter of *tolC* will be genomically truncated to lose consecutively promoters 1 to 4 and the regulator binding sites. This will complement the deletion of the regulators and should mirror the findings if the regulators are involved. Alternatively, since it could be that the mRNA is simply processed or modulated differently, the mRNA itself might responsible for the changed translation, either directly by interacting with enterobactin/antibiotics or via intermediaries. By truncating the promoter region, the 5' untranslated region will also be truncated, and if it played a role in the regulation it will be seen in the time-resolved fluorescence measurements. As *sdsR* was shown to be a regulator of *tolC* (Parker and Gottesman, 2016), it will also be deleted from the *tolC-gfp* strain to see its effect on TolC production in presence/absence of iron but most importantly, of antibiotics.

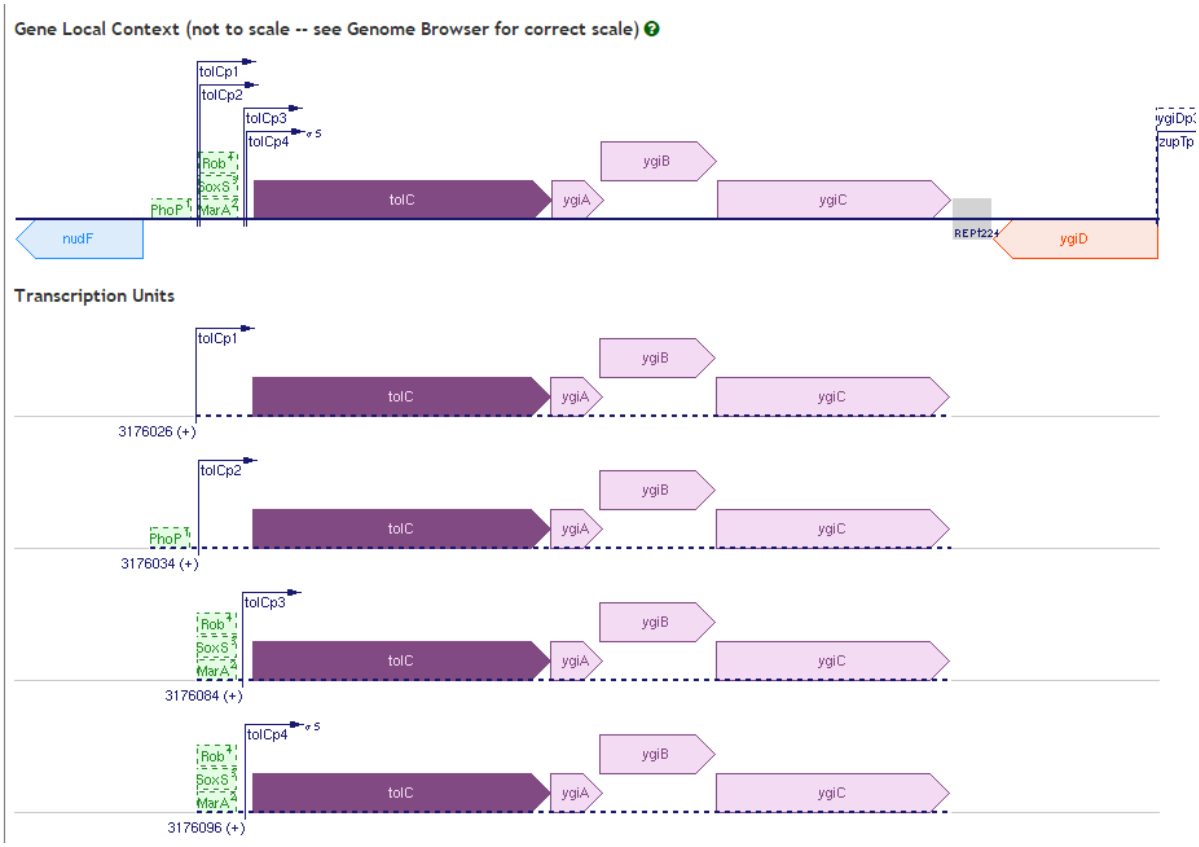

Figure 21: Genomic context showing the promoters and regulator binding sites of *tolC*. Retrieved from EcoCyc.org (Keseler et al., 2013). *tolC* gene is in purple, bent arrows pointing to the left are representing the promoters, and the green boxes are representing the positive regulators of gene expression Rob, MarA, SoxS, PhoP.

A second type of study that will be performed will be microscopy on antibiotics-treated *tolC-gfp* cells. The reason for that is that for efficient efflux out of the cell the respective pumps might adopt certain arrangements. Also, the effect of the antibiotic itself might lead to a change in TolC disposition. A preliminary such study could be seen in Supplemental Figure 4 where WT and *tolC-*

gfp have been grown to an OD_{600} of 0.5 in LB medium (contains iron) and then treated with the sub-lethal novobiocin concentration of 50 µg/mL. The cells are shown 3.5h and 18h after the addition of the antibiotic. Not only do the cells become more fluorescence over time, but a localization pattern with the fluorescence concentrating at either 1 or both cell poles become apparent. The nucleoid was stained with DRAQ5 for better orientation. These preliminary results are promising and raise the question whether other antibiotics will induce a differential localization and how that connects to the phenomenon of multidrug resistance.

1.7 References

Aono, R., N. Tsukagoshi, and M. Yamamoto. "Involvement of Outer Membrane Protein TolC, a Possible Member of the Mar-Sox Regulon, in Maintenance and Improvement of Organic Solvent Tolerance of Escherichia Coli K-12." Journal of Bacteriology 180, no. 4 (February 1998): 938–44.

Aronson, Deborah E., Lindsey M. Costantini, and Erik L. Snapp. "Superfolder GFP Is Fluorescent in Oxidizing Environments When Targeted via the Sec Translocon." Traffic (Copenhagen, Denmark) 12, no. 5 (May 2011): 543–48. doi:10.1111/j.1600-0854.2011.01168.x.

Bina, J. E., and J. J. Mekalanos. "Vibrio Cholerae tolC Is Required for Bile Resistance and Colonization." Infection and Immunity 69, no. 7 (July 2001): 4681–85. doi:10.1128/IAI.69.7.4681-4685.2001.

Bleuel, Corinna, Cornelia Grosse, Nadine Taudte, Judith Scherer, Dirk Wesenberg, Gerd J. Krauss, Dietrich H. Nies, and Gregor Grass. "TolC Is Involved in Enterobactin Efflux across the Outer Membrane of Escherichia Coli." Journal of Bacteriology 187, no. 19 (October 2005): 6701–7. doi:10.1128/JB.187.19.6701-6707.2005.

Datsenko, K. A., and B. L. Wanner. "One-Step Inactivation of Chromosomal Genes in Escherichia Coli K-12 Using PCR Products." Proceedings of the National Academy of Sciences of the United States of America 97, no. 12 (June 6, 2000): 6640–45. doi:10.1073/pnas.120163297.

Dinh, T., and T. G. Bernhardt. "Using Superfolder Green Fluorescent Protein for Periplasmic Protein Localization Studies." Journal of Bacteriology 193, no. 18 (September 15, 2011): 4984–87. doi:10.1128/JB.00315-11.

Du, Dijun, Zhao Wang, Nathan R. James, Jarrod E. Voss, Ewa Klimont, Thelma Ohene-Agyei, Henrietta Venter, Wah Chiu, and Ben F. Luisi. "Structure of the AcrAB–TolC Multidrug Efflux Pump." Nature 509, no. 7501 (April 20, 2014): 512–15. doi:10.1038/nature13205.

Eicher, Thomas, Lorenz Brandstätter, and Klaas M. Pos. "Structural and Functional Aspects of the Multidrug Efflux Pump AcrB." Biological Chemistry 390, no. 8 (January 1, 2009). doi:10.1515/BC.2009.090.

Feilmeier, B. J., G. Iseminger, D. Schroeder, H. Webber, and G. J. Phillips. "Green Fluorescent Protein Functions as a Reporter for Protein Localization in Escherichia Coli." Journal of Bacteriology 182, no. 14 (July 2000): 4068–76.

Gibbs, Karine A., Daniel D. Isaac, Jun Xu, Roger W. Hendrix, Thomas J. Silhavy, and Julie A. Theriot. "Complex Spatial Distribution and Dynamics of an Abundant Escherichia Coli Outer Membrane Protein, LamB." Molecular Microbiology 53, no. 6 (September 2004): 1771–83. doi:10.1111/j.1365-2958.2004.04242.x.

Graham, L. L., R. Harris, W. Villiger, and T. J. Beveridge. "Freeze-Substitution of Gram-Negative Eubacteria: General Cell Morphology and Envelope Profiles." Journal of Bacteriology 173, no. 5 (March 1991): 1623–33.

Hantke, K., K. Winkler, and J. E. Schultz. "Escherichia Coli Exports Cyclic AMP via TolC." Journal of Bacteriology 193, no. 5 (March 1, 2011): 1086–89. doi:10.1128/JB.01399-10.

Hiraga, S., H. Niki, T. Ogura, C. Ichinose, H. Mori, B. Ezaki, and A. Jaffé. "Chromosome Partitioning in Escherichia Coli: Novel Mutants Producing Anucleate Cells." Journal of Bacteriology 171, no. 3 (March 1989): 1496–1505.

Horiyama, Tsukasa, and Kunihiko Nishino. "AcrB, AcrD, and MdtABC Multidrug Efflux Systems Are Involved in Enterobactin Export in Escherichia Coli." PloS One 9, no. 9 (2014): e108642. doi:10.1371/journal.pone.0108642.

Jaffé, A., and R. D'ari. "Growth of the Escherichia Coli Cell Envelope." Biochimie 67, no. 1 (January 1985): 141–44.

Johnson, J. M., and G. M. Church. “Alignment and Structure Prediction of Divergent Protein Families: Periplasmic and Outer Membrane Proteins of Bacterial Efflux Pumps.” Journal of Molecular Biology 287, no. 3 (April 2, 1999): 695–715. doi:10.1006/jmbi.1999.2630.

Keseler, Ingrid M., Amanda Mackie, Martin Peralta-Gil, Alberto Santos-Zavaleta, Socorro Gama-Castro, César Bonavides-Martínez, Carol Fulcher, et al. “EcoCyc: Fusing Model Organism Databases with Systems Biology.” Nucleic Acids Research 41, no. Database issue (January 2013): D605-612. doi:10.1093/nar/gks1027.

Koronakis, V., J. Li, E. Koronakis, and K. Stauffer. “Structure of TolC, the Outer Membrane Component of the Bacterial Type I Efflux System, Derived from Two-Dimensional Crystals.” Molecular Microbiology 23, no. 3 (February 1997): 617–26.

Koronakis, Vassilis, Jeyanthy Eswaran, and Colin Hughes. “Structure and Function of TolC: The Bacterial Exit Duct for Proteins and Drugs.” Annual Review of Biochemistry 73 (2004): 467–89. doi:10.1146/annurev.biochem.73.011303.074104.

Lau, Sze Yi, and Helen I. Zgurskaya. “Cell Division Defects in Escherichia Coli Deficient in the Multidrug Efflux Transporter AcrEF-TolC.” Journal of Bacteriology 187, no. 22 (November 2005): 7815–25. doi:10.1128/JB.187.22.7815-7825.2005.

Masi, Muriel, Guillaume Duret, Anne H. Delcour, and Rajeev Misra. “Folding and Trimerization of Signal Sequence-Less Mature TolC in the Cytoplasm of Escherichia Coli.” Microbiology (Reading, England) 155, no. Pt 6 (June 2009): 1847–57. doi:10.1099/mic.0.027219-0.

Masi, Muriel, Phu Vuong, Matthew Humbard, Karen Malone, and Rajeev Misra. “Initial Steps of Colicin E1 Import across the Outer Membrane of Escherichia Coli.” Journal of Bacteriology 189, no. 7 (April 2007): 2667–76. doi:10.1128/JB.01448-06.

Nikaido, H. “Multidrug Efflux Pumps of Gram-Negative Bacteria.” Journal of Bacteriology 178, no. 20 (October 1996): 5853–59.

Ohtsu, Iwao, Natthawut Wiriyathanawudhiwong, Susumu Morigasaki, Takeshi Nakatani, Hiroshi Kadokura, and Hiroshi Takagi. “The L-cysteine/L-Cystine Shuttle System Provides Reducing Equivalents to the Periplasm in Escherichia Coli.” The Journal of Biological Chemistry 285, no. 23 (June 4, 2010): 17479–87. doi:10.1074/jbc.M109.081356.

Palade, G. E. “A Study of Fixation for Electron Microscopy.” The Journal of Experimental Medicine 95, no. 3 (March 1952): 285–98.

Parker, Ashley, and Susan Gottesman. “Small RNA Regulation of TolC, the Outer Membrane Component of Bacterial Multidrug Transporters.” Journal of Bacteriology 198, no. 7 (January 25, 2016): 1101–13. doi:10.1128/JB.00971-15.

Paulsen, I. T., J. H. Park, P. S. Choi, and M. H. Saier. “A Family of Gram-Negative Bacterial Outer Membrane Factors That Function in the Export of Proteins, Carbohydrates, Drugs and Heavy Metals from Gram-Negative Bacteria.” FEMS Microbiology Letters 156, no. 1 (November 1, 1997): 1–8.

Pédelacq, Jean-Denis, Stéphanie Cabantous, Timothy Tran, Thomas C. Terwilliger, and Geoffrey S. Waldo. “Engineering and Characterization of a Superfolder Green Fluorescent Protein.” Nature Biotechnology 24, no. 1 (January 2006): 79–88. doi:10.1038/nbt1172.

Porcheron, Gaëlle, and Charles M. Dozois. “Interplay between Iron Homeostasis and Virulence: Fur and RyhB as Major Regulators of Bacterial Pathogenicity.” Veterinary Microbiology 179, no. 1–2 (August 31, 2015): 2–14. doi:10.1016/j.vetmic.2015.03.024.

“PubMed Entry.” Accessed May 7, 2017. http://www.ncbi.nlm.nih.gov/pubmed/23143106.

Ramakers, Christian, Jan M. Ruijter, Ronald H. Lekanne Deprez, and Antoon F. M. Moorman. “Assumption-Free Analysis of Quantitative Real-Time Polymerase Chain Reaction (PCR) Data.” Neuroscience Letters 339, no. 1 (March 13, 2003): 62–66.

Raymond, Kenneth N., Emily A. Dertz, and Sanggoo S. Kim. “Enterobactin: An Archetype for Microbial Iron Transport.” Proceedings of the National Academy of Sciences of the United States of America 100, no. 7 (April 1, 2003): 3584–88. doi:10.1073/pnas.0630018100.

Saier, M. H., I. T. Paulsen, M. K. Sliwinski, S. S. Pao, R. A. Skurray, and H. Nikaido. “Evolutionary Origins of Multidrug and Drug-Specific Efflux Pumps in Bacteria.” FASEB Journal: Official Publication of the Federation of American Societies for Experimental Biology 12, no. 3 (March 1998): 265–74.

Sambrook, J., E. Fritsch, and T. Maniatis. Molecular Cloning: A Laboratory Manual: Vol. 2. 2. ed. S.l.: Cold Spring Harbor, 1989.

Sharff, A., C. Fanutti, J. Shi, C. Calladine, and B. Luisi. "The Role of the TolC Family in Protein Transport and Multidrug Efflux. From Stereochemical Certainty to Mechanistic Hypothesis." European Journal of Biochemistry 268, no. 19 (October 2001): 5011–26.

Skals, M., N. R. Jorgensen, J. Leipziger, and H. A. Praetorius. "-Hemolysin from Escherichia Coli Uses Endogenous Amplification through P2X Receptor Activation to Induce Hemolysis." Proceedings of the National Academy of Sciences 106, no. 10 (March 10, 2009): 4030–35. doi:10.1073/pnas.0807044106.

Sobko, Alexander A., Elena A. Kotova, Yuri N. Antonenko, Stanislav D. Zakharov, and William A. Cramer. "Lipid Dependence of the Channel Properties of a Colicin E1-Lipid Toroidal Pore." The Journal of Biological Chemistry 281, no. 20 (May 19, 2006): 14408–16. doi:10.1074/jbc.M513634200.

Tatsumi, Ryoko, and Masaaki Wachi. "TolC-Dependent Exclusion of Porphyrins in Escherichia Coli." Journal of Bacteriology 190, no. 18 (September 2008): 6228–33. doi:10.1128/JB.00595-08.
Thomas, Sabrina, I. Barry Holland, and Lutz Schmitt. "The Type 1 Secretion Pathway - the Hemolysin System and beyond." Biochimica Et Biophysica Acta 1843, no. 8 (August 2014): 1629–41. doi:10.1016/j.bbamcr.2013.09.017.

Urban, Johannes H., and Jörg Vogel. "Translational Control and Target Recognition by Escherichia Coli Small RNAs in Vivo." Nucleic Acids Research 35, no. 3 (2007): 1018–37. doi:10.1093/nar/gkl1040.

Vega, Daniel E., and Kevin D. Young. "Accumulation of Periplasmic Enterobactin Impairs the Growth and Morphology of Escherichia Coli tolC Mutants." Molecular Microbiology 91, no. 3 (February 2014): 508–21. doi:10.1111/mmi.12473.

Voorhout, W. F., J. J. Leunissen-Bijvelt, J. L. Leunissen, and A. J. Verkleij. "Steric Hindrance in Immunolabelling." Journal of Microscopy 141, no. Pt 3 (March 1986): 303–10.

Vos-Scheperkeuter, G. H., E. Pas, G. J. Brakenhoff, N. Nanninga, and B. Witholt. "Topography of the Insertion of LamB Protein into the Outer Membrane of Escherichia Coli Wild-Type and Lac-lamB Cells." Journal of Bacteriology 159, no. 2 (August 1984): 440–47.

Wiriyathanawudhiwong, Natthawut, Iwao Ohtsu, Zhao-Di Li, Hirotada Mori, and Hiroshi Takagi. "The Outer Membrane TolC Is Involved in Cysteine Tolerance and Overproduction in Escherichia Coli." Applied Microbiology and Biotechnology 81, no. 5 (January 2009): 903–13. doi:10.1007/s00253-008-1686-9.

Wright, Patrick R., Andreas S. Richter, Kai Papenfort, Martin Mann, Jörg Vogel, Wolfgang R. Hess, Rolf Backofen, and Jens Georg. "Comparative Genomics Boosts Target Prediction for Bacterial Small RNAs." Proceedings of the National Academy of Sciences of the United States of America 110, no. 37 (September 10, 2013): E3487-3496. doi:10.1073/pnas.1303248110.

Yamashita, Daichi, Takaki Sugawara, Miyu Takeshita, Jun Kaneko, Yoshiyuki Kamio, Isao Tanaka, Yoshikazu Tanaka, and Min Yao. "Molecular Basis of Transmembrane Beta-Barrel Formation of Staphylococcal Pore-Forming Toxins." Nature Communications 5 (September 29, 2014): 4897. doi:10.1038/ncomms5897.

Zgurskaya, Helen I., Ganesh Krishnamoorthy, Abigail Ntreh, and Shuo Lu. "Mechanism and Function of the Outer Membrane Channel TolC in Multidrug Resistance and Physiology of Enterobacteria." Frontiers in Microbiology 2 (2011): 189. doi:10.3389/fmicb.2011.00189.

1.8 Appendix

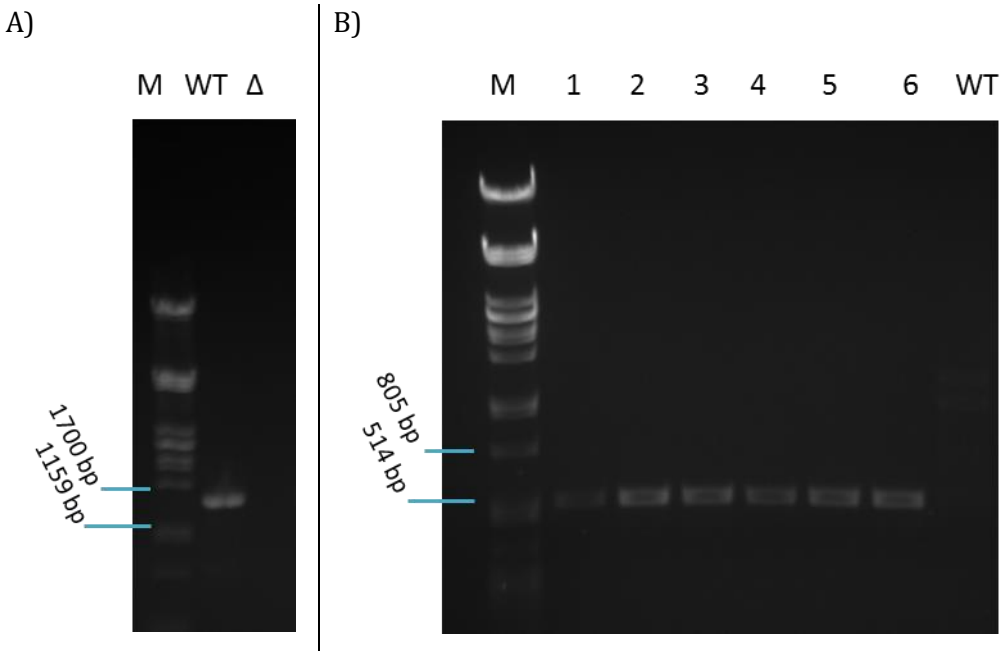

Supplemental Figure 1: PCR check of the generated strains, with genomic DNA as template. Λ Phage DNA digested with PstI was used as the marker (M). A) *tolC* amplification in WT and Δ*tolC*: product size 1482 bp. B)amplification of the *tolC-sfgfp* junction in 5 colonies (1 to 5) and WT: product size 534 bp.

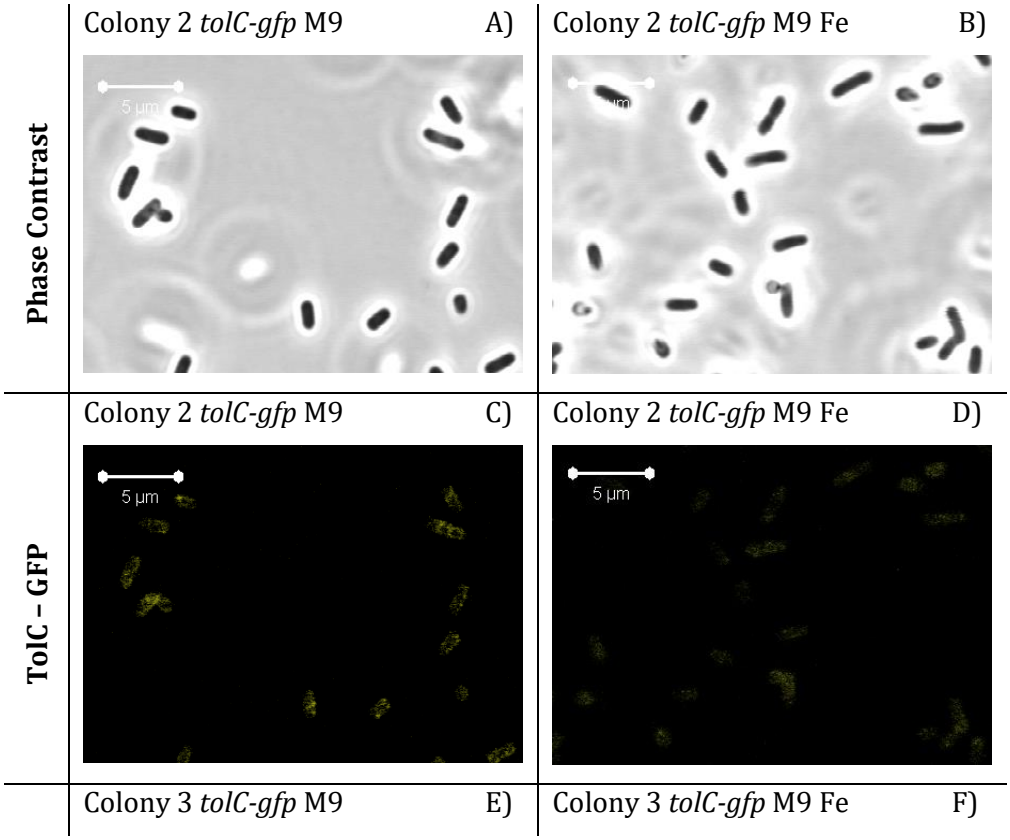

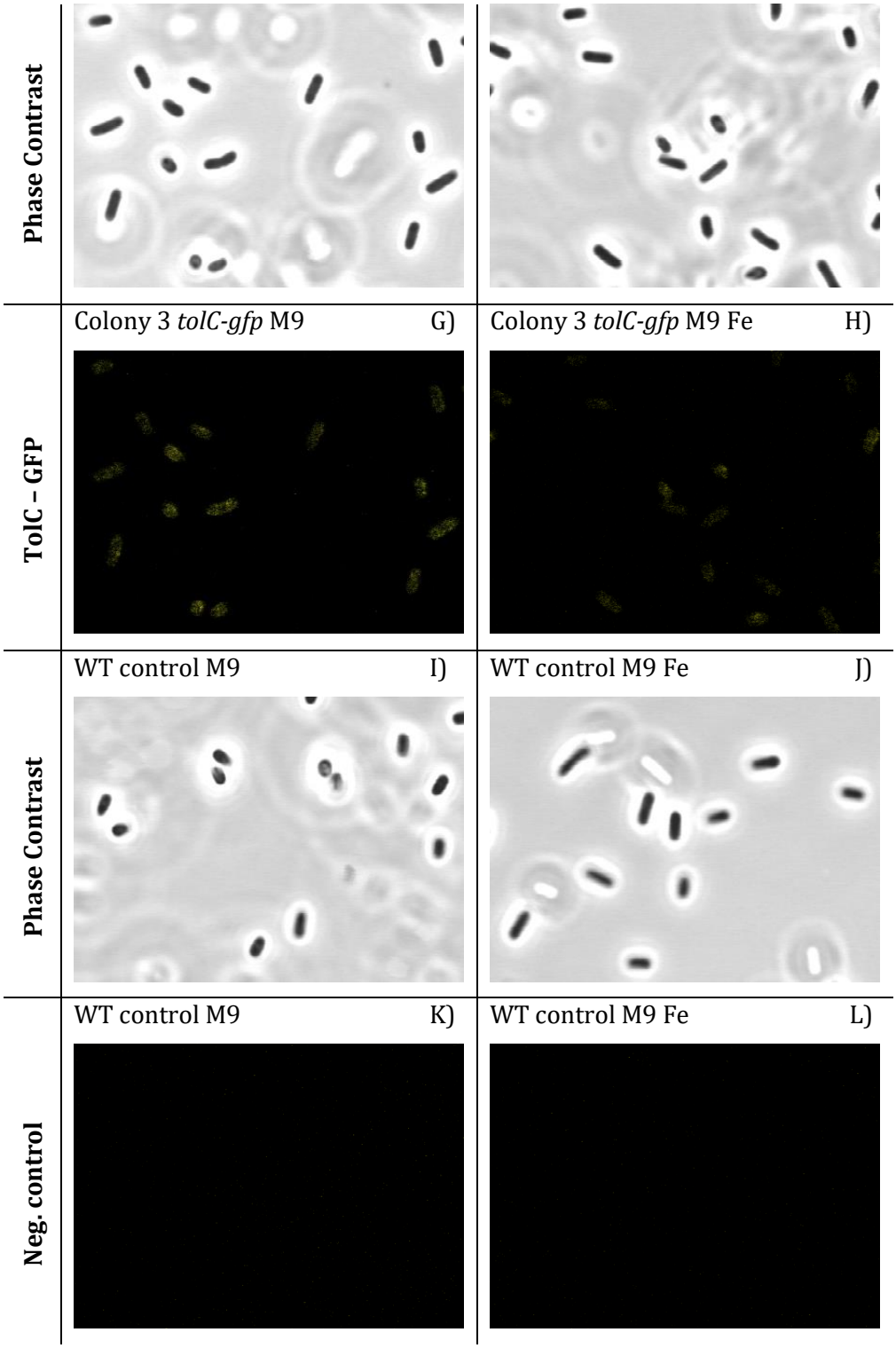

Supplemental Figure 2: Microscopy of M9/M9Fe grown *tolC-gfp* cells. Lack of iron C), G) increases the production TolC as cells are more fluorescent than D),H). WT control K), L).

A)

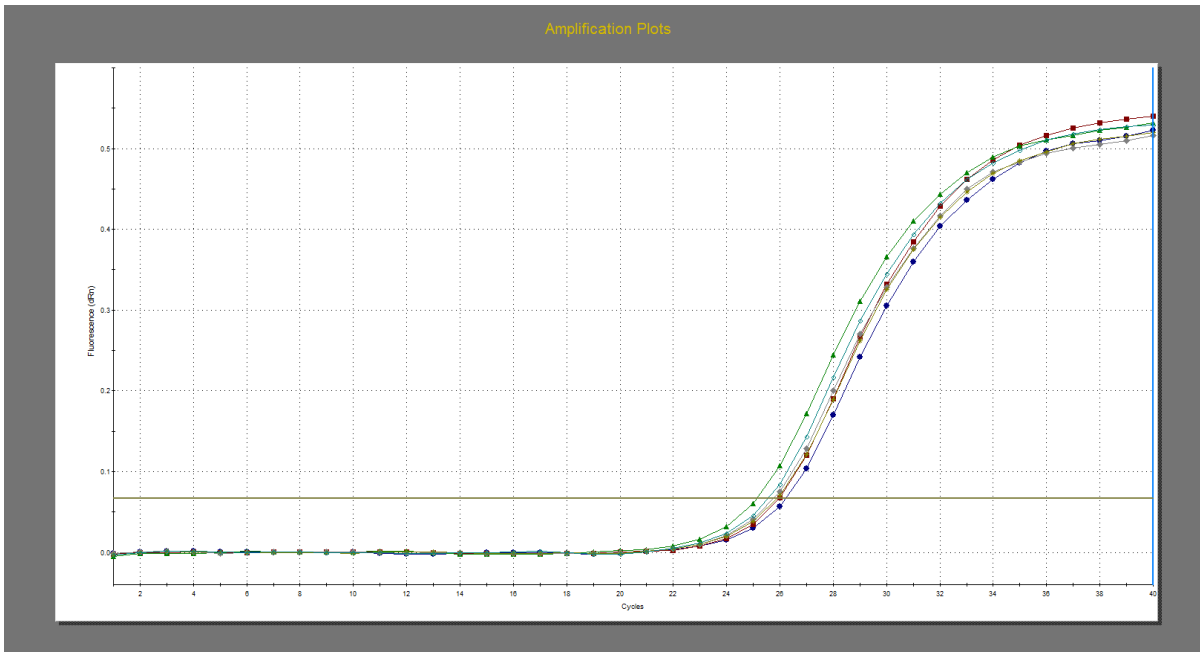

B)

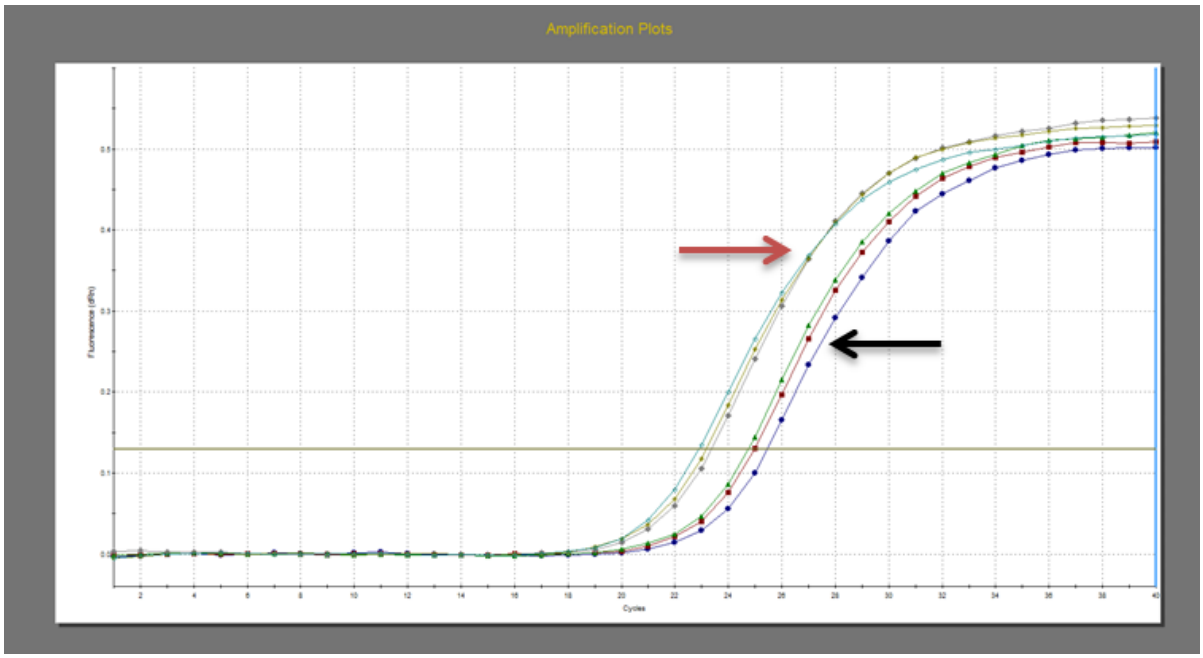

Supplemental Figure 3: Amplification plot from the qRT PCR. A) samples after 18h growth, 3 curves for M9, 3 for M9Fe and B)samples after 10h growth, red arrow showing the 3 samples grown in M9Fe and the black arrow showing the 3 samples grown in M9. Each amplification curve represents the average of 2 technical replicates.

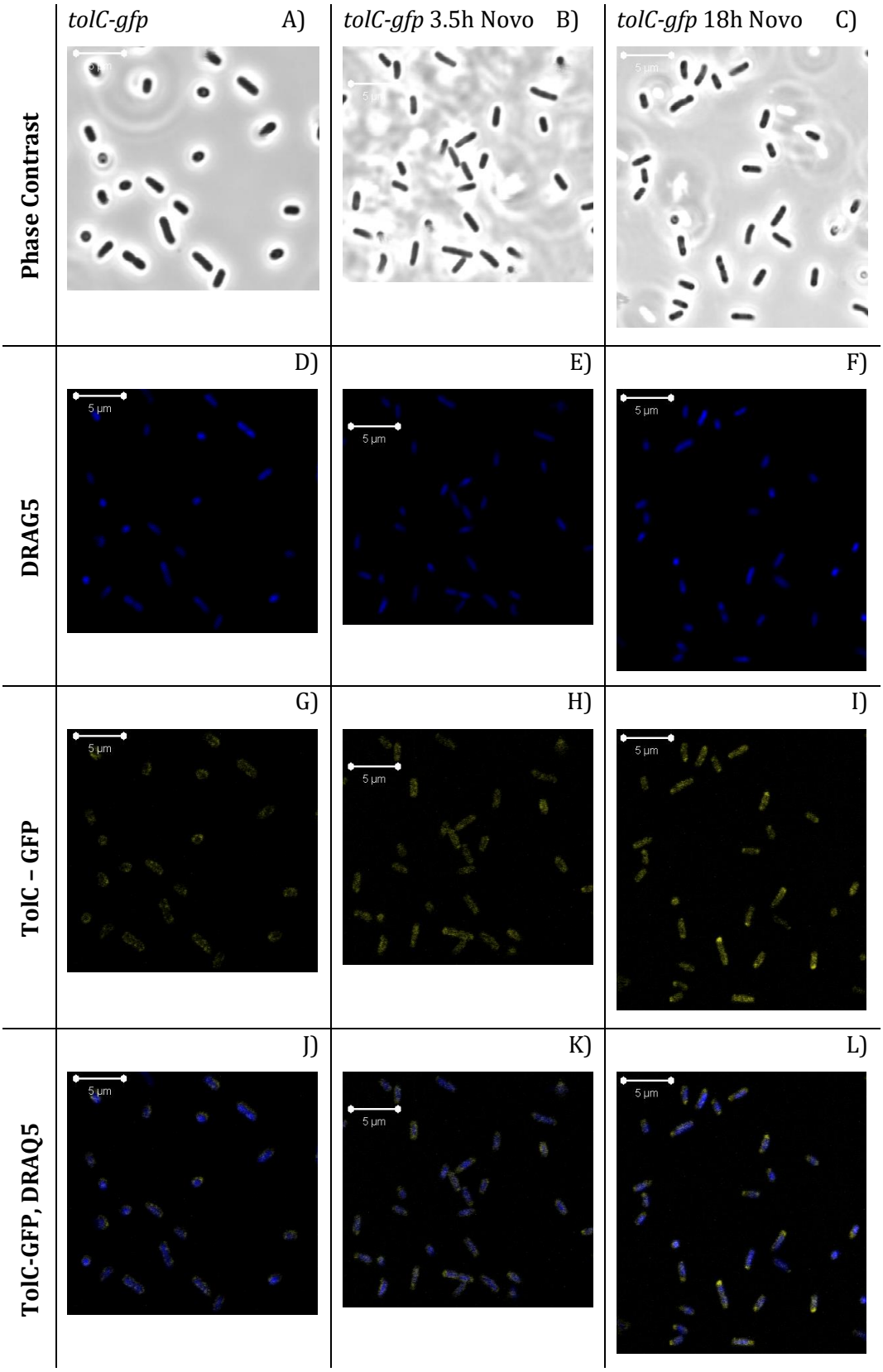

Supplemental Figure 4: Microscopy of a time-course *tolC-gfp* under Novobiocin treatment. A), D), G), J) before treatment. B), E), H), K) 3.5h after 50 µg/mL Novo addition. C), F), I), L) 18h after 50 µg/mL Novo addition

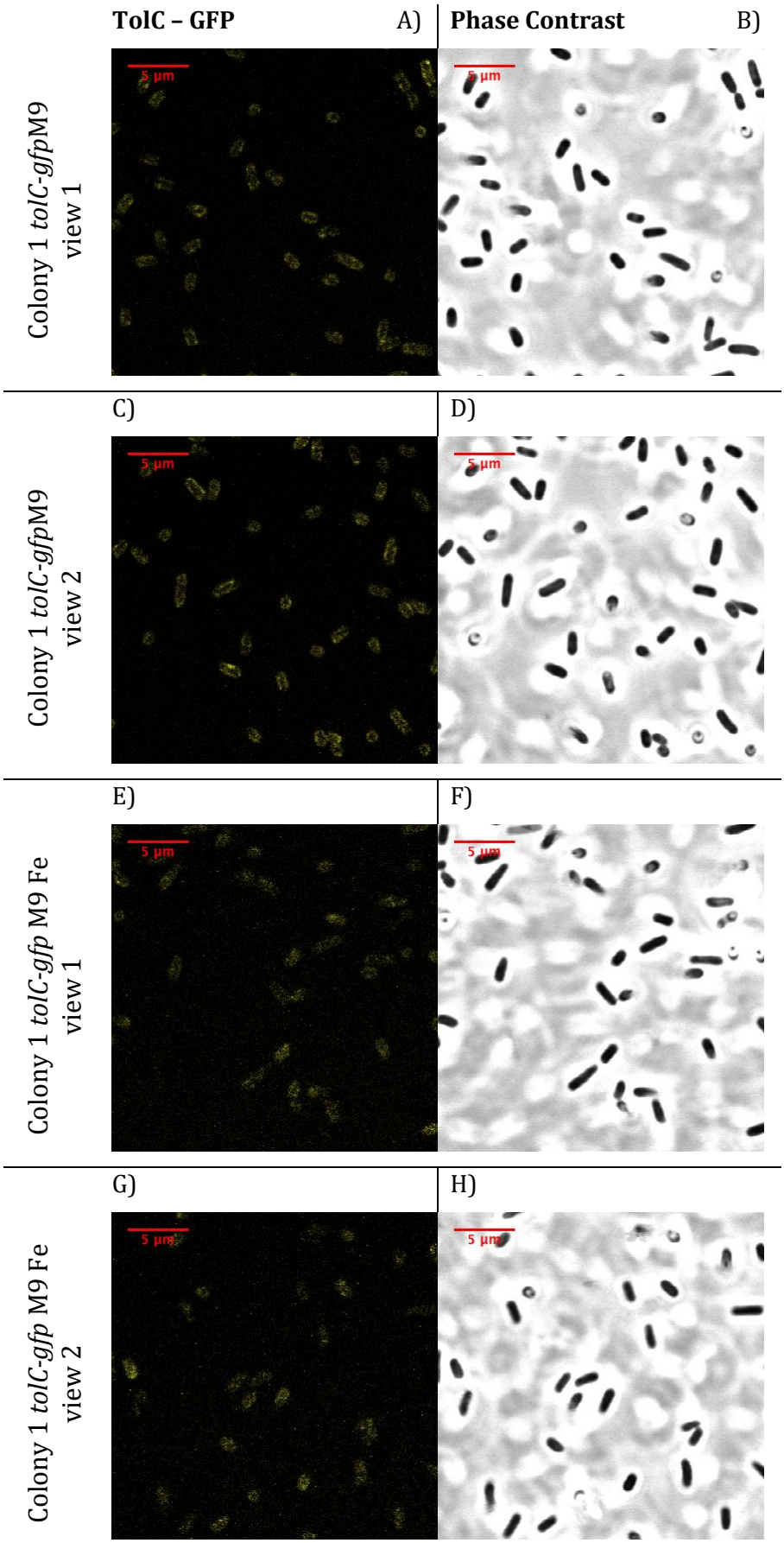

Supplemental Figure 5: Cells from Colony 1 grown without antibiotics. A), B), C) and D) in M9. E), F), G) and H) in M9Fe.

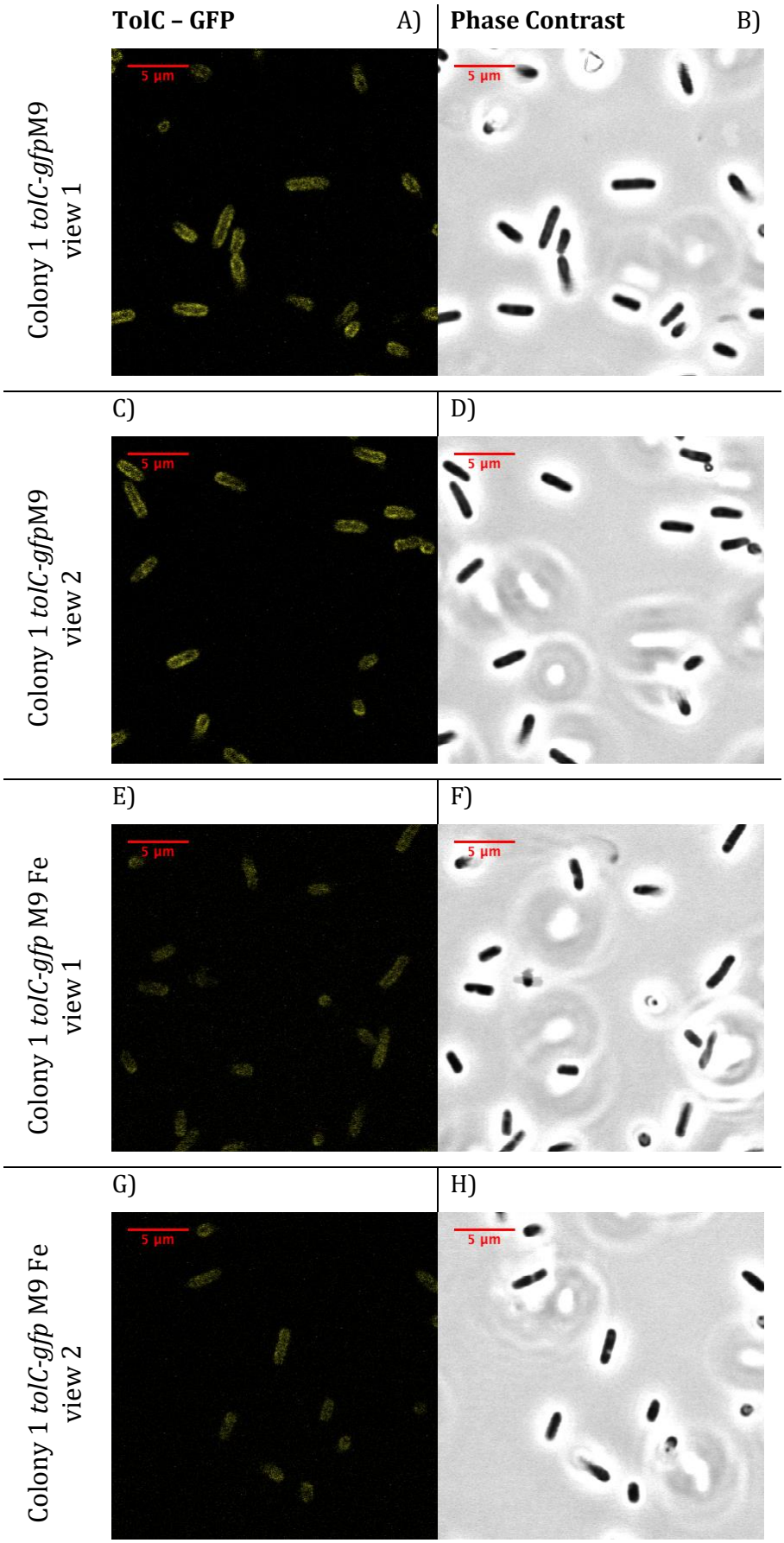

Supplemental Figure 6: Cells from Colony 1 grown in the presence of Erythromycin (3 µg/mL). A), B), C) and D) in M9. E), F), G) and H) in M9Fe.

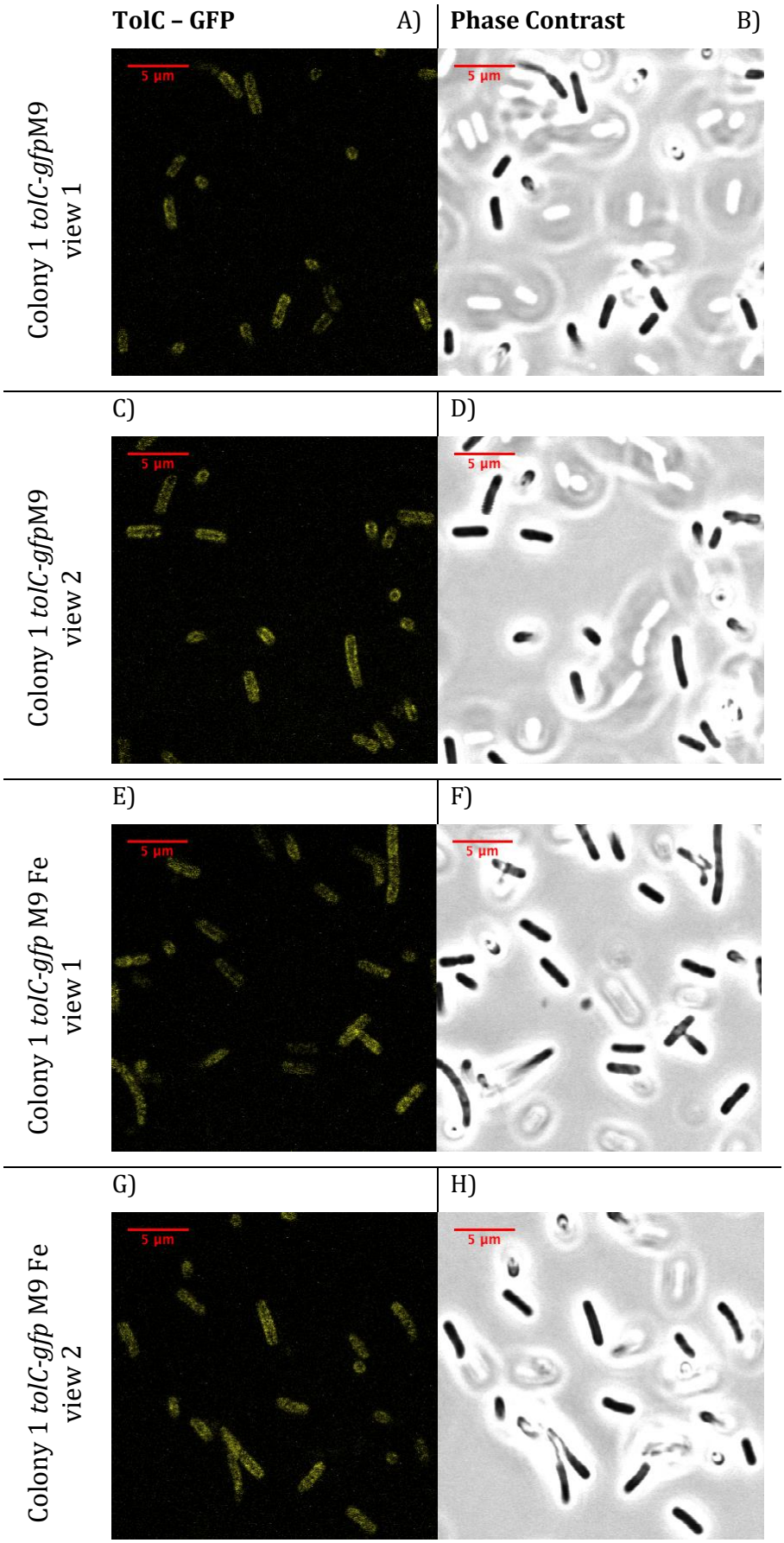

Supplemental Figure 7: Cells from Colony 1 grown in the presence of Novobiocin (100 µg/mL). A), B), C) and D) in M9. E), F), G) and H) in M9Fe.

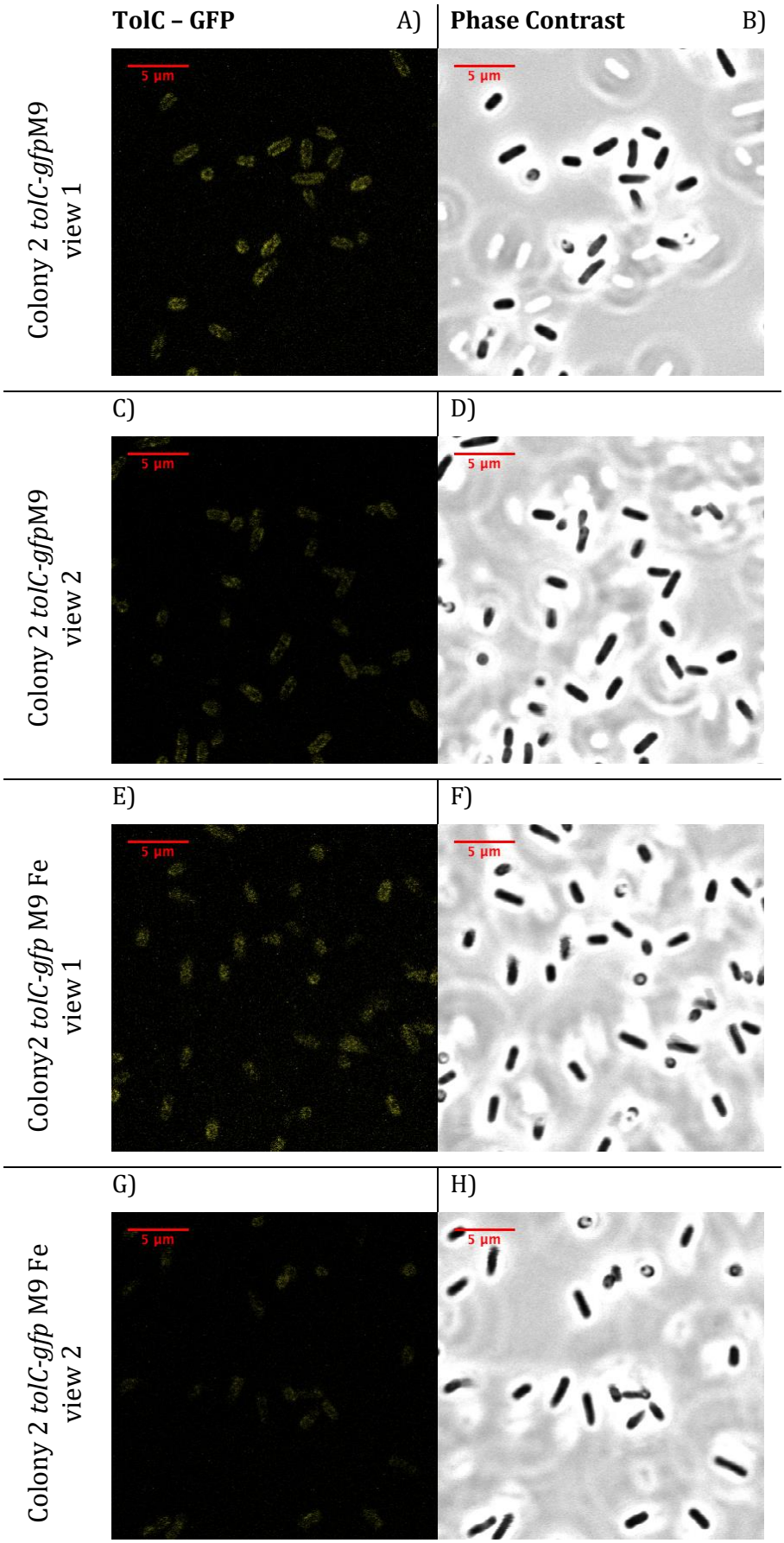

Supplemental Figure 8: Cells from Colony 2 grown without antibiotics. A), B), C) and D) in M9. E), F), G) and H) in M9Fe.

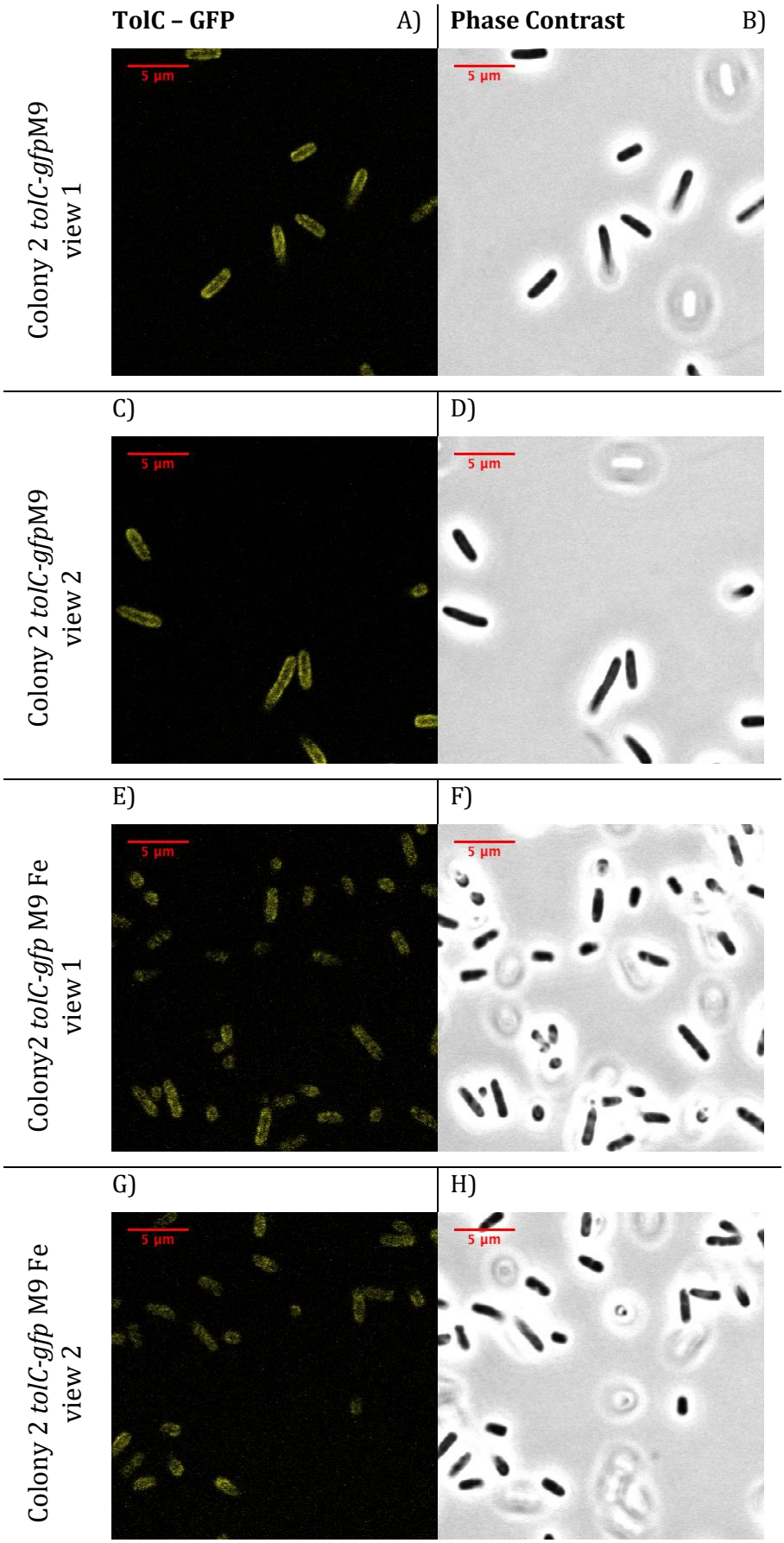

Supplemental Figure 9: Cells from Colony 2 grown in the presence of Erythromycin (3 µg/mL). A), B), C) and D) in M9. E), F), G) and H) in M9Fe.

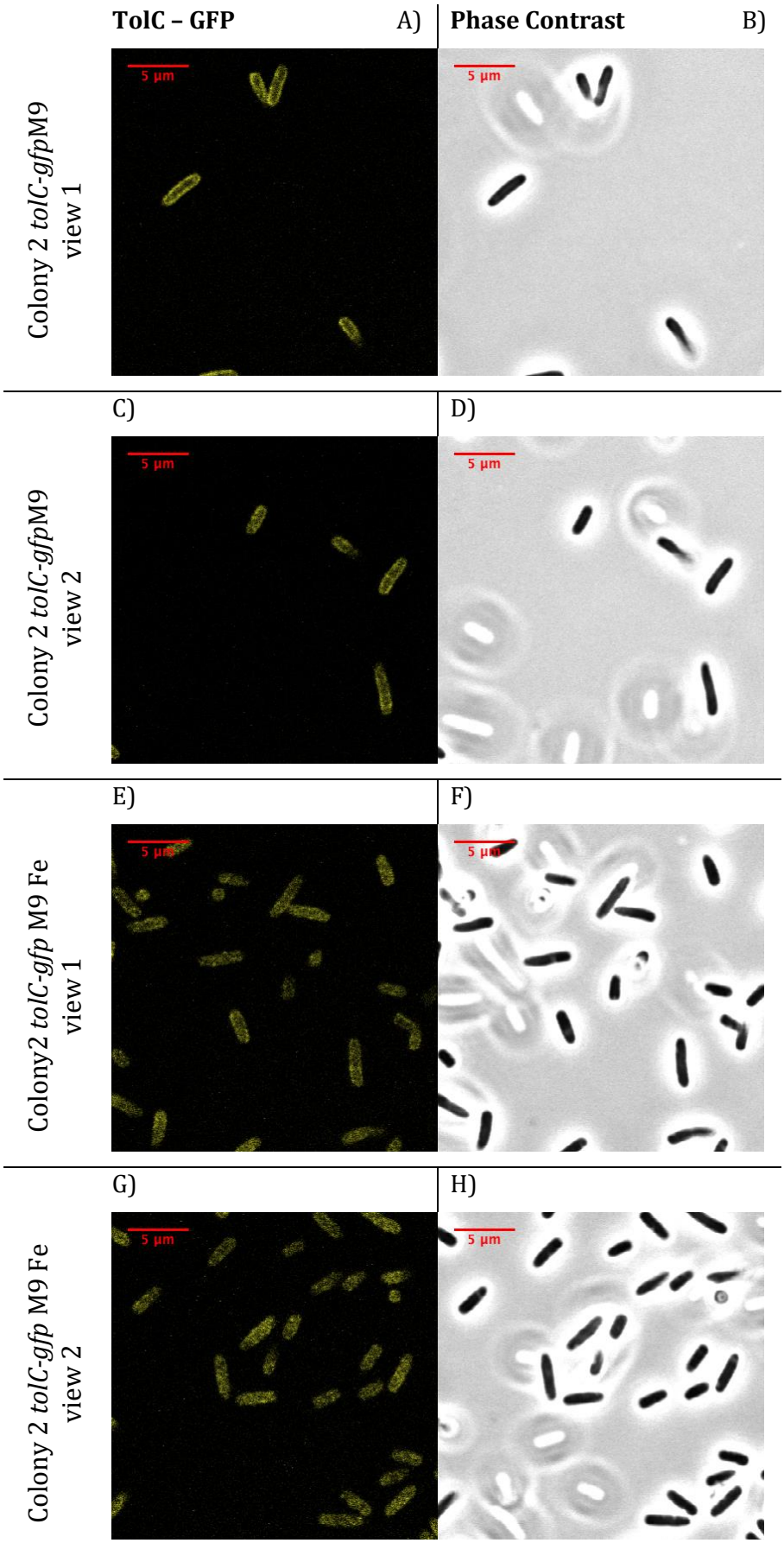

Supplemental Figure 10: Cells from Colony 2 grown in the presence of Clarythromycin (3 µg/mL). A), B), C) and D) in M9. E), F), G) and H) in M9Fe.

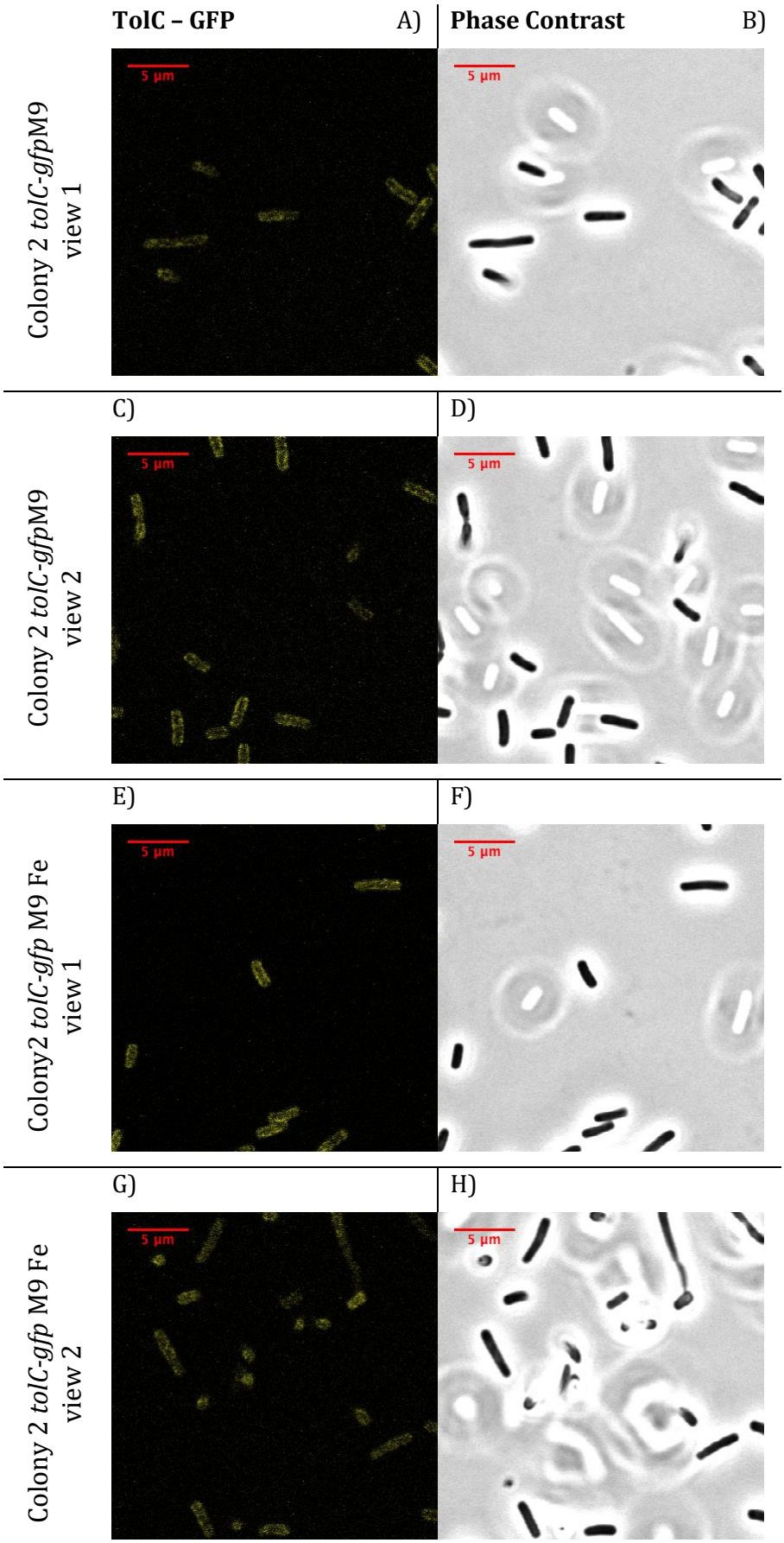

Supplemental Figure 11: Cells from Colony 1 grown in the presence of Novobiocin (100 µg/mL). A), B), C) and D) in M9. E), F), G) and H) in M9Fe.

2 Paper: Bridging timescales and Length Scales: From Macroscopic Flux to the Molecular Mechanism of Antibiotic Diffusion through Porins.

Authors: Eric Hajjar, Kozhinjampara R. Mahendran, Amit Kumar, Andrey Bessonov, **Mircea Petrescu**, Helge Weingart, Paolo Ruggerone, Mathias Winterhalter, and Matteo Ceccarelli

2.1 Declaration of contribution

The present study investigates outer membrane protein F and 2 single point mutations thereof: D113N and R132A. I have designed the cloning of these mutants, I have done the mutagenesis, the overexpression of WT, D113N and R132A and their subsequent purifications. I took part in discussions and manuscript writing.

Biophysical Journal Volume 98 February 2010 569–575

Bridging Timescales and Length Scales: From Macroscopic Flux to the Molecular Mechanism of Antibiotic Diffusion through Porins

Eric Hajjar,[†] Kozhinjampara R. Mahendran,[‡] Amit Kumar,[†] Andrey Bessonov,[‡] Mircea Petrescu,[‡] Helge Weingart,[‡] Paolo Ruggerone,[†] Mathias Winterhalter,[‡] and Matteo Ceccarelli[†*]

[†]Department of Physics, Universita degli Studi di Cagliari and Sardinian Laboratory for Computational Materials Science, Monserrato, Italy; and [‡]School of Engineering and Science, Jacobs University, Bremen, Germany

ABSTRACT Our aim in this study was to provide an atomic description of ampicillin translocation through OmpF, the major outer membrane channel in *Escherichia coli* and main entry point for β-lactam antibiotics. By applying metadynamics simulations, we also obtained the energy barriers along the diffusion pathway. We then studied the effect of mutations that affect the charge and size at the channel constriction zone, and found that in comparison to the wild-type, much lower energy barriers are required for translocation. The expected higher translocation rates were confirmed on the macroscopic scale by liposome-swelling assays. A microscopic view on the millisecond timescale was obtained by analysis of temperature-dependent ion current fluctuations in the presence of ampicillin and provide the enthalpic part of the energy barrier. By studying antibiotic translocation over various timescales and length scales, we were able to discern its molecular mechanism and rate-limiting interactions, and draw biologically relevant conclusions that may help in the design of drugs with enhanced permeation rates.

INTRODUCTION

Bacteria develop mechanisms of resistance that render the use of antibiotics ineffective (1). Moreover, an increase in multidrug-resistant pathogens is appearing at a time when only a few novel active antibacterial compounds are in clinical trials (2). To respond to this alarming situation, we need to reinforce and reinvent antibacterial research. Microscopically based drug design, starting from molecular knowledge of resistant mechanisms, represents a potentially efficient way to bring new agents to the market (3). A key resistance mechanism in Gram-negative bacteria is the prevention of antibiotic uptake, mediated by outer-membrane porins. For example, the resistance of pathogenic bacteria to β-lactams has been attributed to alterations in the expression or the molecular structures of porins (4). The OmpF porin in *Escherichia coli* has an hourglass shape and the channel structure reveals a spatial constriction created by loop L3, which folds back into the channel. As shown in Fig. 1, this region is also characterized by a transversal electric field created by acidic residues on the L3 side (D113 and E117) facing a cluster of arginines (R42-R82-R132) (5). Several studies have raised questions concerning the role of these amino acids in diffusion processes through OmpF. For example, the single substitutions R132A and D113A were found to dramatically increase the uptake of β-lactams antibiotics (6,7). Such findings provide investigators with an opportunity to tune the uptake of antibiotics based on only slight chemical modifications. This attractive strategy requires the development of better-tuned quantitative methods to elucidate the rate-limiting molecular interactions between drug and channel residues. In this work, we studied antibiotic diffusion by combining atomic-level descriptions provided by molecular-dynamics (MD) simulations (8), electrophysiology techniques at the single-molecule level (9), and liposome-swelling assays (10). Our findings reveal, for the first time to our knowledge, the complete pathways of ampicillin permeation through wild-type (WT) OmpF as well as D113N and R132A mutants, from their macroscopic flux down to their molecular mechanism.

MATERIALS AND METHODS

MD simulations

For the MD simulations, we followed a previously described protocol (8), starting from the crystal structure (Protein Data Bank code: 2OMF) and residue protonation state as described by Im and Roux (11). We used the program ORAC and the Amber force field (12) for system setup and simulation (13). The porin mutants were obtained by substituting the single amino acid residue starting from the high-resolution structure of OmpF (2OMF) using the MD package ORAC. After the molecular replacement was completed, we further equilibrated the mutant system for ~2 ns of a standard MD simulation. All simulated systems were validated for convergence and stabilization of energy, temperature, and root mean-square deviation (RMSD) with respect to the starting structure. Based on previous findings (7,8,14), we chose the following collective variables to simulate antibiotic translocation using metadynamics (15): 1), the distance Z, defined as the difference between the center of mass of the antibiotic and the center of mass of the system (porin + detergent) along the z axis; and 2), the angle θ, defined as the orientation of the long axis of the molecule with respect to the z axis. All simulated systems were validated for convergence and stabilization of energy, temperature, and RMSD with respect to the starting structure. Our choice of OmpF as a monomer is supported by previous studies that reported a mutual independence of the three monomers (i.e., no cooperativity) for ions, small-molecule transport, and antibiotics (16–18). Using this biased simulation strategy, we obtained translocation of ampicillin through WT OMPF, D113N, and R132A after 38, 27, and 15 ns, respectively. The metadynamics algorithm enables one to reconstruct the free energy in the subspace of the collective variables by integrating the

Submitted August 20, 2009, and accepted for publication October 15, 2009.

*Correspondence: matteo.ceccarelli@dsf.unica.it

Editor: Benoit Roux.

0006-3495/10/02/0569/7 $2.00

doi: 10.1016/j.bpj.2009.10.045

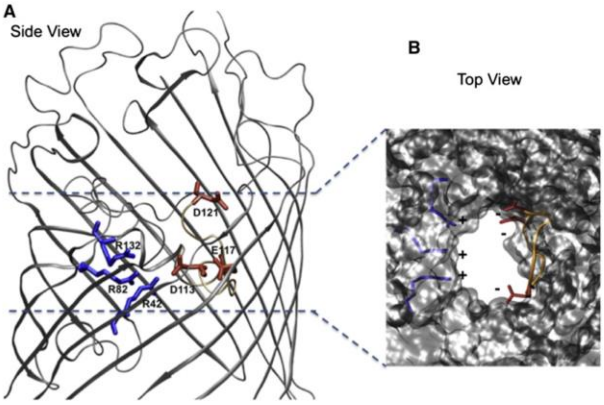

FIGURE 1 Structural details of OmpF. (*A*) The backbone of OmpF is displayed in gray cartoons. The charged residues at the constriction region (D113, E117, and D121 on the L3 side, and R42, R82, and R132 on the anti-L3 side) are colored by residue type (positively charged in *blue*, negatively charged in *red*). (*B*) The OmpF structure is displayed in gray molecular surface to highlight the space available. Loop L3 is colored in orange and the charged residues at the constriction region are colored as in *A*.

history-dependent terms (15). Because of the complexity of the process studied, we calculated the free energy after obtaining the first translocation path, which is considered to be the most probable path because it passes through the lowest saddle point, as was previously done for the unthreading of a molecule (19). We used the resulting approximated free-energy surface to select the regions of energy minima. Additional metadynamics simulations were launched starting from each minimum, which enabled us to reconstruct the one-dimensional (1D) free-energy profile for the translocation of ampicillin through WT OmpF and the two mutants. The profiles only report the energetic barriers from the time the antibiotic enters the channel to when it reaches the highest barrier (also called the main or effective barrier). In fact, once the antibiotic crosses the constriction region, we expect a diffusive regime, with no significant affinity sites. The error bars associated with the energy barrier calculations were assessed as previously described (19) and were 2 kT at most. Furthermore, to decipher the molecular details of the translocation mechanism, additional equilibrium MD simulations (1 ns length) were started from each visited minimum along the ampicillin diffusion path. In-depth analysis included the calculation of 1), atomic fluctuations; 2), hydrogen (H)-bonds (the criteria were a distance of at most 2.8 Å and a donor-hydrogen-acceptor angle of at least 130°) and hydrophobic interactions (the criterion was a distance of at least 3 Å between nonpolar atoms) of ampicillin; 3), the residence time of water molecules around ampicillin (20); and 4), the cross-sectional solvent-accessible surface area (SASA) (21) using both an in-house program and the software VMD (22).

Experiments

The chemicals used in this study were arabinose, raffinose, KCl, MES, *n*-pentane, hexadecane, squalene, ampicillin anhydrous, Dextran 40000 (Sigma-Aldrich, Buchs, Switzerland), Octyl-POE (Alexis, Switzerland), 1,2-diphytanoyl-*sn*-glycero-3-phosphatidylcholine (DPhPC), and *E. coli* total lipid extract (Avanti Polar Lipids, Alabaster, AL). Reconstitution experiments and single-channel analyses were performed as previously described (18). A stable planar lipid bilayer was formed on a 25-μm-thick Teflon film (aperture diameter: 40–50 μm), and spontaneous channel insertion was obtained under high applied voltage. A Peltier element was used for temperature regulation (Dagan), and ion current blockages were measured after the addition of ampicillin to the chamber. The data in Table 1 were obtained by a fluctuation, single-channel analysis as outlined in previous studies (4,9,18,23,24). The on-rate was calculated from the number of binding events ($k_{on} = \upsilon / (3[c])$, where υ is the number of events and c is the concentration of antibiotic). The off-rate ($t \gg k_{off} - 1$) was calculated from the residence time, as described previously. The flux of antibiotic through the channel is proportional to the k_{on} rate ($J = k_{on}\ \Delta c/2$). WT OmpF and mutants (1 mg/mL) in 1% Octyl-POE were reconstituted into liposomes as described by Nikaido and Rosenberg (25). *E. coli* total lipid extract (Avanti Polar Lipids, Alabaster, AL) was used for liposome formation, and 17% Dextran (molecular weight: 40,000; Fluka) was used for liposome filling. After incubation, multilamellar liposomes were formed by sonication in a water bath sonicator. The size of the formed liposomes was checked with the use of a Nano-ZS ZEN3600 zetasizer (Malvern Instruments, UK). Control liposomes were prepared in the same manner but without the addition of porin. The isotonic concentration was determined by diluting the proteoliposomes into different concentrations of raffinose (Sigma) with an Osmomat 30 osmolarimeter (Gonotec). Each batch (containing WT, D113N, or R132A) was separated into smaller aliquots assuming a homogeneous distribution. One aliquot of each batch was tested for arabinose, a smaller molecule for which we expect maximum permeation, and this swelling rate was set as our reference 100% for the respective batch. By normalizing each batch separately, we were able to reduce the

TABLE 1 Kinetic analysis of the ampicillin-binding events: k_{on}, k_{off}, K (binding constant), and J (flux) of ampicillin for WT OmpF and the mutant D113N

Ampicillin at $\Delta C = 10$ mM	Threshold gating potential [mV]	k_{oncis} [1/(s M)]	$k_{ontrans}$ [1/(s M)]	k_{off} [1/s]	K [1/M]	Flux J *cis* to *trans* [molecule/s]
OmpF	100–150	2800 ± 280	2700 ± 270	5300 ± 530	1.0	14
50 mV		3000 ± 300	2600 ± 260	4800 ± 480	1.2	15
−50 mV						
D113N	200	17000 ± 1700	3200 ± 320	10000	2	80
50 mV		4100 ± 420	2500 ± 250	10000	0.7	22
−50 mV						

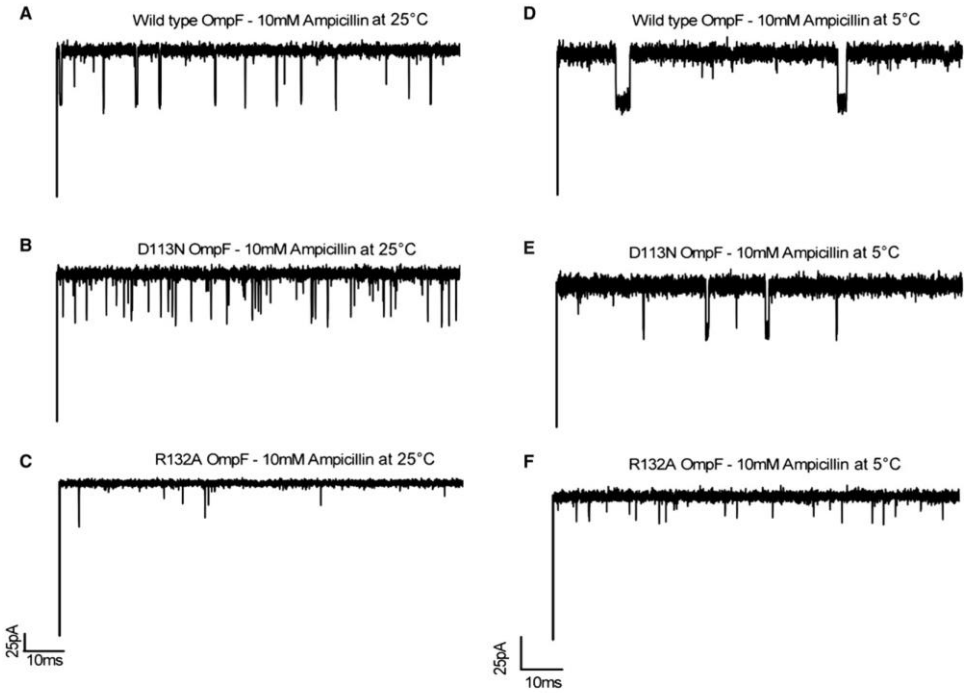

FIGURE 2 Typical tracks of ion current through a single WT OmpF channel and mutants D113N and R132A, reconstituted into DPhPC lipid membranes in the presence of 10 mM ampicillin and 1 M KCl at pH 6. Applied voltage is 50 mV.

effects of the variable reconstitution efficiencies of different preparations. Changes in the optical density were monitored at 400 nm with a Cary 100 Scan spectrophotometer (Varian). The swelling rates were taken as averages from at least three different sets of experiments, calculated as described by Nikaido and Rosenberg (25), and then normalized to the rate obtained with arabinose.

RESULTS

First, we measured ion current fluctuations through single trimeric OmpF (WT and mutants R132A and D113N) reconstituted into lipid bilayers, which allowed us to extract the kinetic rates (18). As shown in Fig. 2, *A–C*, at 25°C ampicillin causes significant ion current fluctuations in both WT OmpF and mutant D113N, but, surprisingly, few blocking events are visible in the case of R132A. The average residence time of ampicillin is calculated to be 180 ± 20 μs for WT OmpF and as low as 100 ± 20 μs for the D113N mutant. In the case of both mutants, our findings highlight a possible underestimation of the number of events due to the resolution limit of the method. To rule out this possibility, we repeated the measurements at lower temperatures, as slowing down the diffusion should reveal potential fast events.

At 5°C, as shown in Fig. 2, *D–F*, we measure fewer blocking events but elongated residence times for both the WT and D113N OmpF. Lowering the temperature brings the residence time of D113N well above the resolution limit (Fig. 3 *B*). In the case of R132A, we observe more events, but they are still partial blocking events, and thus we cannot calculate the binding kinetics. To sum up, the number of binding events is much higher in the case of D113N compared to WT OmpF at all applied temperatures (Fig. 3 *A*). Of interest, the fitting procedure reveals that beyond 25°C, in the range of physiological temperatures, the number of measured events is underestimated in the case of D113N, which is as expected when the residence time approaches the resolution limit of the method (inverse filter frequency: 100 μs).

According to a simple kinetic model, at low substrate concentration the flux J is only proportional to the on-rate k_{on}, $J = (k_{on}/2)\,\Delta c$, where Δc is the concentration gradient (23,26). The kinetic analysis (Table 1) yielded $k_{on} = 3000 \pm 300\ s^{-1}M^{-1}$ for WT OmpF and $17000 \pm 1700\ s^{-1}M^{-1}$ for the D113N mutant, resulting in the translocation of ~6 times more ampicillin molecules for D113N than for WT OmpF.

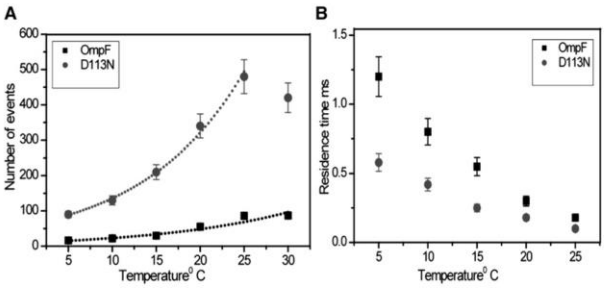

FIGURE 3 (*A*) Statistical analysis revealing temperature-dependent blocking events of ampicillin with WT OmpF and D113N. The continuous line represents the exponential fit. (*B*) Effect of temperature on the antibiotic residence time (τ) for WT OmpF and D113N mutant.

We then used additional methods to bridge the timescales and length scales of transport, to clarify the case of R132A in which only partial blocking events were observed at all measured temperatures.

To elucidate the energetic details of transport, we performed metadynamics simulations of ampicillin translocation through WT OmpF, D113N, and R132A mutants. From the reconstructed 1D free-energy profiles (Fig. 4), we observe that the effective barrier for ampicillin to translocate is higher in the case of WT OmpF (14 kT) and lower for R132A (9 kT) and D113N (5 kT). To compare these findings with our predictions, we quantified the in vitro macroscopic flux of ampicillin using a liposome-swelling assay, a method that has been successfully applied to such problems in previous studies (10,25). The advantage of this technique is that the penetration rates of ampicillin in proteoliposomes generally mimic those of the intact cells, and swelling rates are directly proportional to the permeability of the antibiotic. As shown in Fig. 5, we find a higher diffusion rate of ampicillin for both mutants, as it increases by 25% for R132A and 40% for D113N compared to the WT OmpF. The trend of the flux is in good agreement with that of the energy barriers obtained from the molecular simulations. Taken together, our results demonstrate that a single point mutation at the constriction region can remarkably affect the kinetics of ampicillin and thus its uptake.

To elucidate the molecular mechanism and rationalize our findings, we then deciphered the physicochemical and structural properties of the diffusion process. Each relevant minimum identified by the metadynamics (as labeled in Fig. 4) was used as a starting point for the additional equilibrium MD simulations for which we analyzed the solvation, flexibility, SASA, and interaction patterns between ampicillin and the OmpF residues.

In the case of the WT, when ampicillin is above the constriction region (in the structures sampled along the equilibrium simulations at Minimum-I), it interacts only transiently with channel residues, as the antibiotic undergoes numerous reorientations and attempts to enter the constriction zone. This is confirmed by the averaged atomic fluctuations of ampicillin of 0.78 Å (along Minimum-I), which is close to the antibiotic fluctuation calculated in bulk water (Table 2).

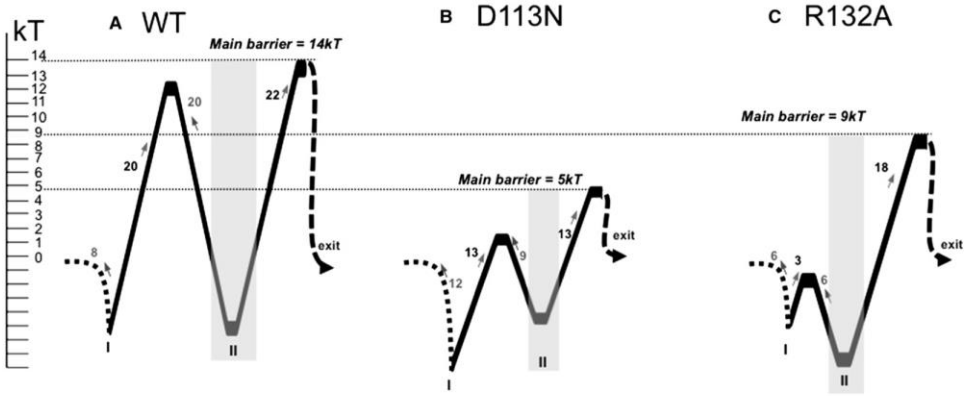

FIGURE 4 One-dimensional free-energy profiles for the translocation of ampicillin through WT OmpF (*A*), D113N (*B*), and R132A (*C*). The minima at the constriction region are highlighted in gray and the energy barriers are reported in kT. The "exit" label refers to the periplasmic side.

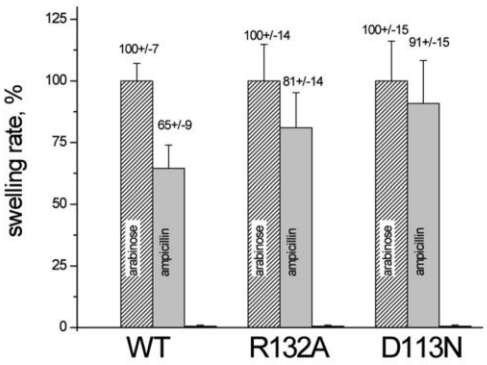

FIGURE 5 Liposome-swelling assay with proteoliposomes containing WT OmpF or mutants D113N and R132A. Arabinose, a small molecule that is able to penetrate perfectly, was used as a reference to normalize the swelling rates (=100%). A second control was performed with raffinose, which does not permeate through OmpF.

Such extensive rearrangements above the constriction region were also previously described in the case of diffusion of glycerol through aquaglyceroporin (27). Furthermore, when it reaches the affinity site at the constriction region (Minimum-II), the ampicillin fluctuations are as low as 0.35 Å, and such a decrease in entropy was also previously shown upon ligand binding (28). The entropy-enthalpy compensation is made possible via specific interactions between ampicillin and OmpF through both H-bonds (with D113 and R42-R82-R132) and hydrophobic contacts (Fig. 6 *A*). In this affinity site (Minimum-II), we also find that ampicillin has durable interactions with slow water molecules or "bound waters" (Table 2). Such a strong network of interactions of ampicillin at the constriction region explains the high-energy barrier calculated to exit the channel, which correlates well with the long residence time measured.

In the case of D113N, ampicillin does not reorient extensively above the constriction region, and the fluctuations calculated along Minimum-I are only of 0.29 Å (Table 2). In contrast to the WT, the antibiotic finds the optimal orientation rapidly (Fig. 6) to fit the constriction region. This explains the lower energy barrier to enter the constriction region and agrees with the higher number of measured events. At the constriction region, ampicillin maintains a favorable network of interactions (Fig. 6 *B*) in which the side chain of the residue E117 now repositions in the lumen of the channel to make H-bonds with the positive group of ampicillin. However, once ampicillin crosses the constriction region, its positive group does not find a salt-bridge partner, and this facilitates its diffusion further down. The lack of interactions retarding the antibiotic's exit through the channel constitutes a major difference compared to the WT and explains the lower energetic barrier and measured residence time.

Of interest, a different molecular path is found by ampicillin in the case of the mutant R132A, which explains the partial blocking events measured (Fig. 2 *C*). In the case of this mutant, ampicillin takes advantage of the structural and polarity changes in the channel to rapidly reach the constriction region (the barrier is reduced to 3 kT; see Fig. 4 *C*), and translocates with its phenyl group pointing down (Fig. 6 *C*). Furthermore, when it is at the constriction region, ampicillin neither accommodates in the hydrophobic pocket at the L3 side nor makes H-bonds with the basic residues at the anti-L3 side (Fig. 6 *C*). Compared to the WT OmpF, the only conserved interaction in this case is the salt-bridge between the amino positive group of ampicillin and D113. Still, in the case of R132A, we observe that ampicillin interacts with some novel residues (Fig. 6 *C*), has a low flexibility, and interacts with slow "bound waters" (Table 2). This well-defined affinity site once again explains the high-energy barrier needed to exit the channel (Fig. 4 *C*).

The occlusion of the channel is well illustrated by the MD simulation snapshots (Fig. 7, *A–C*), which show that it is only in the case of the mutant R132A that ampicillin is not positioned centrally and instead leaves a large portion of space available. We quantified the available area (Fig. 7, *D–F*) and found that ampicillin only significantly occludes the pore upon translocation in the cases of the WT OmpF and the D113N mutant. For the mutant R132A, there is still at least 60% of space available. This means that the antibiotic diffusion would not interfere significantly with the ionic current, which would explain the lack of well-resolved ionic current blockage at any measured temperature in this case (Fig. 2 *C*).

DISCUSSION

In all three systems (WT OmpF, D113N, and R132A), we found an affinity site for ampicillin in OmpF, defined by

TABLE 2 Structural details obtained from the equilibrium MD simulations

	Averaged atomic fluctuations (Å)			Interaction with "bound waters" (% of the total number of interacting water molecules)		
Region of analysis	WT	D113N	R132A	WT	D113N	R132A
Mini I (above constriction region)	0.74	0.39	0.59	0	0	0
Mini II (at constriction region)	0.35	0.29	0.32	10	5	7
Mini III (below constriction region)	0.60	0.75	1.00	4	0	0

First column reports the averaged atomic fluctuations of ampicillin, and the second column provides the number of "bound waters", defined as the molecules that interact with ampicillin with a residence time of >30% of the simulation time.

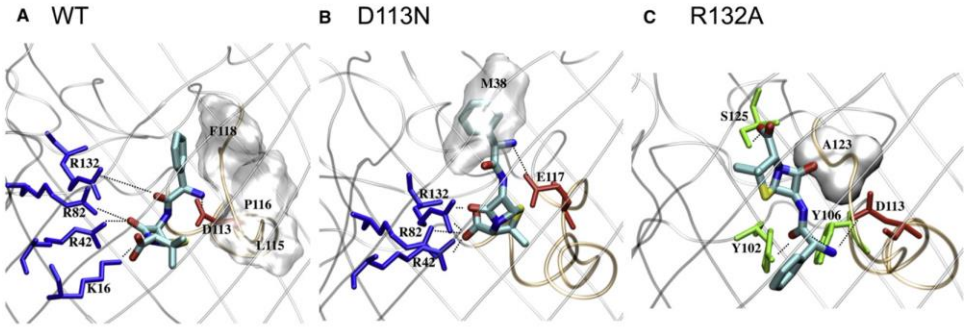

FIGURE 6 Molecular details (*side views*) of ampicillin at the binding site of the constriction region of (*A*) WT OmpF, (*B*) D113N, and (*C*) R132A. The views and orientations in this figure are the same as in Fig. 1 (the *top* is toward the vestibule, the *bottom* is toward the periplasmic space). The antibiotic is displayed in stick representation and colored by atom type (*blue* for nitrogen, *red* for oxygen, *cyan* for carbon) where hydrogens are not shown. The backbone of OmpF is displayed in gray cartoons to highlight its secondary structures. The constriction region is highlighted by loop L3 (colored in *orange*). Residues of OmpF that are seen as strongly interacting with the antibiotic are labeled using the one-letter amino acid code; those making H-bonds are colored by residue type (positively charged in *blue*, negatively charged in *red*, polar in *green*), and those making hydrophobic contacts are displayed with their molecular surface, highlighting their shape.

specific interactions with key residues of the constriction region and with strongly ordered water molecules. For the concentration used here (far from saturation and within the limit of the physiological dose), the only parameter that makes a difference in the flux is k_{on}. Of interest, we can conclude from our results that k_{on} can be tuned by mutations at the constriction region that affect, very locally, the molecular interactions. The fact that ampicillin uptake can be tuned by

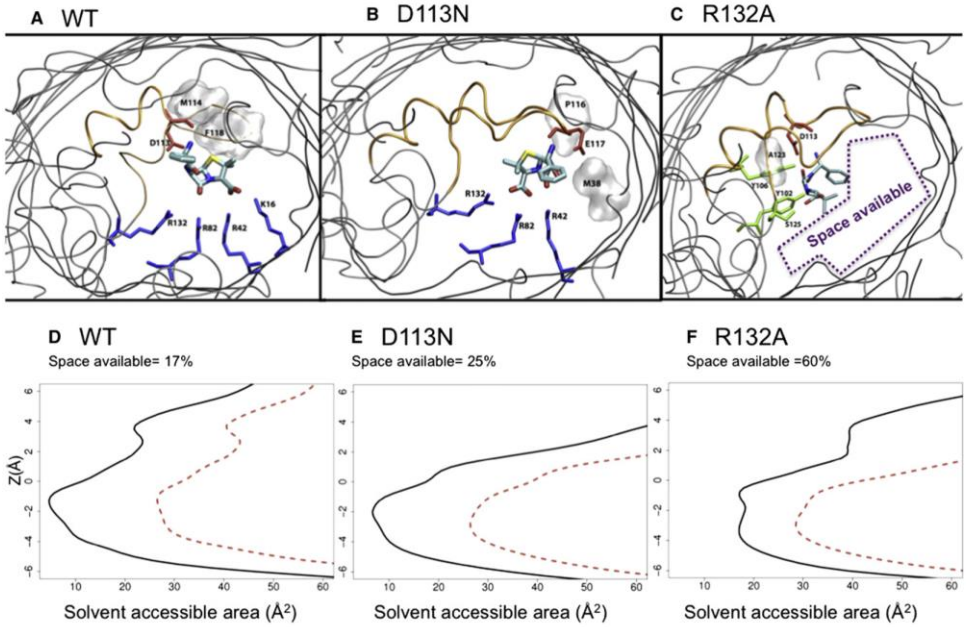

FIGURE 7 Molecular details (*top view*) from equilibrium simulations started at Minima-II for WT OmpF (*A*), D113N (*B*), and R132A (*C*) mutants. Ampicillin is displayed in stick representation and colored according to atom type. The backbone of OmpF is shown by gray cartoons (L3 is colored *orange*). The residues making H-bonds are colored by residue type, and those making hydrophobic contacts are displayed by gray molecular surface. Below, the average SASA is reported for WT OmpF (*D*), D113N (*E*), and R132A (*F*) in the presence (*black*) and absence (*red*) of ampicillin.

specific interactions inside the channel is in agreement with previous theoretical and experimental studies (11,23,29–31). Cornell et al. (12) assumed that k_{on} is only dependent on the diffusion coefficient of the molecule and the radius of attraction. This implies that, surprisingly, even very local interactions at the constriction region must be taken into account in the definition of this radius.

We conclude that the bottleneck for antibiotic translocation stems from the difficulty of overcoming the constriction region. In the case of WT OmpF, ampicillin has to deal with a particularly reduced size and a strong electrostatic field. Using computer simulations, we were able to predict when the presence of an ampicillin molecule would block the ion current, and thus rationalize the ion current fluctuations induced by antibiotics upon translocation.

By combining different approaches, we were able to follow the ampicillin translocation process over various timescales and length scales. This allowed us to reveal the complete molecular mechanism of diffusion and relate it to biologically relevant conclusions. The identification of crucial antibiotic-channel interactions will benefit the design of novel molecules with enhanced permeation rates. Finally, we believe that our multiscale approach can be conveniently employed to study porin-antibiotic interactions in other enterobacterial pathogens (1,4), such as those involved in persistent tuberculosis.

We thank Tivadar Mach, Malcom Page, and Jurg Dreier for their support and productive discussions.

This study was supported by the European Union, FP6 grant MRTN-CT-2005-019335 (Translocation), and by the computer center and consortiums Cybersar, CASPUR, and CINECA through CPU hours.

REFERENCES

1. Arias, C. A., and B. E. Murray. 2009. Antibiotic-resistant bugs in the 21st century—a clinical super-challenge. *N. Engl. J. Med.* 360:439–443.
2. Spellberg, B., J. H. Powers, …, J. E. Edwards, Jr. 2004. Trends in antimicrobial drug development: implications for the future. *Clin. Infect. Dis.* 38:1279–1286.
3. Barker, J. J. 2006. Antibacterial drug discovery and structure-based design. *Drug Discov. Today.* 11:391–404.
4. Pagès, J. M., C. E. James, and M. Winterhalter. 2008. The porin and the permeating antibiotic: a selective diffusion barrier in Gram-negative bacteria. *Nat. Rev. Microbiol.* 6:893–903.
5. Cowan, S. W., T. Schirmer, …, J. P. Rosenbusch. 1992. Crystal structures explain functional properties of two *E. coli* porins. *Nature.* 358:727–733.
6. Simonet, V., M. Malléa, and J. M. Pagès. 2000. Substitutions in the eyelet region disrupt cefepime diffusion through the *Escherichia coli* OmpF channel. *Antimicrob. Agents Chemother.* 44:311–315.
7. Vidal, S., J. Bredin, …, J. Barbe. 2005. β-Lactam screening by specific residues of the OmpF eyelet. *J. Med. Chem.* 48:1395–1400.
8. Ceccarelli, M., C. Danelon, …, M. Parrinello. 2004. Microscopic mechanism of antibiotics translocation through a porin. *Biophys. J.* 87:58–64.
9. Kozhinjampara, M., C. Chimerel, …, M. Winterhalter. 2009. Antibiotic translocation through membrane channels: temperature-dependent ion current fluctuation for catching the fast events. *Eur. Biophys. J.*, in press.
10. Yoshimura, F., and H. Nikaido. 1985. Diffusion of β-lactam antibiotics through the porin channels of *Escherichia coli* K-12. *Antimicrob. Agents Chemother.* 27:84–92.
11. Im, W., and B. Roux. 2002. Ions and counterions in a biological channel: a molecular dynamics simulation of OmpF porin from *Escherichia coli* in an explicit membrane with 1 M KCl aqueous salt solution. *J. Mol. Biol.* 319:1177–1197.
12. Cornell, W. D., P. Cieplak, …, P. Kollmann. 1995. J. Am. Chem. Soc. 117:5179–5197.
13. Procacci, P., T. A. Darden, …, M. Marchi. 1997. ORAC: a molecular dynamics program to simulate complex molecular systems with realistic electrostatic interactions. *J. Comput. Chem.* 18:1848–1862.
14. Danelon, C., E. M. Nestorovich, …, S. M. Bezrukov. 2006. Interaction of zwitterionic penicillins with the OmpF channel facilitates their translocation. *Biophys. J.* 90:1617–1627.
15. Laio, A., and M. Parrinello. 2002. Escaping free-energy minima. *Proc. Natl. Acad. Sci. USA.* 99:12562–12566.
16. Robertson, K. M., and D. P. Tieleman. 2002. Orientation and interactions of dipolar molecules during transport through OmpF porin. *FEBS Lett.* 528:53–57.
17. Rostovtseva, T. K., E. M. Nestorovich, and S. M. Bezrukov. 2002. Partitioning of differently sized poly(ethylene glycol)s into OmpF porin. *Biophys. J.* 82:160–169.
18. Nestorovich, E. M., C. Danelon, …, S. M. Bezrukov. 2002. Designed to penetrate: time-resolved interaction of single antibiotic molecules with bacterial pores. *Proc. Natl. Acad. Sci. USA.* 99:9789–9794.
19. Laio, A., A. Rodriguez-Fortea, …, M. Parrinello. 2005. Assessing the accuracy of metadynamics. *J. Phys. Chem. B.* 109:6714–6721.
20. Sterpone, F., M. Ceccarelli, and M. Marchi. 2001. Dynamics of hydration in hen egg white lysozyme. *J. Mol. Biol.* 311:409–419.
21. Mach, T., P. Neves, …, P. Gameiro. 2008. Facilitated permeation of antibiotics across membrane channels—interaction of the quinolone moxifloxacin with the OmpF channel. *J. Am. Chem. Soc.* 130: 13301–13309.
22. Humphrey, W., A. Dalke, and K. Schulten. 1996. VMD: visual molecular dynamics. *J. Mol. Graph.* 14:33–38, 27–28.
23. Berezhkovskii, A. M., and S. M. Bezrukov. 2005. Optimizing transport of metabolites through large channels: molecular sieves with and without binding. *Biophys. J.* 88:L17–L19.
24. Weingart, H., M. Petrescu, and M. Winterhalter. 2008. Biophysical characterization of in- and efflux in Gram-negative bacteria. *Curr. Drug Targets.* 9:789–796.
25. Nikaido, H., and E. Y. Rosenberg. 1983. Porin channels in *Escherichia coli*: studies with liposomes reconstituted from purified proteins. *J. Bacteriol.* 153:241–252.
26. Nekolla, S., C. Andersen, and R. Benz. 1994. Noise analysis of ion current through the open and the sugar-induced closed state of the LamB channel of *Escherichia coli* outer membrane: evaluation of the sugar binding kinetics to the channel interior. *Biophys. J.* 66:1388–1397.
27. Hénin, J., E. Tajkhorshid, …, C. Chipot. 2008. Diffusion of glycerol through *Escherichia coli* aquaglyceroporin GlpF. *Biophys. J.* 94: 832–839.
28. Jusuf, S., P. J. Loll, and P. H. Axelsen. 2003. Configurational entropy and cooperativity between ligand binding and dimerization in glycopeptide antibiotics. *J. Am. Chem. Soc.* 125:3988–3994.
29. Berezhkovskii, A. M., M. A. Pustovoit, and S. M. Bezrukov. 2003. Channel-facilitated membrane transport: average lifetimes in the channel. *J. Chem. Phys.* 119:3943–3951.
30. Berezhkovskii, A. M., G. Hummer, and S. M. Bezrukov. 2006. Identity of distributions of direct uphill and downhill translocation times for particles traversing membrane channels. *Phys. Rev. Lett.* 97:020601.
31. Tieleman, D. P., and H. J. Berendsen. 1998. A molecular dynamics study of the pores formed by *Escherichia coli* OmpF porin in a fully hydrated palmitoyloleoylphosphatidylcholine bilayer. *Biophys. J.* 74:2786–2801.

3 Paper: Biophysical characterization of In- and Efflux in Gram-Negative Bacteria

Authors: Helge Weingart, **Mircea Petrescu**, Mathias Winterhalter

3.1 Declaration of contribution

For the present review article, I prepared figures, discussed content and participated in manuscript writing.

Biophysical Characterization of In- and Efflux in Gram-Negative Bacteria

Helge Weingart, Mircea Petrescu and Mathias Winterhalter*

Jacobs University Bremen, School of Engineering and Science, 28759 Bremen, Germany

Abstract: Gram-negative bacteria developed a number of tools to avoid accumulation of cell-toxic compounds. The outer membrane as a first defense system is tightly packed reducing permeation through the lipid membrane. Water-soluble compounds may penetrate through membrane channels called porins. Once inside the periplasmic space special enzymes may welcome the foreign molecule for inactivation. The molecules entering the inner membrane will be harvested by efflux pumps and ejected back to the extra-cellular space. Bacteria modulate all these barriers through the level of protein expression or mutations. In order to understand the function of the involved proteins a quantification of the individual transport elements is necessary. Here we describe recent biophysical methods to characterize molecular transport across membranes.

INTRODUCTION

With the upcoming advances nanotechnology new fields like investigating reactions in small volumes, characterisation of single enzymes or watching motion of single molecules became feasible. However, despite its relevance, the transport of molecules across the bacterial cell envelope has not yet been investigated directly. To date, for example, the efficiencies of antibiotics are characterized by their minimal inhibitory concentration (MIC). The MIC is defined as the lowest concentration of an antimicrobial compound sufficient to prevent visible growth of a microorganism. This value reflects the integral success of an antibiotic to cross all barriers and to fulfill its activity in a given type of bacteria. Clearly, the MIC value is a very complex function. Different resistance mechanisms may interact to increase the level or spectrum of resistance and cooperative effects cannot be deduced without a careful measurement. Inhibition of one resistance mechanism by an antibiotic may increase the susceptibility of the bacterium to a specific antibacterial agent; however, it may also restore or enhance the activity of a second class of antibiotics. In order to optimize the drug efficiency it is most helpful to quantify the individual contribution of given resistance mechanisms to the resistance of an organism.

Gram-negative bacteria possess an asymmetric outer membrane consisting of an inner layer containing phospholipids and an outer layer containing lipopolysaccharides (LPS). First, the antibiotic molecule has to overcome the outer membrane, than diffuse through the periplasmic space to find its target. If the latter is not localized in the periplasmic space the antibiotic has to permeate across the inner membrane to reach its cytoplasmic target. Bacteria may avoid this intoxication by an extreme tight packing of the outer membrane, thereby reducing the permeation of hydrophobic agents across the highly-charged LPS. The influx of small water-soluble substances through porins can be lowered by mutational changes in size, selectivity or the copy number of the hydrophilic channels [1-3]. The periplasmic space may contain enzymes that inactivate the antimicrobial agent. Once the toxic molecule has reached the inner membrane it might be recognised by an efflux pump and actively expelled from the cell. Here we outline several biophysical methods that can be successfully used to separate the effects and to understand the process of antibiotic resistance (Fig. **1**).

Compounds of the β-lactam family belong to the most important and most widely used group of antibacterial agents. They interfere with the biosynthesis of the peptidoglycan, a complex polymer of sugars and amino acids constituting the major component of the bacterial cell wall. The antibacterial efficacy of the β-lactam family of antibiotics is dependent on their structural similarity to the substrate of the DD-transpeptidases located in the periplasmic space. Inhibition of these enzymes by β-lactams leads to structural instability and death of the bacteria. Before reaching the target, β-lactam antibiotics have to cross the outer membrane. Permeation across the cell envelope is facilitated by an attractive interaction of the antibiotic with the lipid phase or with a particular channel protein in the membrane. These interactions can be characterized by equilibrium studies using several techniques. For example, optically active molecules such as β-lactams show often a solvent-dependent spectrum [4]. Depending on whether the molecule is in the aqueous or lipid phase, the absorption and emission spectra are shifted. Therefore, these environment-sensitive spectra allow the partition coefficient to be determined. Furthermore, the change in mobility can be recorded using fluorescence anisotropy [5]. Another technique is based on calorimetric measurements. For example, a titration of a β-lactam antibiotic to a liposome preparation using Isothermal Titration Calorimetry (ITC) allows conclusions on possible partitioning [6]. It should be noted that drugs may bind to lipids or rather partition into lipids. Moreover, the affinity may change in presence of already bound molecules as in case of charged molecules. Thus, a binding constant does often not exist but rather a binding isotherm. Usually, such an analysis

*Address correspondence to this author at the Campus Ring 1, 28759 Bremen, Germany; Tel: +49 421 200-3248; Fax: +49 421 200-3249; E-mail: m.winterhalter@jacobs-university.de

1389-4501/08 $55.00+.00

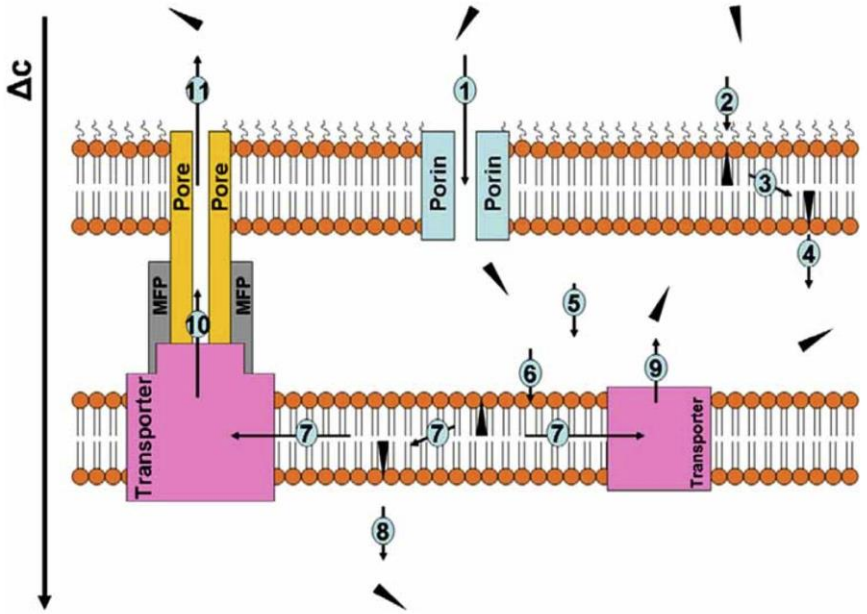

Fig. (1). Schematic view of the different barriers along the pathway of an antibiotic from the outside to the cellular target. The drug follows the concentration gradient Δc.

1: Entry of hydrophilic drugs through a channel, 2: Partitioning of hydrophobic drugs into the outer membrane, 3: Diffusion or flip-flop across the hydrophobic layer, 4: Partitioning into the periplasmic space, 5: Diffusion through the periplasmic space, 6: Partitioning into the inner membrane. 7: Lateral diffusion, flip-flop across the inner membrane 8: Partitioning into the cytoplasm, 9: Active efflux into the periplasmatic space, 10: Active efflux bypassing the periplasmic space. 11: Diffusion into the extracellular space. All processes are either in equilibrium or approaching the equilibrium. Only steps 9 and 10 require energy supply using the proton motive force or ATP hydrolysis.

is not included in the usual software packages but it is straightforward [7]. Optical spectroscopy, conductance or calorimetric studies have also been applied to reveal the affinity of substrates to transporters and channels. For example, the binding of hydrophobic compounds like ethidium to the multidrug efflux transporter EmrE has been studied by ITC [8]. ITC allows under favourable conditions the direct quantification of the entropic and enthalpic contributions to the binding. Another possibility for such a separation is to quantify the binding constant at different temperatures. Applying Van't Hoff equation $\ln K = -\Delta G^{\varnothing}/RT$ relating the temperature-dependent binding constant K with the free standard enthalpy $-\Delta G^{\varnothing}$ allows also to separate entropic from enthalpic contribution. However, equilibrium measurements do not allow direct conclusions on the kinetics of transport.

Some of the charged β-lactams have very low membrane permeability and subsequently translocate more rapidly through membrane channels. The most prominent candidate is the general diffusion porin OmpF (outer membrane protein F) which is considered to be the primary gateway for antibiotics. Indeed, some β-lactam resistant strains of *Escherichia coli* have shown a deficiency in OmpF expression [9]. Also, mutations in the central loop leading to structural alterations of OmpF, such as a decrease in the pore radius, seriously inhibit antibiotic uptake [10]. High resolution crystal structure and conductance measurements revealed a pore size of about one nanometre [11]. As typical antibiotic molecules have about the same size, free diffusion through the channel can be excluded. As typical antibiotic molecules have about the same size, free diffusion through the channel can be excluded. Thus, interactions with the surface of the channel determine the antibiotic permeation.

Efflux is a further important determinant of intrinsic and/or acquired resistance to antimicrobials. Bacterial multidrug efflux (MDE) transporters are members of a limited number of families. In Gram-negative bacteria, members of the resistance-nodulation-cell division (RND) family are the most relevant in terms of resistance to clinically important agents including β-lactams [12-14]. RND transporters are located in the inner membrane and function in concert with a periplasmic, so-called membrane fusion protein and a channel-forming outer membrane protein of the TolC family. This tripartite complex allows drug transport from the cytoplasmic or periplasmic space directly into the external medium, bypassing the outer membrane barrier [15]

In *Escherichia coli*, the constitutively expressed RND-type efflux system AcrAB was shown to contribute significantly to the intrinsic β-lactam resistance [16]. A comparison

of various β-lactam antibiotics showed a quantitative relationship between the β-lactam side chain lipophilicity and MICs in *E. coli* and *Salmonella typhimurium*. β-lactams with lipophilic side chains appeared to be good substrates of the AcrAB pump because wild-type strains producing a functional AcrAB system were far more resistant than the corresponding *acrAB*-negative mutants. In contrast, β-lactams with hydrophilic side chains are poor substrates of the pump, as judged by the similar MICs obtained for the AcrAB producer and the *acrAB* mutant. This correlation suggests that those molecules that partition at least partially into the lipid bilayer of the inner membrane are more effectively captured by the AcrAB pump [17].

Beside AcrAB, *E. coli* possess four other RND-type MDE systems (AcrD, AcrEF, MdtEF, and MdtABC) which all need the outer membrane channel TolC for their functions. Nishno *et al.* overexpressed all five RND-type drug exporters in the *acrB* deletion strain *E. coli* KAM3 [18]. They found that all of them conferred resistance to β-lactams. Among these, AcrAB and AcrEF conferred the highest level of β-lactam resistance to *E. coli*. Overexpression of AcrD, MdtEF, and MdtABC caused an intermediate resistance to the β-lactams tested.

TRANSLOCATION ACROSS LIPOSOMES

Liposomes are used as model system for membrane transport using radioactive compounds for the uptake. However, the time resolution is limited by the separation method necessary to distinguish the free from the captured molecule and to the availability of radioactive tracer [19, 21]. Recently, an interesting study to reveal slow kinetics of H.K-ATPase in Oocytes has been presented. Using atomic absorption spectroscopy allowed quantifying the Rb^+ uptake with 0.1 pmol precission. [22].

Permeation of β-lactams across the lipid bilayer has been analysed by liposome swelling assays [1, 23, 24]. This method detects a change in optical density caused by osmotic swelling. For example, ampicillin does not permeate across lipid membranes. As β-lactams are charged, water-soluble substances they may translocate more rapidly through membrane channels. Subsequently, in absence of membrane channels iso-osmotic addition of millimolar concentrations to a liposome preparation does not change the internal osmotic pressure and the optical density will not change. It is expected that the permeation is even less for tighter LPS-lipid membranes but to date this has not been characterised. In contrast, hydrophobic antibiotics like some of the quinolones (e.g. nalidixic acid) permeate significantly across lipid bilayers. Permeation rates of a large variety of antibiotics have been observed by measuring the swelling of liposomes containing reconstituted porins (see Table **1**). It should be noted that this type of measurements depends crucially on the lipid concentration and small variations will result in arbitrary values. Moreover, the swelling assay provides only relative numbers to assess how the translocation varies from one compound to the other for one preparation. In principle, quantification is possible but rather tedious. In addition, the underlying effect is still under debate. It is expected that an increase in osmotic pressure should stretch the liposome giving raise to an enhanced scattering or enhanced optical density. However, all experiments revealed a reduction in optical density. From mechanical stretching experiment it is known that liposome will leak or rupture after stretching 2-4% [25]. We performed a number of tests to probe for the possible underlying mechanism. It seems that the increasing osmotic pressure cause leakage and thus a decreasing optical density. Thus, the influx is creating a stress causing rupture with subsequent reduction in optical density. In this case, we expect a large scattering as the interlayer distance will vary with buffer composition and multi-lamellar liposome preparation.

Table 1. Permeation Through Porins

Penicillins	OmpF
Ampicillin	Yes (46)
Amoxicillin	Yes
Carbenicillin	No translocation (5)
Azlocillin	No translocation
Piperacillin	No translocation (<5)
Penicillin G	No translocation
Fluoroquinolones	
Moxifloxacin	Yes
Nalidixic Acid	No translocation
Enrofloxacin	Yes

Various antibiotics have been tested for possible interaction using the ion current fluctuation analysis through OmpF/OmpC. In brackets we indicate the relative values for the corresponding liposome swelling (data from [30]).

Characterization of active energy-requiring transport is possible. An elegant method is to create a transmembrane electric potential to drive an efflux pump. For example, transport proteins are reconstituted in a potassium buffer into liposomes and dialysed with a potassium free buffer. Addition of valinomycin will increase the permeability of the lipid membrane for potassium and thus create a gradient able to drive a pump [26,27]. Similar systems have been used to characterize a variety of uptake systems including efflux pumps [28, 29].

TRANSLOCATION REVEALED BY ELECTROPHYSIOLOGY

Recently, we have shown that substance permeation through porins can be quantified on a single molecular level. Purified porins are reconstituted into planar also called black lipid bilayer (BLM). BLM´s are formed according to Montal and Mueller with some slight modifications [31-34]. After equilibration, a small quantity of porins from a diluted stock solution is added. The porins will spontaneously insert and depending on the dilution the first insertion will occur after a few minutes. To avoid multiple insertions the cuvette is quickly flushed with buffer. Acoustic screening of the set-up, the small membrane area and an anti-vibration table allow

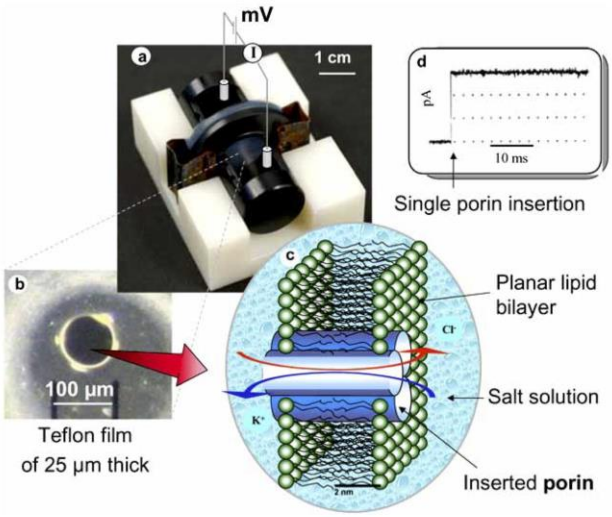

Fig. (2). Set-up of the planar lipid bilayer. A planar bilayer is formed across an aperture separating two aqueous solutions. A single porin spontaneously inserts, allowing a constant ionic current. (**a**) Measurement cell. The volume of each cell is about 250 µl. Further miniaturization is possible [47] (**b**) View of the hole under the microscope, (**c**) Scheme of the bilayer with an incorporated porin and (**d**) Typical current recording of a single porin insertion (adopted from [20]).

ion conductance measurements with time resolution better than milliseconds. Titration of the substrate molecules to one or to both sides of the porin will allow the molecule to diffuse inside the channel and subsequently, cause an ion current fluctuation due to blockage of the channel (Fig. **2**).

Time-dependent ion current fluctuations can be analysed to identify translocation events. If the channel has a similar size as the diffusing particle, the ion flow will be interrupted for a short period. This is visible as fluctuation in the ion current, reflecting the molecular interactions with the channel wall. This observation was used about 10 years ago to reveal substrate affinity and translocation across maltoporin [35, 36].

More recently, this method was optimized to analyze the interaction of antibiotics with outer membrane proteins on a single molecular level. In Fig. (**3**), the presence of a 5.7 mM ampicillin solution caused a rapid closure of the pore for about a few milliseconds. Increasing the concentration increases the number of events but not the mean residence time. Previously for maltose permeation through maltoporin the quantification of the actual flux has been shown [37-38].

This method has been applied to characterize the translocation of a number of antibiotics. For example it has been shown that the β-lactam antibiotics ampicillin and amoxicillin interact strongly with OmpF but not with OmpC. Noise analysis enables us to perform measurements on a wide range of parameters. Depending on voltage and pH, the characteristic residence time varied in the range of microseconds to hundreds of microseconds. For cephradine, a first generation cephalosporin antibiotic, the residence time is 8.8 ms, for ampicillin it is about 110 ms. These times should be compared with several nanoseconds expected in the case of purely diffusional relaxation for molecules of this size. A different case was found with fluoroquinolones. For example, moxifloxacin seems to permeate through OmpF whereas the more hydrophobic nalidixic acid permeates rather quickly across the lipid membrane itself. Typical translocation numbers for reasonable antibiotic concentration in the µM range are around 1-10 molecule per channel and per second. To date this is beyond the range accessible by molecular modelling (about a few ns).

TRANSLOCATION THROUGH A CHANNEL: LIMITING FACTORS

OmpF and OmpC are attractive candidates for the study of the influence of the channel surface on the permeation of antibiotics. For both a high resolution crystal structure is now available which reveals a sixteen β-strands trimeric channel with a pore size of about 1 nm, as expected from earlier conductance studies [11,39]. The fundamental question is how to design antibiotic molecules in order to optimize their influx through the porin channels. In a macroscopic approach the flux of molecules J (substrate molecules per unit time) through a cylinder is given by

$$J = -(D\pi a^2/l)\,\Delta c \qquad (1)$$

with D as the diffusion constant of the particle, usually in the order of 10^{-9}- 10^{-10} m^2/s in aqueous solution depending on the viscosity and size of the drug, a is the pore radius of about 0.5 nm, l is the approximate channel length of about 4 nm and Δc is the concentration gradient.. Inserting the above mentioned approximate values and presuming a concentration gradient of $\Delta c \approx 1$ µM results in a flux of about 10-100

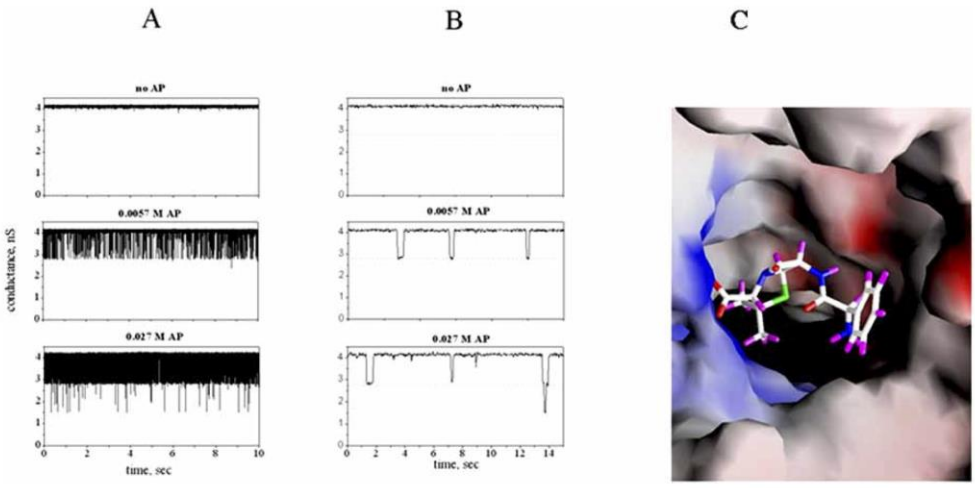

Fig. (3). Typical recording of the ion current through the *E. coli* porin OmpF. Top, left side.

A. 1 M KCl solution produces a current of about 4 nS at room temperature and pH 7. Addition of ampicillin (about 5.7 mM) creates strong ion fluctuations, increasing the concentration (27mM) enhances the blockages.

B. Zooming in with a higher time resolution shows no closure in absence, at 2.7 mM some closures and at 27 mM closures of two channels. These closures correspond to the penetration of ampicillin molecules into the channel, hindering the ions passing through. Note that the blocking is in the range of milliseconds which is remarkable long for diffusion.

C. the result of our molecular modelling: ampicillin showing a high affinity to the OmpF channel (adopted from Reference [34]).

molecules per second. This corresponds to the fastest possible permeation through a cylinder of this size and is limited only by diffusion towards the channel. However, at distances below 1 nm molecular interaction with the channel becomes dominant. This is reflected by the molecular specificity: evidence suggests that it is the chemical structure, rather than the size that exerts the dominant influence on permeation pathways [37].

Recently, the affinity of molecules into the porin channel has been measured [33-38]. Antibiotics have been titrated on both sides of the channel and fluctuations in the ion current show the occupancy of the binding pocket inside the channel. An analysis of the equilibrium fluctuation readily provides the chemical rates for entering and leaving the binding site inside the channel. Determining the on- and off-rates allows the net permeation to be obtained. In a similar study, the analysis of maltose translocation through Maltoporin leads to the development of a symmetric one-binding-site model [37-38]. To simplify, we assume a symmetric barrier and a one side drug addition giving raise to a concentration gradient. The measured rates can be included in equation (1) in which the geometrical factors are replaced by kinetic rates. The flux is given by

$$J = [\, K \cdot k_{off}/(\, 2 + K\,\Delta c)]\ \Delta c \approx [k_{on}\,/(2 + K\,\Delta c)\,]\ \Delta c$$

with K as the binding constant, k_{off}, and k_{on} are the off-rates [37-38]. The net flux J, in molecules per second, is at low concentrations (non-saturated condition) proportional to the concentration gradient Δc. It should be noted that for a strong binding the permeation is limited by the off-rate and that for a large gradient Δc the flux is independent on the concentration gradient. More sophisticated models have been suggested and allow the inclusion of detailed binding parameters [40-42]. However, within the limited accuracy of the measurements and the limited knowledge of molecular parameters the above simplified model may satisfy most of the current needs.

It is also interesting to discuss the relevance of substrate binding for translocation. Inspection of the experimental values for the on and off-rate in the biological relevant concentration gradient range (μM) yields that $k_{off} >> k_{on}\,\Delta c$. This simplifies the flux to $J = k_{on}\,\Delta c/2$. In other words, increasing the on-rate will directly result in an increase in translocation and subsequently, the drug efficiency should increase.

The permeation through OmpF has been measured for several penicillins like ampicillin and amoxicillin. In addition, the translocation of several other β-lactams (carbapenems, cephalosporins) through Omp36 (an OmpC homologue) has been quantified (C. James *et al.,* submitted 2008). Inserting experimental values for $k_{on} = 10^6\ [Ms]^{-1}$ and K = 1 $[Ms]^{-1}$ gives about 3 molecules/second at 1 μM concentration gradient per monomer. This value is about a factor of ten lower than the above derived diffusion limit. In order to discuss the efficiency one has to understand more about the

molecular interaction involved in diffusion at the nanoscale level, for which molecular details are lacking.

NANOPORE ASSAY

In this context it is interesting to note that a very neat whole cell permeation assay was developed for eukaryotic cells which might be possible to apply also to bacteria [43]. Transport across membranes depends on the permeability coefficient for the particular molecule and the concentration gradient, or, in case of transport proteins, also on the number of transporters (or channels). In general, the number of molecules translocated per unit area can vary by several orders of magnitudes. Optical detection methods require usually active molecules in micromolar concentration range. Peters and coworkers suggested placing eukaryotic cells on a microstructured array containing holes of a given size [43]. Depending on transport rates the size of the holes will be adjusted to collect the necessary concentration range per unit time. For adherent eukaryotic cells this technique is rather straightforward but it could be also adapted to bacteria using nanostructured arrays. These structured arrays will allow to have the right time range to measure optically fast as well as slow permeation (Fig. **4**).

PROTON DRIVEN PUMPS

Typical turn-over numbers for proton driven pumps are about 1-1000 ions per second. Thus the ion current generated by such pumps on a single molecular level is not feasible with the current instrumentation for which the limit is around a few pA ($=5\cdot10^5$ ions/s). The search for inhibitors of such pumps is pharmacologically important, as compounds able to block such transporter may restore the activity of other antibiotics and therefore, techniques for screening are currently developed. For example, membrane fragments or reconstituted liposomes are coupled to solid supported bilayers on a gold electrode and the transported charges are integrated over a large surface [44-45]. This technique allows for example to study the charge transfer in ATP-ase and reveals insight in the electrogenic steps.

MOLECULAR MODELLING OF TRANSPORT

To understand which structural features of β-lactam antibiotics determine their permeation properties through the OmpF porin, molecular modelling of ampicillin transport has been performed [33, 34, 46]. The charge distribution of the antibiotic complements the charge distribution at the narrowest part of the bacterial porin. Interaction of these charges creates a zone of attraction inside the channel and compensates the penetrating molecule's entropy loss and dehydration energy. For example, the phenyl group of ampicillin provides an additional favorable energetic contribution during translocation by interacting with the hydrophobic environment. This facilitates translocation through the narrowest part of the channel. Molecular modelling provides new tools to interpret results obtained with other antibiotics and possibly, stimulate intelligent drug design for enhanced permeation.

A different approach to model the pathway would be to apply a force to drag the antibiotic molecule through the channel. A similar approach has already been performed with ions. Application of sufficiently high voltages will bring enough ions throughout the calculation time through the channel to achieve a reasonable statistics. The modelling is in good agreement with the experimentally measured conductance (C. Chimerel *et al.* submitted, 2008).

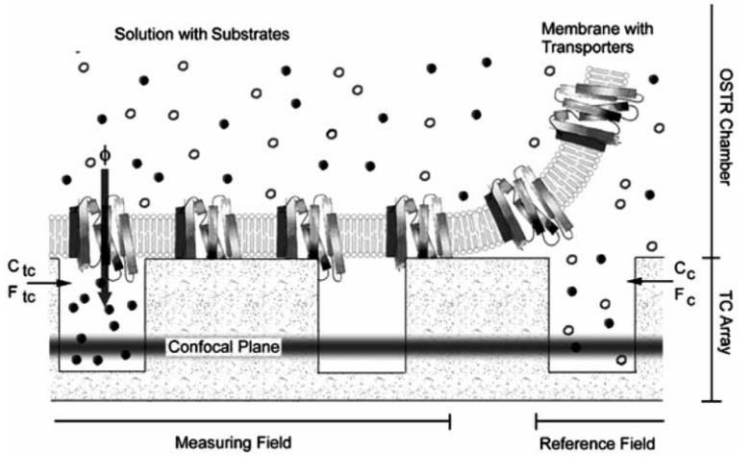

Fig. (4). Schematic drawing of the microchamber set-up for optical transporter recording. A cellular membrane is attached to a microarray of small test compartments. A transport substrate (filled circles) and a control substrate (open circles) are added to the chamber. The time-dependent appearance of the substrates in the test chambers is recorded by confocal scans. In the measuring field the membrane seals the test chambers and only the transport substrate appears in the test chambers. In the reference field the test chambers are not sealed, and both transport and control substrates appear. C_{tc}, F_{tc}, C_c, and F_c are the concentration and fluorescence in test chambers and chamber, respectively [taken from [43] with permission].

For OmpF and OmpC high resolution crystal structures are known. Together with a new generation of powerful computer and new software, the modelling of the transport pathway became possible [33,34,46]. Molecular dynamics simulations allow the investigation of a number of processes at atomic level by integrating Newton's equation of motion. However, the current available computation time limits the system to about 100 000 molecules and a few nanoseconds. Clearly, permeation of antibiotics is far beyond this range and would require a less detailed approach like a coarse grained description. Another solution to catch such rare-events is called Metadynamics and is based on an algorithm that limits backward motions. In a first work, Ceccarelli and coworker [47] applied a new algorithm to elucidate possible pathways of the antibiotic through the channel. In a more recent publication the pathway of five different β-lactams (ampicillin, amoxicillin, piperacillin, azlocillin and carbenicillin) through OmpF has been evaluated [33]. It is interesting to note that the mid-channel constriction L3 loop of OmpF hardly moves at all in the presence of antibiotics. Azlocillin and piperacillin did not permeate through the channel. Likely, they are too bulky. In contrast, ampicillin and amoxicillin permeate nicely and two binding pockets have been elucidated. The energy gain related to the binding pocket has to be related to the kinetics of permeation. This is approximated following the transition state theory through

$$k = (1/\tau)\ \exp(-\Delta G/k_B T)$$

with k as the corresponding rate constant and τ as the pre-exponential. In the exponent ΔG is the energy difference calculated from the molecular modelling and $k_B T$ is the Boltzmann factor. Originally, this theory was derived for reactions in the gas phase and the pre-exponential corresponds to the number of hits. In condensed phase this values is to be replaced by a more complex relation.

Another possible approach is to apply a force to the antibiotic molecule and drag it through the channel. In both cases the pathway, possible interaction and interaction with the channel can be obtained. However the actual permeation values are obtained in a rather indirect manner through an extrapolation into the experimentally available millisecond range and thus conclusions must be taken with a certain caution. Current efforts to model the flux of ions through OmpF suggest that this approach is able to predict macroscopic parameter like ion current.

ACKKNOWLEDGEMENTS

Financial support for this project was obtained through EU-grant MRTN-CT-2005-019335 (Translocation).

REFERENCES

[1] Nikaido, H. (2003) *Microbiol. Mol. Biol. Rev.*, **67,** 593-656.
[2] Simonet, V.; Malléa, M. and Pagès, J.-M. (2000) *Antimicrob. Agents Chemother.*, **44**, 311-315.
[3] Pagès, J.-M. (2004) In "Bacterial and Eukaryotic Porins", R. Benz, ed., Wiley-VCH, pp. 41-59.
[4] Rodrigues, C.; Gameiro, P.; Prieto, M. and de Castro, B. (2003) *Biochim. Biophys. Acta.*, **1620**, 151-159.
[5] Su, C.C.; Rutherford, D.J. and Yu, E.W. (2007) *Biochem. Biophys. Research. Com.*, **361**, 85-90; Su, C.C., Nikaido, H. and Yu, E.W. (2007) *Febs. Lett.* **581**, 4972-76
[6] Howe, J.; Andrä, J.; Conde, R.; Iriarte, M.; Garidel, P.; Koch, M.H.; Gutsmann, T.; Moriyón, I. and Brandenburg K. (2007) *Biophys. J.*, **92**, 2796-2805.
[7] Schwarz G, Damian L, and Winterhalter M. (2007) *Eur. Biophys. J.*, **36,** 571-9.
[8] Sikora, C.W. and Turner, R.J. (2005) *Biophys. J.*, **88**, 475-482.
[9] Harder, K. J.; Nikaido, H. and Matsuhashi, M. (1981) *Antimicrob. Agents Chemother.*, **20**, 549-552.
[10] Simonet, V.; Malléa, M. and Pagès, J.-M. (2000) *Antimicrob. Agents Chemother.*, **44**, 311-315.
[11] Cowan, S.W.; Schirmer, T.; Rummel, G.; Steiert, M.; Ghosh, R.; Pauptit, P.A.; Jansonius, J.N. and Rosenbusch, J.P. (1992) *Nature*, **358,** 727-733.
[12] Poole, K. (2004) *Clin. Microbiol. Infect.*, **10**, 12-26.
[13] Piddock, L. J. V. (2006) *Clin. Microbiol., Rev.*, **19**, 382-402.
[14] Kumar, A. and Schweizer, H.P. (2005) *Adv. Drug Deliv. Rev.*, **57**, 1486-513.
[15] Zgurskaya, H.I.; Krishnamoorthy, G.; Tikhonova, E.B.; Lau, S.Y. and Stratton, K.L. (2003) *Front Biosci.*, **8**, 862-873.
[16] Mazzariol, A.; Cornaglia, G. and Nikaido, H. (2000) *Antimicrob. Agents Chemother.*, **44**, 1387-1390.
[17] Nikaido, H.; Basina, M.; Nguyen, V. and Rosenberg, E.Y.(1998) *J. Bacteriol.*, **180**, 4686-4692.
[18] Nishino, K.; Yamada, J.; Hirakawa, H.; Hirata, T. and Yamaguchi,A. (2003) *Antimicrob. Agents Chemother.*, **47**, 3030-3033.
[19] Hong, J.S. and Kaback, H.R. (1972) *Proc. Natl. Acad. Sci. USA*, **69**, 3336-3340.
[20] Berkane, E.; Orlik, F.; Charbit, A.; Danelon, C.; Fournier, D.; Benz, R. and Winterhalter, M. (2005) *J. Nanobiotechnol.*, **3**,3.
[21] Michéa-Hamzehpour, M., Furet, Y.X., and Pechère, J.C. (1991). *Antimicrobial Agent Chemotherapy*, **35**, 2091-97.
[22] Dürr, K.L.; Tavraz, N.N.; Zimmermann, D.; Bamberg, E. and Friedrich, T. (2008) *Biochemistry*, **47**, 4288-4297.
[23] Luckey, M. and Nikaido, H. (1980) *Proc. Natl. Acad. Sci. USA*, **77**, 167-171.
[24] Nikaido, H. and Rosenberg, E.Y. (1983) *J. Bacteriol.*, **153**, 241-252.
[25] Needham, D. and Nunn, R.S. (1990) Biophys. J., **58**, 997-1009.
[26] Ward, A.; Hoyle, C.; Palmer, S.; Griffith, J.; Pos, M.; Morrison, S.; Poolman, B.; Gwynne, M. and Henderson, P. (2001) *J. Mol. Microbiol. Biotechnol.*, **3**, 193-200.
[27] Gbaguidi, B.; Hakizimana, P.; Vandenbussche, G. and Ruysschaert, J.-M. (2007) *Cell. Mol. Life Sci.*, **64**, 1571-1582.
[28] Bolhuis, H.; Van Veen, H.W.; Brands, J.R.; Putman, M.; Pooolman, B.; Driessen, A.J.M. and Konigs, W.N. (1996) *J. Biol. Chem.*, **271**, 24123-24128.
[29] Elbaz, Y.; Tayer, N.; Steinfels, E.; Steiner-Mordoch, S. and Schuldiner, S. (2005) *Biochemistry*, **44**, 7369-7377.
[31] Winterhalter, M. (1999) *Coll. Surface Sci.*, **149**, 161-169.
[30] Yoshimura, F. and Nikaido, H. (1985) *Antimicrob. Agents Chemother.*, **27**, 84-92.
[32] Montal, M. and Mueller, P. (1972) *Proc. Natl. Acad. Sci. USA*, **69**, 3561-3566.
[33] Danelon, C.; Nestrovich, E.M.; Winterhalter, M.; Ceccarelli, M. and Bezrukov, S.M. (2006) *Biophys. J.*, **90**, 1617-1627.
[34] Nestorovich, E.M.; Danelon, C.; Winterhalter, M. and Bezrukov, S.M. (2002) *Proc. Natl. Acad. Sci. USA.*, **99**, 9789-9794.
[35] Benz, R.; Schmid, A. and Hancock, R.E.W. (1985) *J. Bacteriol.*, **162**, 722–727.
[36] Nekolla, S.; Andersen, C. and Benz, R. (1994) *Biophys. J.*, **66**, 1388-1397.
[37] Danelon, C.; Brando, T. and Winterhalter, M. (2003) *J. Biol. Chem.*, **278**, 35542-35551.
[38] Schwarz, G.; Danelon, C. and Winterhalter, M. (2003) *Biophy. J.*, **84**, 2990-2998.
[39] Baslé, A.; Rummel, G.; Storici, P.; Rosenbusch, J.P. and Schirmer, T. (2006) *J. Mol. Biol.*, **362**, 933-942.
[40] Berezhkovskii, A.M. and Bezrukov, S.M. (2005) *Biophys. J.*, **88**, L17-19.
[41] Bauer, W.R. and Nadler, W. (2006) *Proc. Natl. Acad. Sci. USA*, **103**, 11446-11451.

[42] Bezrukov, S.M.; Berezhkovskii, A.M. and Szabo, A. (2007) *J. Chem. Phys.*, **127**, 115101-115108.
[43] Peters, R. (2003) *Annu. Rev. Biophys. Biomol. Struct.*, **32**, 47-67.
[44] Tadini-Buonisegni, F., Bartolommei, G., Monelli, M.R., and Fendler, K. (2008). *Arch. Biochem. Biophys*. In press.
[45] Geibel, S., Flores-Herr, N., Licher, T., and Vollero, H. (2006) *J. Biomol. Screen*, **11**, 262-268.
[46] Ceccarelli, M.; Danelon, C.; Laio, A. and Parrinello, M. (2004) *Biophys. J.*, **87**, 58-64.
[47] Mach, T.; Chimerel, C.; Fritz, J.; Fertig, N.; Winterhalter, M. and Fuetterer, C. (2008) *Anal. Bioanal. Chem.*, **390**, 841-846.

Received, June 1, 2008 **Accepted, June 10, 2008**